

FEDERAL UNIVERSITY OF ITAJUBA
GRADUATE PROGRAM IN MECHANICAL ENGINEERING

MASTER'S DISSERTATION

By

Okafor Geoffrey Onyebuchi

Energy analysis of low-GWP refrigerants R513A and R516A as alternatives to R134a in heat pumps for simultaneous heating and cooling of water.

Dissertation Submitted to the Graduate Program Degree in Mechanical Engineering as part of the requirements for obtaining the Degree Master of Science in Mechanical Engineering.

Area of Concentration: Thermal, Fluids, and Flow Machine (Energy Analysis of Systems)

Advisor: Prof. Juan José García Pabón. - Universidade Federal de Itajubá, Brazil

Co-Advisor: Prof. Juan Manuel Belman Flores - Universidade de Guanajuato, México

Itajubá, December 2024

ACKNOWLEDGMENTS

I would like to express my deepest gratitude to God Almighty for His unwavering strength, wisdom, and guidance throughout this research journey.

My heartfelt thanks go to UNIFEI for providing the resources and a supportive environment that fostered my academic growth. I am profoundly grateful to TETFUND Nigeria for their generous financial support and to the collaborative efforts of TETFUND-FARA-ARIFA and UFV, which laid the foundation for this valuable research partnership.

I am especially indebted to my advisor, Prof. Juan José García Pabón, for his invaluable guidance, patience, and insightful feedback throughout this work. I also extend my sincere thanks to my co-advisor, Prof. Juan Manuel Belman Flores from the Universidade de Guanajuato, México, for his constructive contributions and unwavering support.

I would like to thank FAPEMIG for funding project APQ 01477-21. This master's research focused on refrigerant fluids, which would serve as substitutes under the conditions in which the funded heat pump could operate. This support was crucial for advancing our research and developing new technologies.

I am grateful to the staff of the Graduate Program in Mechanical Engineering at UNIFEI, as well as to the professors whose teachings greatly enriched my academic experience: Prof. Juan José García Pabón, Prof. Sandro Metrevelle Marcondes de Lima e Silva, Prof. Electo Eduardo Silva Lora, Prof. Osvaldo J. Venturini, Prof. Diego M.Y. Maya, Prof. Paulo Fernando Ribeiro, Prof. Christian Coronado, Prof. Maria Elizabete Villela Santiago, and Prof. Marcia de Souza Luz Freitas. I also extend my appreciation to Ms. Claudia Rosa Rezende de Oliveira from UNIFEI's Directorate of International Relations for her invaluable assistance.

I am deeply thankful to the residents of RepCassino for their warm hospitality during my stay, making my time in a new environment more comfortable and enriching.

Finally, I express my profound gratitude to my beloved family, especially my wife, Mrs. Okafor Peace Ozioma, for their constant encouragement, prayers, and unwavering support throughout this journey.

To all the individuals I encountered and who contributed to making this dream a reality, I am truly grateful. May God bless you all abundantly.

CONTENTS

ACKNOWLEDGMENTS	2
LIST OF TABLES	5
LIST OF FIGURES	6
NOMENCLATURE	7
1. INTRODUCTION	14
1.1. Background and motivation	14
1.2. Research objectives	15
1.3. Structure of the work	16
2. THEORETICAL AND LITERATURE REVIEW	17
2.1. Heat pumps for simultaneous heating and cooling	17
2.1.1. Vapor-compression cycle overview	18
2.1.2. Heat pump overview	19
2.1.3. Applications of heat pump for simultaneous heating and cooling	22
2.2. Theoretical concepts of heat exchanger:	24
2.2.1. Evaporator	24
2.2.2. Condenser	26
2.3. Low-GWP refrigerants and their properties	28
2.4. Previous studies and research gaps	30
3. METHODOLOGY	36
3.1. Experimental setup and procedure	36
3.2. Preliminary calculations	41
3.2.1. Volumetric efficiency of compressor	41
3.2.2. Isentropic efficiency of compressor	42
3.2.3. Heat transfer coefficient into a brazed plate heat exchanger	42

3.3.	Mathematical model.....	51
3.3.1	<i>Evaporator balance</i>	52
3.3.2.	<i>Condenser balance</i>	53
3.3.3.	<i>Compressor</i>	54
3.3.4.	<i>Heat pump model</i>	55
3.4.	Model validation parameters.....	59
3.5.	Simulations conditions.....	60
4.	RESULTS AND DISCUSSION.....	61
4.1.	Experimental results.....	61
4.2.	Validation of mathematical model.....	67
4.3.	Simulation of systems	72
5.	CONCLUSION AND FUTURE WORKS	79
5.1.	Conclusion	79
5.2.	Future works	80
	REFERENCE.....	82
	APPENDIX I. EXPERIMENTAL DATA.....	89
	APPENDIX II. AVERAGE HEAT TRANSFER COEFFICIENT EXPERIMENTAL ANALYSIS.....	92
	APPENDIX III. EXAMPLE OF HEAT TRANSFER COEFFICIENT CALCULATION FOR REFRIGERANT SIDE	95

LIST OF TABLES

Table 1: Properties of R134a, R513A, and R516A (Kim et al. 2021); (*Li 2021).	29
Table 2: Geometrical characteristics of the BPHE (Longo et al. 2016).	43
Table 3: Mean percentage error (MPE) and mean absolute percentage error (MAPE) of R134a, R513A, and R516A.....	67
Table 4: Simulation results for the medium-temperature scenario.	73
Table 5: Simulation results for the high-temperature scenario.	74
Table 6: Experimental data for R134a.	89
Table 7: Experimental data for R513A.....	90
Table 8: Experimental data for R516A.....	91
Table 9: Average Heat transfer coefficient Experimental data for R134a.....	92
Table 10: Average Heat transfer coefficient Experimental data for R513A.	93
Table 11: Average Heat transfer coefficient Experimental data for R516A.	94

LIST OF FIGURES

Figure 1: Vapor-compression cycle of heat pump (Incropera, 1996).....	19
Figure 2: Air-cooled and water-cooled systems for condenser.	20
Figure 3: Different energy sources for heat pumps in heating mode (EHPA, 2019).....	20
Figure 4: Heat pump in reversible mode (heating and cooling) (Trane, 2022).	21
Figure 5: Heat pump configuration for simultaneous heating and cooling.	22
Figure 6: Temperature profile in the evaporator.....	25
Figure 7: Temperature profile in the condenser.....	27
Figure 8: Instrumentation diagram of the refrigeration installation (Méndez-Méndez et al. 2023).	39
Figure 9: Flowchart of variable measures.....	40
Figure 10: Operational diagram of the BPHE (Danfoss A/S, 2014).....	44
Figure 11: Modeling of system components.....	55
Figure 12: Fluxgram (flow diagram) of heat pump model solution using MATLAB.....	57
Figure 13: T_{evap} and T_{cond} vs number of data for R134a, R513A, and R516A.	61
Figure 14: Effect of T_{evap} and T_{cond} on m_{ref}	62
Figure 15: Q_{evap} , Q_{cond} , and W_{comp} vs T_{evap} for R134a, R513A, and R516A.	63
Figure 16: COP_h and COP_c vs T_{evap} for R134a, R513A, and R516A.	64
Figure 17: U_{evap} and U_{cond} vs m_{ref} for R134a, R513A, and R516A.	65
Figure 18: Volumetric and isentropic efficiency vs compression ratio.	66
Figure 19: Theoretical vs experimental T_{evap} and T_{cond}	69
Figure 20: Theoretical vs experimental Q_{evap} , Q_{cond} , and W_{comp}	70
Figure 21: Theoretical vs experimental COP for cooling and heating.	71
Figure 22: COP vs mass flow rate of water for R134a: (A) $m_{wc} = 0.1 \text{ kg/s}$ and $T_{inwc} = 35 \text{ }^\circ\text{C}$. (B) $m_{we} = 0.1\text{kg/s}$ and $T_{inwe} = 5 \text{ }^\circ\text{C}$	75
Figure 23: COP vs mass flow rate of water for R134a: (A) $m_{wc} = 0.1 \text{ kg/s}$ and $T_{inwc} = 50 \text{ }^\circ\text{C}$. (B) $m_{we} = 0.1\text{kg/s}$ and $T_{inwe} = 15 \text{ }^\circ\text{C}$	75
Figure 24: COP vs mass flow rate of water for R134a for two scenarios.	77
Figure 25: COP for all fluids, with $m_{wc} = 0.15 \text{ kg/s}$ and $m_{we} = 0.15\text{kg/s}$	78

NOMENCLATURE

a_1, a_2, a_3	Polynomial coefficients for volumetric efficiency (-)
A_{ch}	Cross-sectional area of BPHE channel (m ²).
A_{cond}	Heat transfer area of the condenser (m ²)
$A_{eff,BPHE}$	Effective heat transfer area of BPHE (m ²)
A_{evap}	Heat transfer area of the evaporator in the heat exchanger (m ²)
b	Corrugation depth of plate BPHE (m)
b_1, b_2, b_3	Polynomial coefficients for isentropic efficiency (-)
COP_c	Coefficient of performance for the cooling side (-)
COP_h	Coefficient of performance for the heating side (-)
$c_{p_{ref_l}}$	Specific heat capacity of liquid refrigerant (kJ kg ⁻¹ K ⁻¹)
c_{p_w}	Specific heat capacity of water (kJ kg ⁻¹ K ⁻¹)
$c_{p_{wc}}$	Specific heat capacity of water in the condenser (kJ kg ⁻¹ K ⁻¹)
$c_{p_{we}}$	Specific heat capacity of water in the evaporator (kJ kg ⁻¹ K ⁻¹)
d_h	Hydraulic diameter (m)
$F_{sc,c}$	Subcooled liquid area factor for BPHE as a condenser (-)
$F_{sp,c}$	Superheated vapor area factor for BPHE as a condenser (-)
$F_{sp,e}$	Superheated vapor area factor for BPHE as an evaporator (-)
G_{ref}	Mass flux of refrigerant for two-phase flow in BPHE (kg m ⁻² s ⁻¹)
G_w	Mass flux of water (kg m ⁻² s ⁻¹)
h	Enthalpy of refrigerant (kJ kg ⁻¹)
$h_{comp_{in}}$	Enthalpy of refrigerant at the inlet of the compressor (kJ kg ⁻¹)
$h_{comp_{out}}$	Enthalpy of the refrigerant at the outlet of the compressor (kJ kg ⁻¹)
$h_{comp_{out-isen}}$	Enthalpy at the compressor outlet during isentropic compression (kJ kg ⁻¹)
$h_{cond_{in}}$	Enthalpy of refrigerant at the inlet of the condenser (kJ kg ⁻¹)
$h_{cond_{out}}$	Enthalpy of refrigerant at the outlet of the condenser (kJ kg ⁻¹)
$h_{evap_{in}}$	Enthalpy of refrigerant at the inlet of the evaporator (kJ kg ⁻¹)
$h_{evap_{out}}$	Enthalpy of refrigerant at the outlet of the evaporator (kJ kg ⁻¹)

$h_{l,c}$	Liquid saturated enthalpy of the condenser (kJ kg ⁻¹)
$h_{v,c}$	Vapor saturated enthalpy of the condenser (kJ kg ⁻¹)
$h_{v,e}$	Vapor saturated enthalpy of the evaporator (kJ kg ⁻¹)
HTC_{cond}	Local condensation HTC during two-phase flow (W m ⁻² K ⁻¹)
HTC_{evap}	Local evaporation HTC during two-phase flow (W m ⁻² K ⁻¹)
HTC_w	Water-side heat transfer coefficient for single-phase flow (W m ⁻² K ⁻¹)
$HTC_{w,c}$	Heat transfer coefficient of water in the condenser (W m ⁻² K ⁻¹)
$HTC_{w,e}$	Heat transfer coefficient of water in the evaporator (W m ⁻² K ⁻¹)
$HTC_{sp,c}$	HTC for superheated vapor flow in the condenser (W m ⁻² K ⁻¹)
$HTC_{sp,e}$	HTC for superheated vapor flow in the evaporator (W m ⁻² K ⁻¹)
\overline{HTC}_{cond}	Average HTC of refrigerant in the condenser (W m ⁻² K ⁻¹)
\overline{HTC}_{evap}	Average HTC of refrigerant in the evaporator (W m ⁻² K ⁻¹)
\overline{HTC}_{ref}	Average heat transfer coefficient of refrigerant (W m ⁻² K ⁻¹)
i	Total number of discrete vapor quality steps
L_p	Length of plates in BPHE (m)
\dot{m}_{ref}	Mass flow rate of refrigerant (kg s ⁻¹)
\dot{m}_w	Mass flow rate of water (kg s ⁻¹)
$\dot{m}_{w,c}$	Mass flow rate of water in the condenser (kg s ⁻¹)
$\dot{m}_{w,e}$	Mass flow rate of water in the evaporator (kg s ⁻¹)
n	Total number of observations (-)
$n_{plt_{ref}}$	Number of plates on the refrigerant side (-)
n_{plt_w}	Number of plates on the water side (-)
$N_{eff-plates}$	Effective number of plates (-)
$p_{comp_{in}}$	Pressure at the compressor inlet (Pa)
$p_{comp_{out}}$	Pressure at the compressor outlet (Pa)
Pr_{ref_l}	Prandtl number of the refrigerant in the liquid phase(-)
\dot{Q}_{cond}	Heat transfer rate of the condenser (kW)
\dot{Q}_{evap}	Heat transfer rate of the evaporator (kW)
$\dot{Q}_{sc,c}$	Heat transfer rate in the subcooling region of the condenser (kW)

$\dot{Q}_{sp,c}$	Heat transfer rate in the superheated vapor region of the condenser (kW)
$\dot{Q}_{sp,e}$	Heat transfer rate in the superheated vapor region of the evaporator (kW)
$\dot{Q}_{tp,c}$	Heat transfer rate in the two-phase region of the condenser (kW)
$\dot{Q}_{tp,e}$	Heat transfer rate in the two-phase region of the evaporator (kW)
Re_{refl}	Reynolds Number of refrigerant in the liquid phase for two-phase flow (-)
T_{cond}	Temperature of condensation (°C)
$T_{cond,in}$	Temperature at the inlet of the condenser (°C)
$T_{cond,out}$	Temperature at the outlet of the condenser (°C)
T_{evap}	Temperature of evaporation (°C)
$T_{evap,out}$	Temperature at the outlet of the evaporator (°C)
T_{inwc}	Water temperature at the inlet of the condenser (°C)
T_{inwe}	Water temperature at the inlet of the evaporator (°C)
T_{mw_c}	Mean temperature of water in the condenser (°C)
T_{mw_e}	Mean temperature of water in the evaporator (°C)
T_{outwc}	Water temperature at the outlet of the condenser (°C)
T_{outwe}	Water temperature at the outlet of the evaporator (°C)
$T_{x_{wc}}$	Water temperature when refrigerant starts condensation (°C)
$T_{x_{we}}$	Water temperature when refrigerant is completely evaporated (°C)
$T_{y_{wc}}$	Water temperature when condensation process ends (°C)
U_{cond}	Overall heat transfer coefficient of the condenser ($W m^{-2}K^{-1}$)
U_{evap}	Global heat transfer coefficient of the evaporator ($W m^{-2}K^{-1}$)
V_d	Compressor's volumetric displacement (m^3s^{-1})
v_{compin}	Specific volume at the compressor inlet (m^3kg^{-1})
\dot{W}_{comp}	Energy transferred from the compressor to refrigerant (kW)
W_p	Width of the plate (m)
x_{in}	Inlet vapor quality (-)
$x_{in_{evap}}$	Inlet vapor quality in the evaporator during two-phase flow (-)
x_m	Mean vapor quality (-)

x_{out}	Outlet vapor quality (-)
y_i	Actual values (observed data) (-)
\hat{y}_i	Predicted values from the model (-)

Acronyms

BPHE	Brazed Plate Heat Exchanger (-)
CFCs	Chlorofluorocarbons (-)
<i>COP</i>	Coefficient of Performance (-)
<i>CR</i>	Compression Ratio (-)
EEV	Electronic Expansion Valve (-)
GWP	Global Warming Potential (-)
HCFCs	Hydrochlorofluorocarbons (-)
HFC	Hydrofluorocarbon (-)
HFO	HydrofluoroOlefin (-)
HPSs	Heat Pumps Systems (-)
<i>HTC</i>	Heat Transfer Coefficient ($\text{W m}^{-2}\text{K}^{-1}$).
HVAC	Heating, Ventilation, and Air Conditioning (-)
IHX	Internal Heat Exchanger (-)
ODP	Ozone Depletion Potential (-)
MPE	Mean Percentage Error for model accuracy (-).
MAPE	Mean Absolute Percentage Error for model accuracy (-)

Greek

β	Angle of the corrugation ($^{\circ}$)
Φ	Enlargement factor (-)
ΔT_{ln}	Logarithmic mean temperature difference ($^{\circ}\text{C}$)
$\Delta T_{ln-cond}$	Logarithmic mean temperature difference of the condenser ($^{\circ}\text{C}$)
$\Delta T_{ln-evap}$	Logarithmic mean temperature difference of the evaporator ($^{\circ}\text{C}$)
$\Delta T_{ln-sc,c}$	ΔT_{ln} of the condenser in the subcooling region ($^{\circ}\text{C}$)
$\Delta T_{ln-sp,c}$	ΔT_{ln} of the condenser in the superheated vapor region ($^{\circ}\text{C}$)

$\Delta T_{\text{In-sp,e}}$	ΔT_{In} of the evaporator in the superheated vapor region ($^{\circ}\text{C}$)
$\Delta T_{\text{In-tp,c}}$	ΔT_{In} of the condenser in the two-phase region ($^{\circ}\text{C}$)
$\Delta T_{\text{In-tp,e}}$	ΔT_{In} of the evaporator in the two-phase region ($^{\circ}\text{C}$)
$\mu_{\text{ref}l}$	Viscosity of refrigerant in liquid phase ($\text{kg m}^{-1}\text{s}^{-1}$)
$\lambda_{\text{ref}l}$	Thermal conductivity of liquid refrigerant ($\text{W m}^{-1}\text{K}^{-1}$)
λ_w	Thermal conductivity of water ($\text{W m}^{-1}\text{K}^{-1}$)
μ_w	Viscosity of water ($\text{kg m}^{-1}\text{s}^{-1}$)
η_{isen}	Isentropic efficiency of the compressor (-)
η_{vol}	Volumetric efficiency of the compressor (-)

Subscripts

<i>comp</i>	Compressor
<i>cond</i>	Condenser
<i>ch</i>	Channel
<i>eff</i>	Effective
<i>evap</i>	Evaporator
<i>in</i>	Inlet
<i>isen</i>	Isentropic
<i>l</i>	Liquid phase
<i>mw</i>	Mean water
<i>out</i>	Outlet
<i>plt</i>	Plate
<i>ref</i>	Refrigerant
<i>sc</i>	Subcooling
<i>sp</i>	Superheating
<i>v</i>	Vapor phase
<i>vol</i>	Volumetric
<i>w</i>	Water
w_c	Water in the condenser
w_e	Water in the evaporator

RESUMO

A transição para refrigerantes de baixo potencial de aquecimento global (GWP) é essencial para lidar com as mudanças climáticas. Este estudo avalia o desempenho energético dos refrigerantes de baixo GWP R513A e R516A como alternativas ao R134a em sistemas de bomba de calor para aplicações simultâneas de aquecimento e resfriamento. Utilizando um modelo matemático validado e dados experimentais, o estudo examina a eficiência termodinâmica (COP) de cada refrigerante sob condições operacionais variáveis, incluindo variações de temperatura e vazão no evaporador e condensador. A pesquisa examinou dois casos principais: um cenário de temperatura média (cenário 1), onde as temperaturas de entrada do evaporador da mistura de água-glicol variam de 0 a 5 °C, e as temperaturas de entrada da água do condensador variam de 35 a 40 °C, simulando aplicações como resfriamento moderado e aquecimento de água quente doméstica. O cenário de alta temperatura (cenário 2) envolve temperaturas de entrada do evaporador entre 10 e 15 °C e temperaturas de entrada da água do condensador de 50 a 55 °C, representando condições adequadas para recuperação de calor residual e aplicações de aquecimento de processos industriais. Embora essas temperaturas se sobreponham a outras tecnologias, como coletores solares de tubo evacuado, sua integração em sistemas de bomba de calor ressalta a versatilidade e a escalabilidade desses sistemas para diversas demandas de energia. Em ambos os cenários, a vazão mássica de água foi ajustada entre 0,05 e 0,15 kg/s no evaporador e no condensador. Os resultados indicam que o R513A e o R516A alcançaram desempenho comparável ao R134a, com o R516A demonstrando um COP ligeiramente maior sob condições de alta temperatura. Para os três fluidos, o COP médio no modo de resfriamento (COP_c) foi de 3,3, e no modo de aquecimento (COP_h), foi de 4,6 nas condições testadas. Essas descobertas destacam o potencial de R513A e R516A como substitutos eficazes para refrigerantes de alto potencial de aquecimento global, apoiando a transição para tecnologias de refrigerantes sustentáveis.

Palavras-chave: Refrigerante de baixo GWP, BPHE, bomba de calor, aquecimento e resfriamento simultâneos, R513A, R516A, substitutos do R134a.

ABSTRACT

The transition to low global warming potential (GWP) refrigerants is essential in addressing climate change. This study evaluates the energy performance of low-GWP refrigerants R513A and R516A as alternatives to R134a in heat pump systems for simultaneous heating and cooling applications. Utilizing a validated mathematical model and experimental data, the study examines the thermodynamic efficiency (COP) of each refrigerant under varying operational conditions, including temperature and flow rate variations in the evaporator and condenser. The research examined two primary cases: a medium-temperature scenario (scenario 1), where the evaporator inlet temperatures of the water-glycol mixture range from 0 to 5°C, and condenser water inlet temperatures range from 35 to 40°C, simulating applications such as moderate cooling and domestic hot water heating. The high-temperature scenario (scenario 2) involves evaporator inlet temperatures between 10 to 15°C and condenser water inlet temperatures from 50 to 55°C, representing conditions suitable for waste heat recovery and industrial process heating applications. Although these temperatures overlap with other technologies like evacuated-tube solar collectors, their integration into heat pump systems underscores the versatility and scalability of these systems for diverse energy demands. In both scenarios, the mass flow rate of water was adjusted between 0.05 and 0.15 kg/s in the evaporator and condenser. The results indicate that R513A and R516A achieved comparable performance to R134a, with R516A demonstrating a slightly higher COP under high-temperature conditions. For the three fluids, the average COP in cooling mode (COP_c) was 3.3, and in heating mode (COP_h), it was 4.6 across the tested conditions. These findings highlight the potential of R513A and R516A as effective replacements for high-GWP refrigerants, supporting the transition to sustainable refrigerant technologies.

Keywords: Low-GWP refrigerant, BPHE, heat pump, simultaneous heating and cooling, R513A, R516A., R134a replacement.

1. INTRODUCTION

1.1. Background and motivation

In recent years, global leaders have been collaborating to tackle the effects of global warming. One of the key areas of focus is addressing the impact of refrigeration systems, particularly those using refrigerants with high global warming potential (GWP) (Liu et al. 2021);(Bobbo et al. 2024). These traditional refrigerants have been identified as significant contributors to greenhouse gas emissions and ozone depletion (UNEP, 2020). As a result, there have been international efforts to phase out these high-GWP refrigerants and transition to alternatives that have a lower environmental impact. Consequently, the Heating, Ventilation, and Air Conditioning (HVAC) industry faces the challenge of developing innovative and eco-friendly refrigeration systems that can meet the demands of cooling and heating applications while minimizing their adverse effects on the environment (UNEP, 2014).

The chlorine compound in chlorofluorocarbons (CFCs) and hydrochlorofluorocarbons (HCFCs) damage the Earth's ozone layer and contributes to global warming by trapping additional heat in the atmosphere (UNITED NATIONS, 2016). According to Vuppaladadiyam et al. (2022), an ideal refrigerant should exhibit characteristics such as low global warming potential (GWP), non-toxicity, non-flammability, zero-ozone depletion potential (ODP), and excellent thermodynamic and thermophysical properties. High-GWP gases are gradually being phased out, with the GWP of a refrigerant measured relative to the heat-trapping capability of carbon dioxide (CO₂), which is assigned a GWP value of 1, over a standard time period, typically 100 years (Vaccaro et al. 2024). CO₂ offers several advantages, such as non-toxic, non-flammable, affordable, and widely available, but its high critical pressure and low critical temperature often necessitate less efficient transcritical operation. Various cycle modifications improve trans-critical CO₂ COP to match or exceed HFC systems (Toffoletti et al. 2025).

HydroFluoroOlefins (HFOs) such as R1234yf, and mixtures like R513A and R516A, have emerged as low-GWP refrigerants and are increasingly considered viable alternatives to R134a. R134a is widely used in refrigeration and air conditioning applications due to its favorable thermodynamic properties, but its high global warming potential (GWP=1300) makes it a target

for replacement in favor of more environmentally friendly alternatives. Several studies have already explored these refrigerants in different types of conventional refrigeration systems. Several studies have already explored these refrigerants in different types of conventional refrigeration systems.

Beyond the environmental impact of refrigerants, increasing energy efficiency in HVAC system is also a critical global demand. Simultaneous heating and cooling systems represent a dynamic approach to optimizing energy usage in HVAC applications. These systems are designed to harness waste heat from cooling processes and redirect it for heating purposes, thereby improving overall energy efficiency. In conventional cooling cycles, waste heat is often released into the surrounding environment, but simultaneous heating and cooling systems capture and utilize this waste heat for space heating, ventilation, and domestic hot water preparation. This recovery process helps reduce the need for supplementary energy sources (Girip; Ilie; Calota, 2023).

This study focuses on analyzing the performance of low-GWP refrigerants R513A and R516A through energy simulations of water-to-water refrigeration systems operating under conditions of simultaneous cooling and heating. This research aligns with global sustainability goals, such as those outlined in the Kigali Amendment to the Montreal Protocol goals (UNEP, 2020), and aims to contribute to the development of innovative refrigeration systems that reduce carbon emissions and enhance energy efficiency.

1.2. Research objectives

The main objective compares the energy performance of low-GWP refrigerants R513A and R516A as alternatives for R134a in refrigeration systems for simultaneous heating and cooling water using a mathematical model validated with experimental data.

Specific objectives are:

- To model the refrigeration system, including critical components such as the evaporator, compressor, condenser, and expansion device, with emphasis on accurately representing the thermodynamic and heat transfer characteristics of these components.

- To validate the mathematical model using experimental data obtained by evaluating the performance of R134a, R513A, and R516A, ensuring the accuracy and reliability of the model against real-world operating conditions.
- To evaluate the energy performance of each refrigerant within the modeled refrigeration system under two specific scenarios: (1) a medium-temperature chiller with waste heat recovery for heating space, and (2) a cooling space with waste heat recovery for residential hot water heating.

1.3. Structure of the work

Chapter 1, the Introduction, sets the stage by introducing the research topic, background, motivation, objectives, scope, and structure of the work. This chapter aims to provide the readers with a clear understanding of the context and purpose of the study.

Chapter 2, the Theoretical and literature Review, delves into the existing body of knowledge relevant to low-GWP refrigerants and simultaneous heating and cooling systems. This chapter draws upon academic research literature to identify gaps that the current study aims to address.

Chapter 3, The methodology chapter explains the mathematical model, detailing the equations used for each component and describing how these components are interconnected. It also presents the flowchart for solving the model, along with the input requirements and minimum parameters needed to utilize the model. Additionally, the chapter provides background information on the experimental data used for validating the model, as well as the expected outcomes from the simulations.

Chapter 4, Results and discussion, presents the findings obtained from the experimentation and modeling efforts. The thermodynamic analysis of the refrigerants, performance comparison, and energy efficiency assessment are discussed in this chapter. The results are then contextualized and analyzed in relation to the research objectives.

Chapter 5, Conclusion and future work, summarizes the key findings, implications, and contributions of the research study. It revisits the research objectives and highlights the value of the study outcomes in addressing environmental concerns and advancing HVAC technology. Additionally, this chapter suggests areas for future research and exploration.

2. THEORETICAL AND LITERATURE REVIEW

2.1. Heat pumps for simultaneous heating and cooling

There are numerous situations where simultaneous heating and cooling demands coexist (Byrne, 2022b):

- Space heating and cooling of highly glazed buildings.
- Server room cooling and space heating in office buildings.
- Space cooling and domestic hot water production in hotels.
- Space cooling and desalination in coastal regions.
- Ice rink cooling and swimming pool heating within the same complex.
- Heat recovery in refrigeration systems within the agro-food industry.

In the context of climate change and resource scarcity, the hybridization of systems has emerging as a key solution to reduce energy consumption. Heat pumps for simultaneous heating and cooling (HPSs) are considered multi-energy systems, and heat recovery in refrigeration systems is gaining traction. HPSs can serve multiple buildings with varying thermal demands, increasing the need for simultaneous production. This requires collective supply systems with individualized billing processes. However, HPSs are inherently more complex, which has limited their widespread adoption. This complexity arises from the need to connect and control additional components. All HPSs feature automatic control systems that manage various operating modes, as well as the temperature and flow rates of source fluids. Common balancing sources include outdoor air, geothermal wells, water loops, or gray water. Further optimization of refrigeration cycles, refrigerants, circuit architectures, and technological components is necessary to continue promoting and advancing the adoption of these efficient hybrid systems (Byrne, 2022a). The following subsections explain the theoretical concepts used in heat pumps, with a focus on the vapor compression cycle.

2.1.1. Vapor-compression cycle overview

The vapor-compression cycle operates by transferring heat from a lower temperature area to a higher temperature area, using a refrigerant as the working fluid. This cycle involves four main components: a compressor, a condenser, an expansion valve, and an evaporator (Figure 1). The process follows a series of thermodynamic processes for an ideal vapor compression cycle and the state changes of the refrigerant:

State 1 – 2

- Work is provided by the compressor, usually driven by an electrical motor.
- The refrigerant, in its saturated vapor state, is compressed and becomes a superheated, high-pressure gas.

State 2 - 3

- The condenser releases heat to the environment at constant pressure, typically using air or water as the heat sink.
- The superheated refrigerant gas cools and condenses, transitioning to a saturated liquid at constant pressure.

State 3 - 4

- The refrigerant is throttled to the evaporation pressure using an expansion valve or another device.
- As a result, the refrigerant drops to a much lower temperature.

State 4 - 1

- The evaporator absorbs heat from the load (refrigerated space or fluid stream) at a constant pressure.
- The low-pressure, saturated refrigerant liquid evaporates, transitioning into a saturated refrigerant gas at constant pressure.

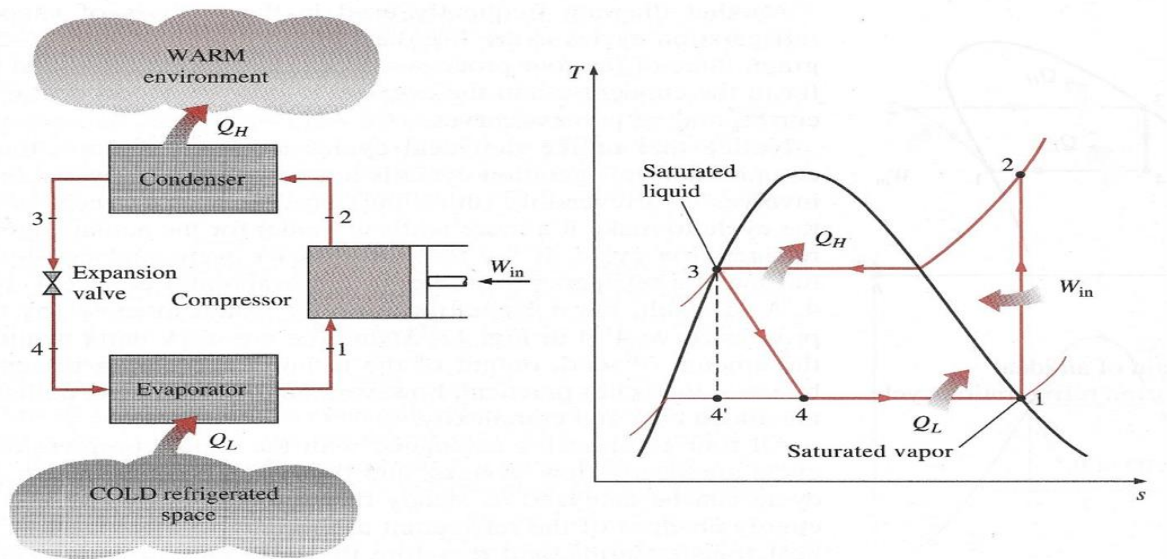


Figure 1: Vapor-compression cycle of heat pump (Incropera, 1996).

2.1.2. Heat pump overview

Heat pumps are designed with the ability to either heat or cool the refrigerant vapor compression cycle.

- The cooling mode: it focuses on removing heat from a space (e.g., split air conditioning, refrigerators, or cold storage room) or from water (e.g., chiller, ice makers) using the evaporator. The condenser, on the other hand, typically exchanges heat with the environment either directly or indirectly (see Figure 2).

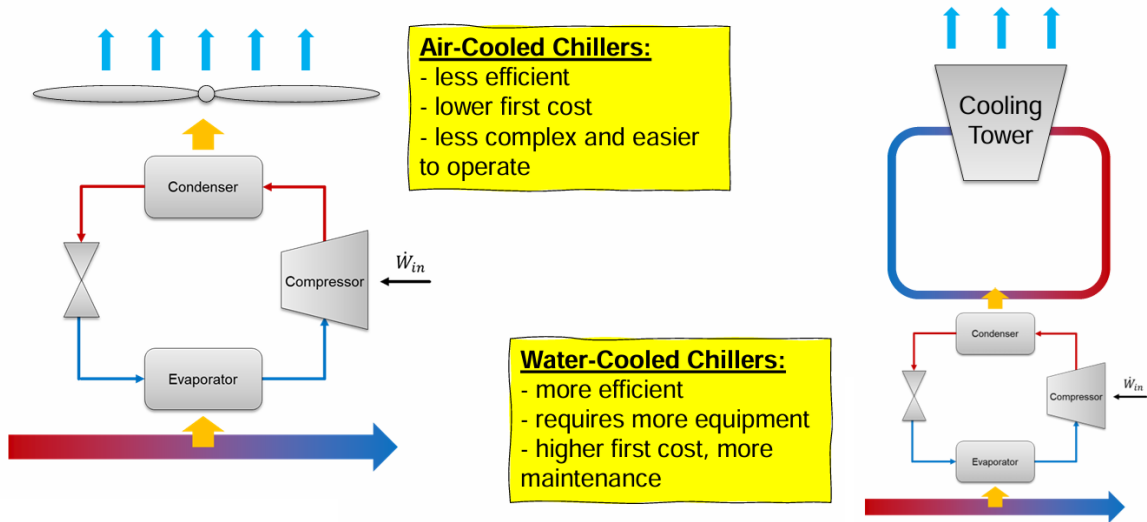


Figure 2: Air-cooled and water-cooled systems for condenser.

- Heating mode: The primary objective of the heating mode in a heat pump is to transfer heat to air or water for residential or industrial applications. This technology often competes with traditional electric heaters and gas boilers. While heat pumps may have a higher initial cost compared to these alternatives, they are significantly more energy-efficient, offering long-term savings and reduced environmental impact. The heat source for heat pumps can be air, ground, lake, or solar, as shown in Figure 3.

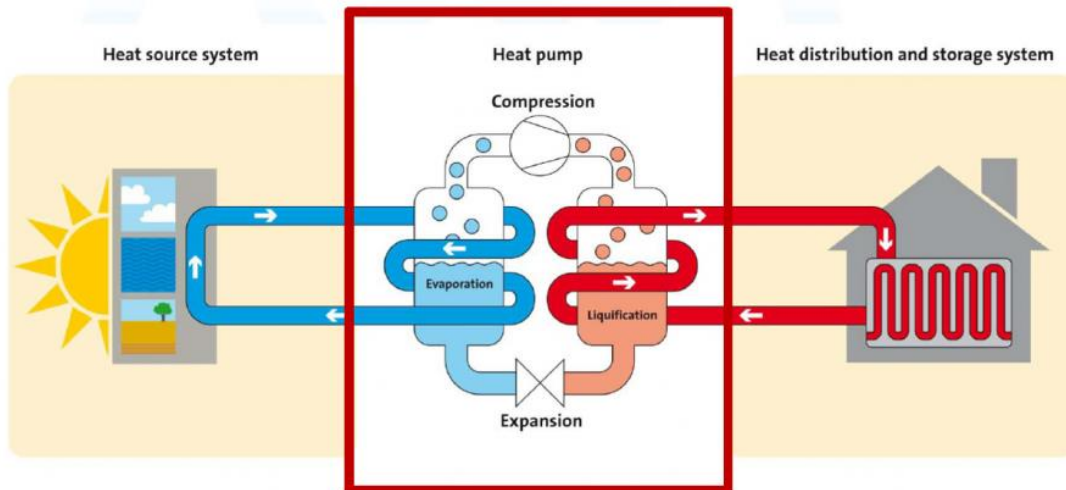


Figure 3: Different energy sources for heat pumps in heating mode (EHPA, 2019).

- Reversible mode: They are versatile systems capable of providing both heating and cooling functions, making them an efficient solution for maintaining comfortable indoor temperatures year-round. Unlike conventional heat pumps that operate in one mode, reversible heat pumps can switch between heating and cooling modes, allowing them to adapt to seasonal changes in temperature. Figure 4 shows that the vapor compression cycle remains consistent; however, the key difference lies in the use of a reversing valve. This valve allows the heat exchanger to alternate between functioning as an evaporator and as a condenser, depending on the operational mode.

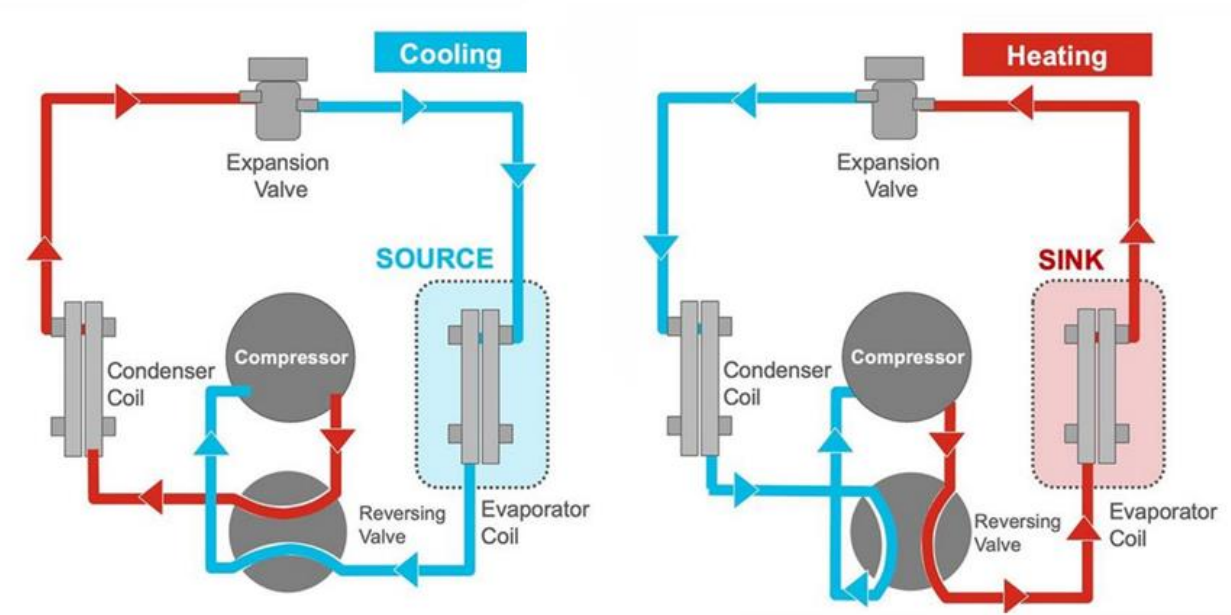


Figure 4: Heat pump in reversible mode (heating and cooling) (Trane, 2022).

- Simultaneous mode: By using both heating and cooling simultaneously (see Figure 5), these systems maximize energy use and can lead to significant savings on energy bills. They reduce the need for separate heating and cooling systems, which can be less efficient.

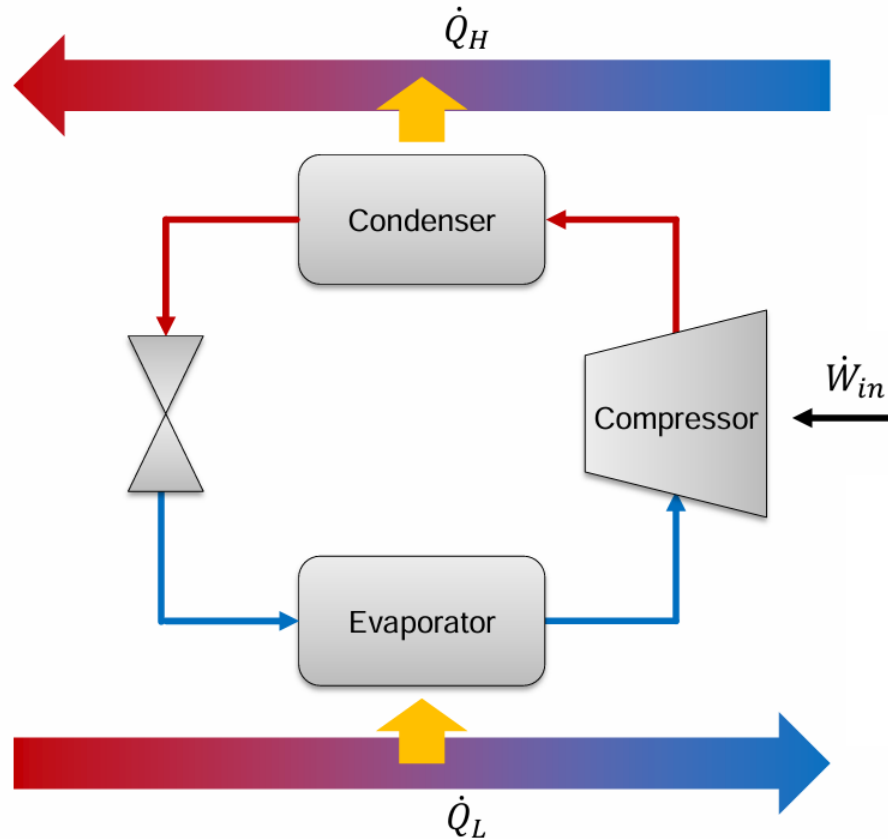


Figure 5: Heat pump configuration for simultaneous heating and cooling.

2.1.3. Applications of heat pump for simultaneous heating and cooling

Previously, some applications of heat pump for simultaneous heating and cooling (HPSs) were mentioned. In this subsection, two cases will be detailed, which will be studied for the fluids R134a, R513A, and R516A. It is important to remember that the use of HPSs is more suitable for situations where there is a balance between the demand for heat and the demand for cooling. These systems operate more efficiently when heating and cooling needs occur simultaneously, allowing for the maximum utilization of recovered heat in the cooling process, and vice versa. When this balance is absent, the performance of the HPS may be less efficient, making it less viable for applications where the demand for one type of energy (cooling or heating) greatly exceeds the other (Dubey et al. 2024).

- **Cooling water and heating space:** This case applies to situations where the ambient temperature ranges between 10°C and 20°C, commonly observed in cooler climates or during transitional seasons (e.g., spring and fall). The cooling demand involves generating cold water at temperatures between 0°C and 5°C, suitable for industrial and commercial applications requiring precise temperature control; achievable through advanced control systems. For example, it is essential in cold storage to maintain low temperatures for perishable goods like fruits, vegetables and certain medical drugs like vaccines. It is also important in precision cooling, for facilities like data centers where server room require strict temperature control to ensure optimal equipment operation. Simultaneously, the system produces hot water in the range of 35°C to 40°C to space heating. In colder climates or regions with mixed seasons, such as Northern Europe, HPSs can support dual operations in small apartment buildings or commercial spaces like offices.
- **Cooling space and producing hot water:** In regions like in tropical or subtropical climates, with ambient temperature ranges between 20°C and 30°C, air conditioning systems are necessary to cool indoor spaces, with water temperatures on the cooling side typically between 10°C and 15°C, applicable in large buildings and residential air conditioning. While the provided cases focus on temperatures up to 30°C, HPSs can also be used in hotter climates where temperatures exceed 30°C e.g. plastic molding or chemical processing, desalination plants, tropical agriculture etc. Simultaneously, hot water is generated at temperatures of 50°C to 55°C, primarily for residential uses such as showering, dishwashing, or laundry. In regions like Southeast Asia or Southern Europe, HPSs can simultaneously provide cooling for living spaces and hot water for household use, ensuring energy savings.

2.2. Theoretical concepts of heat exchanger:

2.2.1. Evaporator

The overall energy balance of the evaporator is given by:

$$\dot{Q}_{evap} = U_{evap} A_{evap} \Delta T_{ln-evap} \quad (1)$$

where U_{evap} and A_{evap} represent the overall heat transfer coefficient and heat transfer area of the evaporator, respectively. The evaporator consists of two distinct regions: the two-phase region (where the refrigerant is undergoing phase change) and the superheating region (where the refrigerant transitions into superheated vapor). Each of these regions has its own heat transfer characteristics, leading to different values of the overall heat transfer coefficient, denoted as $U_{tp,e}$ for the two-phase region and $U_{sp,e}$ for the superheating region (more details see section 3.2.3).

The logarithmic mean temperature difference of the evaporator, $\Delta T_{ln-evap}$, is therefore calculated by dividing the evaporator into two parts: the evaporation part and the superheating part (Fernando et al. 2004). Figure 6 illustrates the temperature profile in the evaporator.

$$\Delta T_{ln-evap} = \frac{\dot{Q}_{evap}}{\frac{\dot{Q}_{sp,e}}{\Delta T_{ln-sp,e}} + \frac{\dot{Q}_{tp,e}}{\Delta T_{ln-tp,e}}} \quad (2)$$

where the subscripts "sp" and "tp" denotes the superheated vapor and two-phase regions, respectively.

The heat transfer from water to refrigerant in the different regions is calculated as follows:

$$\dot{Q}_{tp,e} = \dot{m}_{ref}(h_{v,e} - h_{evap,in}) = \dot{m}_{w_e} c_{p_{w_e}} (T_{x_{w_e}} - T_{out_{w_e}}) \quad (3)$$

$$\dot{Q}_{sp,e} = \dot{m}_{ref}(h_{evap,out} - h_{v,e}) = \dot{m}_{w_e} c_{p_{w_e}} (T_{in_{w_e}} - T_{x_{w_e}}) \quad (4)$$

where \dot{m}_{ref} is the mass flow rate of refrigerant. $h_{evap,in}$ and $h_{evap,out}$ are the enthalpies of the refrigerant at the inlet and outlet of the evaporator, respectively, while $h_{v,e}$ is the saturated vapor

enthalpy. \dot{m}_{w_e} and $c_{p_{w_e}}$ are the mass flow rate and specific heat capacity of the water side. $T_{out_{w_e}}$ and $T_{in_{w_e}}$ are the water temperatures at the outlet and inlet of the evaporator, and $T_{x_{w_e}}$ is the water temperature when refrigerant is completely evaporated.

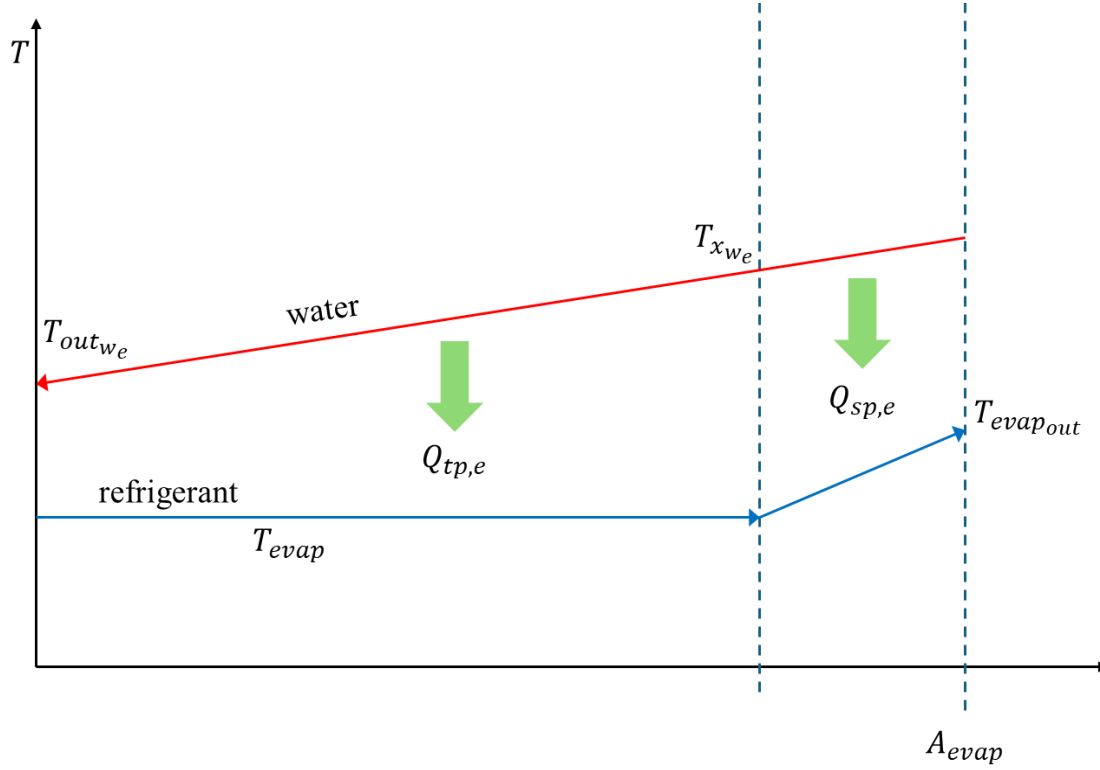


Figure 6: Temperature profile in the evaporator.

The logarithmic mean temperature difference for the two regions (the superheated vapor, $\Delta T_{ln-sp,e}$, and the two-phase region, $\Delta T_{ln-tp,e}$) are calculated as follows:

$$\Delta T_{ln-sp,e} = \frac{(T_{in_{w_e}} - T_{evap_{out}}) - (T_{x_{w_e}} - T_{evap})}{\ln \frac{(T_{in_{w_e}} - T_{evap_{out}})}{(T_{x_{w_e}} - T_{evap})}} \quad (5)$$

$$\Delta T_{\ln-tp,e} = \frac{(T_{x_{we}} - T_{out_{we}})}{\ln \frac{(T_{x_{we}} - T_{evap})}{(T_{out_{we}} - T_{evap})}} \quad (6)$$

In brazed plate heat exchangers operating as evaporator, typically 20% of the area is used for a superheating degree of 5K. Thus, the area superheated vapor factor can be defined as $F_{sp,e} = 0.2$ (Li; Hrnjak, 2021).

2.2.2. Condenser

The overall energy balance of the condenser is given by:

$$\dot{Q}_{cond} = U_{cond} A_{cond} \Delta T_{\ln-cond} \quad (7)$$

where U_{cond} and A_{cond} are the overall heat transfer coefficient and heat transfer area of the condenser, respectively. The logarithmic mean temperature difference of the condenser, $\Delta T_{\ln-cond}$ is calculated by dividing the condenser into three regions: the superheating region, the condensing region and the subcooling region (Fernando et al. 2004). Figure 7 shows the temperature profile of the condenser.

$$\Delta T_{\ln-cond} = \frac{\dot{Q}_{cond}}{\frac{\dot{Q}_{sp,c}}{\Delta T_{\ln-sp,c}} + \frac{\dot{Q}_{tp,c}}{\Delta T_{\ln-tp,c}} + \frac{\dot{Q}_{sc,c}}{\Delta T_{\ln-sc,c}}} \quad (8)$$

where the subscript "sc" refers to the subcooling region.

The heat transfer from water to refrigerant in the different regions is calculated as follows:

$$\dot{Q}_{sp,c} = \dot{m}_{ref}(h_{condin} - h_{v,c}) = \dot{m}_{w_c} c_{p_{w_c}} (T_{out_{w_c}} - T_{x_{w_c}}) \quad (9)$$

$$\dot{Q}_{tp,c} = \dot{m}_{ref}(h_{v,c} - h_{l,c}) = \dot{m}_{w_c} c_{p_{w_c}} (T_{x_{w_c}} - T_{y_{w_c}}) \quad (10)$$

$$\dot{Q}_{sc,c} = \dot{m}_{ref}(h_{l,c} - h_{cond_{out}}) = \dot{m}_{w_c} c_{p_{w_c}} (T_{y_{w_c}} - T_{in_{w_c}}) \quad (11)$$

where $h_{cond_{in}}$ and $h_{cond_{out}}$ are the enthalpies of refrigerant at the inlet and outlet of the condenser. $h_{v,c}$ and $h_{l,c}$ represent the vapor and liquid saturated enthalpies, respectively. Additionally, \dot{m}_{w_c} and $c_{p_{w_c}}$ denotes the mass flow rate and specific heat capacity of the water side. $T_{out_{w_c}}$ and $T_{in_{w_c}}$ are the water temperature at the outlet and inlet of the condenser. $T_{x_{w_c}}$ is the temperature of the water when the refrigerant starts to condense, and $T_{y_{w_c}}$ is the water temperature when condensation process ends.

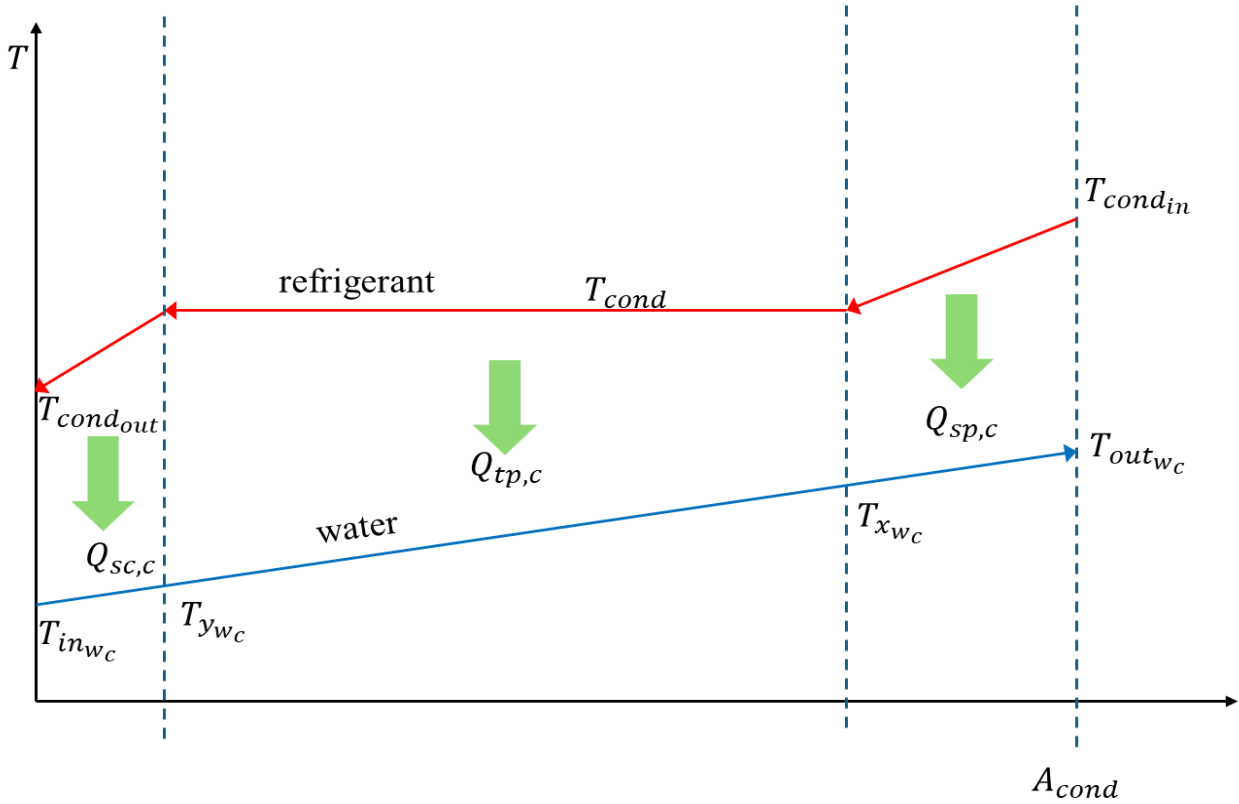


Figure 7: Temperature profile in the condenser.

The logarithmic mean temperature difference for the three regions in the condenser can be expressed as follows:

$$\Delta T_{\ln-sp,c} = \frac{(T_{cond_{in}} - T_{out_{wc}}) - (T_{cond} - T_{x_{wc}})}{\ln \frac{(T_{cond_{in}} - T_{out_{wc}})}{(T_{cond} - T_{x_{wc}})}} \quad (12)$$

$$\Delta T_{\ln-tp,c} = \frac{(T_{y_{wc}} - T_{x_{wc}})}{\ln \frac{(T_{cond} - T_{x_{wc}})}{(T_{cond} - T_{y_{wc}})}} \quad (13)$$

$$\Delta T_{\ln-sp,c} = \frac{(T_{cond} - T_{y_{wc}}) - (T_{cond_{out}} - T_{in_{wc}})}{\ln \frac{(T_{cond} - T_{y_{wc}})}{(T_{cond_{out}} - T_{in_{wc}})}} \quad (14)$$

For brazed plate heat exchangers working as condensers, approximately 34% of the area is typically dedicated for de-superheating vapor, while around 3% is allocated for achieving a 5K degree of subcooling. Consequently, the area factors for the superheating and subcooling regions are defined as: $F_{sp,c} = 0.34$ and $F_{sc,c} = 0.03$ (Sarraf; Launay; Tadrist, 2016).

2.3. Low-GWP refrigerants and their properties

Climate change has elicited significant concern worldwide, leading to research efforts aimed at developing an eco-friendly refrigerant with low global warming potential. This is in a bid to mitigate the adverse effects of refrigerants utilized in cooling and heating systems. Human emissions of greenhouse gases are responsible for climate change, with hydrofluorocarbon refrigerants and Vapor compression systems used in cooling systems being the primary culprits (Yildiz; Yildirim, 2021). Conventional refrigerants had to be replaced with energy-efficient and environmentally friendly alternatives to meet global environmental targets (Padmavathy et al. 2021).

One key example is the phase-out of R134a due to its high GWP of 1300 kg-CO₂-eq, which significantly exceeds the maximum limit of 750 kg-CO₂-eq set by global regulatory frameworks,

such as the European Union’s F-Gas Regulation (Regulation (EU) No 517/2014). This phase-out, set for completion by 2025, necessitates finding a substitute refrigerant with comparable thermodynamic properties but a much lower GWP (Islam et al. 2023).

HydrofluoroOlefins (HFOs) have emerged as highly promising contenders for replacing high-GWP refrigerants, owing to their minimal environmental impact. HFOs are marked by unsaturated carbon-carbon double bonds, which account for their low GWP values and short atmospheric lifetimes. For instance, R1234yf or HFO-1234yf has gained considerable attention as a direct replacement for R134a due to its GWP of less than 1—drastically lower than R134a’s GWP of 1300 (Chavhan; Poonawala; Gawande, 2019) (Kersey, 2022) (Direk; Soyly, 2018). However, R1234yf’s limitations includes having some economical and commercial problems due to the fact that R1234yf is a synthetic fluid with high cost. R1234yf is not recommended as an alternative for air conditioner systems working with R410A; and has compatibility challenges with certain system components, which require additional safety measures and design adaptations (Pabon et al. 2020).

Other HFO-based blends, such as R513A and R516A, offer additional alternatives with favorable thermodynamic properties and lower GWPs. R513A, a blend of R134a and R1234yf, has a GWP of approximately 573 and demonstrates balanced performance in heating and cooling applications. On the contrary, R516A is a ternary blend of R1234yf, R152a, and R134a, resulting in a GWP below 200, making it one of the lowest-GWP options available for such systems. Kim et al. (2021), in their study, presented the properties of R134a, R513A, and R516A as outlined in Table 1.

Table 1: Properties of R134a, R513A, and R516A (Kim et al. 2021); (*Li 2021).

REFRIGERANTS	R134a	R513A	R516A
Group	HFC	HFC/HFO	HFC/HFO
*Composition (mass %)	Pure	R1234yf/R134a (56.0/44.0)	R1234yf/R152a/R134a (77.5/14.0/8.5)
GWP _{100year} (AR5)	1300	573	131
ASHRAE 34 Safety Classification	A1	A1	A2L
Molecular Mass (g/mol)	102.0	108.4	102.6
*Critical Temperature (°C)	101.1	96.5	96.8
*Critical Pressure (kPa)	4056	3766	3615

Normal Boiling Point ($^{\circ}\text{C}$)	-26.3	-29.6	-29.6
Glide (K)	0	0	0
Vapor Density (kg/m^3) at 25°C	32.4	37.6	34.5
Liquid Density (kg/m^3) at 25°C	1207	1134	1069
Vapor Pressure (kPa) at 25°C	665.4	713.5	692.5
* Vapor viscosity ($\mu\text{Pa s}$) at 25°C	11.693	11.626	11.416
*Liquid viscosity ($\mu\text{Pa s}$) at 25°C	194.89	166.00	164.01
*Liquid therm. cond. ($\text{mW}/\text{m}\cdot\text{K}$) at 25°C	81.134	69.931	70.092
*Vapor therm. cond. ($\text{mW}/\text{m}\cdot\text{K}$) at 25°C	13.825	14.032	14.380
*Latent heat at boiling point Δh_{LV} (kJ/kg)	216.98	194.48	202.77
*Latent heat (kJ/kg) at 25°C	177.79	156.35	64.01
*Liquid C_p (kJ/kgK) at 25°C	1.4246	1.4117	1.4563
*Vapor C_p (kJ/kgK) at 25°C	1.0316	1.0565	1.0890

The potential replacements for R134a present a series of trade-offs regarding flammability, GWP, efficiency, and volumetric capacity. Of the two fluids possessing an ultra-low GWP, R1234ze(E) exhibits a low volumetric capacity but is more appealing than R1234yf due to its superior efficiency. R516A and R513A demonstrate comparable efficiency and volumetric capacity, while also presenting a trade-off between flammability and coefficient of performance (COP). In general, the non-flammable R513A represents a viable interim option, whereas R516A may be considered as a long-term solution (Domanski; Yana Motta, 2021).

2.4. Previous studies and research gaps

Several low-GWP refrigerants have been proposed as potential substitutes for R134a, including R1234yf, R516A, R513A, R32, R450A, R1234ze(E), R1270, R744 (CO_2), R290 (propane), and R600a (isobutane)(Aissani; Zid; Bencharif, 2024). Researchers have been actively exploring these options to identify the most effective and sustainable replacements for various applications.

Schultz; Kujak; Majurin, (2015) presented a comprehensive assessment of R513A, as a potential substitute for R134a. The study highlighted the environmental and safety benefits of R513A, such as its negligible impact on stratospheric ozone, 56% lower global warming potential

than R134a, absence of significant secondary environmental effects, low toxicity, and non-flammability.

Mota-Babiloni et al. (2018) found that R513A had slightly higher exergy efficiency than R134a, despite greater exergy destruction, at evaporating temperatures between $-15\text{ }^{\circ}\text{C}$ and $5\text{ }^{\circ}\text{C}$ and condensing temperatures of $30\text{ }^{\circ}\text{C}$ and $35\text{ }^{\circ}\text{C}$. The system maximum global efficiency was influenced by lower cooling water temperatures, particularly for R513A. The compressor caused the highest irreversibility and lowest exergy efficiency due to rotary parts and ambient losses. The condenser and expansion valve had the highest exergy efficiency, while the evaporator had intermediate values. The average global exergy efficiency of R513A was 0.4% higher than R134a, and the compact design of the plate heat exchanger reduced the exergy destruction rate of the water-cooled condenser. R513A could be used in R134a refrigeration systems without redesign, but the rotary compressor should be replaced with a technology capable of efficiently operating with small cooling capacities.

In a comparative experimental study conducted by Yang et al. (2019), R134a and its low-GWP alternative, the R1234yf/R134a mixture (R513A, 44/56% weight), were tested in a domestic refrigerator under identical ambient conditions. The study performed three types of tests, revealing that the optimal charge for R513A was 80 g, 5.9% lower than R134a's 85 g. R513A demonstrated a 21% reduction in pull-down time compared to R134a and a 3.5% reduction in 24-hour energy consumption. During the freezing test, R513A saved 43.2 minutes compared to the baseline test, indicating that the freezing capacity of R513A was superior to that of R134a. Furthermore, R513A (at 80g charge) exhibited similar behavior to the baseline test, with the discharge temperature and compressor pressure ratio of R513A being lower than those of R134a.

Mota-Babiloni et al. (2019) carried out an experiment to investigate the impact of an Internal Heat Exchanger (IHX) on the performance of a vapor compression system using R513A and R134a. The results showed that the cooling capacity of the system increased by 5.6% for R513A and 3% for R134a. Additionally, the coefficient of performance (COP) increased by 8% for R513A and 4% for R134a, with minimal power consumption reduction. The authors recommend the use of a high-effectiveness IHX for R513A, particularly for high compression ratio operations, as long as the discharge temperature remains below critical values.

Kumar et al. (2024) conducted an experimental study comparing the thermal performance of a heat pump condenser using R22 and R134a refrigerants. Heat pumps, recognized for their

potential to reduce global warming emissions, require advancements in condenser design and environmentally friendly refrigerants for higher efficiency. Their study standardized a heat pump and analyzed refrigerants for water heating, evaluating COP, heat transfer rate, and Log Mean Temperature Difference (LMTD). Results showed R134a outperformed R22 in efficiency, indicating that using optimized refrigerants can significantly enhance energy savings in heat pump systems.

You, (2024) study introduces "You's Principle," which determines the optimal ratio of temperature differences for heat transfer in refrigeration and heat pump systems. The principle is derived from second-law (entropy or exergy) analysis, optimizing the ratio based on the temperatures of the low-temperature heat source (evaporator) and the high-temperature heat sink (condenser). This method provides a scientific alternative to traditional "rule-of-thumb" design approaches, enhancing system efficiency and performance.

Zhang et al. (2020) conducted theoretical and experimental research on the performance of twin-screw compressors using R513A as a replacement for R134a. The study revealed that the differences in volumetric efficiency and adiabatic efficiency between the two refrigerants were negligible and acceptable. Moreover, the coefficient of performance (COP) of R513A was only slightly lower than that of R134a. Therefore, considering the cost of equipment replacement and global warming potential (GWP), R513A can be a direct substitute for R134a in twin screw compressors.

The study conducted by Li (2021) utilized a thermodynamic process model, component sizing methodology, and life cycle environmental performance methodology to assess various refrigerants as substitutes for R134a. The performance evaluation was for a two-stage centrifugal chiller application with a fixed cooling capacity of 1.750 kW. R515A, R515B, and R1234ze(E) exhibited a 25% decrease in volume capacity due to low suction density, while R134a alternatives necessitated an increased component heat transfer area, with a 5-15% increase for the evaporator and 12-38% for the condenser. Despite R516A requiring adherence to vessel safety codes, R513A, R513B, and R516A are preferable drop-in options for R134a with less component modification, while R515A, R515B, and R1234ze(E) necessitated a compressor size that was more than 18% larger. R134a alternatives can result in significant life cycle emission reductions. However, the poor heat transfer performance and high cost of R1234yf may hinder its use in chillers. The

findings provide valuable insights for stakeholders regarding sustainable and economically feasible refrigerant options.

Blanco Ojeda et al. (2022b) demonstrated that alternative refrigerants have the potential to replace R134a in cascade refrigeration systems. The results indicated that R436A exhibited an average increase in the COP coefficient of performance by 3.1%, while R1234yf and R513A showed a reduction of 3.7% and 4.4%, respectively. The environmental impact analysis was conducted for two scenarios: Chicago (USA) and Curitiba (Brazil). The study found that the total TEWI values for R436A, R1234yf, and R513A were reduced by 46%, 42.1%, and 22.5%, respectively, compared to the originally designed R134a system for the Curitiba scenario. However, for the Chicago scenario, the values increased by 0.3%, 2.4%, and 5.8%, respectively.

Al-Sayyab et al. (2022) presented a comprehensive experimental evaluation of R1234yf-based low GWP working fluids for refrigeration and heat pumps. They discovered that R513A presents the highest overall system performance, with an enhancement of 2% in cooling mode. In the cooling mode, R516A exhibited a system coefficient of performance (COP) improvement at low evaporating temperatures within the range of 1% to 15%. On the other hand, R1234yf demonstrated the highest mass flow rate in cooling mode, surpassing R134a by 33% to 61%. Additionally, R1234yf displayed the highest normalized total equivalent warming impact (TEWI) reduction in both modes, with a 58% reduction in the heating mode and a 93% reduction in the cooling mode. In contrast, R516A exhibited a lower decrease than R513A in the heating mode.

Belman-Flores et al. (2022) presented the performance of a domestic refrigerator using the R513A refrigerant as a direct replacement for R134a. The optimal charge was defined for R513A concerning the minimum energy consumption, which was 100 g, representing a reduction of 16.7% compared to R134a (120 g). For a test period of 24 h, R513A showed a 9% reduction in energy consumption compared to R134a. Finally, the analysis of the total equivalent warming impact presented R513A as a fluid with a lesser impact, around 8.85%, relative to R134a.

In a recent study conducted by Conte et al. (2023), large scroll compressors were experimentally investigated using six low-GWP refrigerants. The results indicated that R516A and R513A exhibited higher cooling capacities than R134a under the same working conditions. However, the study also revealed that only R516A and R513A were capable of achieving higher cooling values than R134a, with average increases of 3.0% and 4.4%, respectively. It is noteworthy that R516A is classified as A2L, while R513A has a GWP of 673.

Méndez-Méndez; Pérez-García; Morales-Fuentes, (2023) conducted an experimental energy evaluation of R516A and R513A as replacement for R134a in refrigeration and air conditioning modes. They concluded that R516A can serve as a substitute for R134a in medium- and low-temperature refrigeration applications due to similar discharge pressures and temperatures. R513A exhibits the highest volumetric refrigeration capacity, making it a viable alternative to R134a in air conditioning applications. R516A energy performance is comparable to R134a and has a GWP that meets the EU517/2014 standard, making it a suitable replacement in refrigeration and air conditioning applications.

In a study conducted by Belman-Flores et al. (2023), R1234ze(E), R513A, and R516A were evaluated in a domestic refrigerator with a volumetric capacity of 513 L. For COP, and considering R134a as a reference, it was observed that R513A presented the greatest reduction of around 28%, while R1234ze(E) showed an increase of 13%. Meanwhile, R513A exhibits promising environmental and energy characteristics, making it a viable option in the short term. However, the high energy consumption of R516A limits its potential, and it may be more suitable for domestic refrigeration with improved refrigerator design. Further research is necessary to enhance the performance of R516A in this context, given its low GWP.

Prasad et al. (2023) conducted an experimental and simulation investigation on HFC/HFO mixtures, including R513A and R516A, as substitute for R134a in a vapor compression refrigeration system. The study revealed significant differences in thermodynamic properties and performance among the various refrigerants, providing valuable insights into refrigerant selection for cooling applications. The study is crucial in addressing the environmental concerns related to traditional refrigerants and guide the development of policies promoting the adoption of environmentally friendly refrigerants in industrial refrigeration.

Hu et al., (2024) experimentally evaluated the impact of replacing R134a with R513A on refrigeration efficiency during rapid refrigerant leaks. It also uses the life cycle climate performance (LCCP) framework to analyze carbon emissions from both refrigerants at different leakage rates. Results show that R513A is more stable than R134a in rapid leak scenarios.

Yasser; Oudah, (2024) studied the flow boiling heat transfer and pressure drop characteristics of R134a, R1234yf, and R513A in smooth and micro-fin tubes to optimize low-GWP refrigerant cycles. R134a demonstrated higher heat transfer coefficients than R1234yf and R513A, with differences of about 5% and 3%, respectively. Pressure drop for R134a was about

8% higher than R1234yf and slightly greater than R513A in smooth tubes, with more pronounced differences in micro-fin tubes. R1234yf and R513A were highlighted as environmentally friendly alternatives to R134a, supporting sustainable refrigeration systems.

Dağdır and Bilen (2024) revealed that R513A operates safely in systems originally designed for R134a, with nearly equivalent mass flow rates and only a modestly greater need for refrigerant mass per unit of cooling capacity, suggesting its viability as a substitute during the transition period to more sustainable refrigerants.

Studies have only tested R513A and R516A in a few types of refrigeration systems. It can be said that R516A is the newer refrigerant, and its research and development are still in an earlier stage compared to R513A. So far, no study has tested these two refrigerants in conventional vapor compression heat pump systems focusing on simultaneous cooling and heating.

3. METHODOLOGY

The refrigeration system comprises of four main components: the condenser, evaporator, compressor, and expansion valve (Modi; Ahir; Student, 2018). The liquid refrigerant undergoes vaporization in the evaporator by absorbing of heat from the surrounding environment. The resulting low-pressure vapor is then directed to the compressor, which circulates the refrigerant throughout the system, simultaneously raising both the pressure and temperature of the refrigerant. The condenser functions to remove heat from the system by transferring it to a cooling medium with a lower temperature than that of the refrigerant. Lastly, high-pressure liquid refrigerant is sent into the evaporator through an expansion device or restrictor which reduces its pressure to match the low pressure existing in an evaporator. The primary role of an expansion valve is to regulate and control the flow of liquid refrigerants towards the evaporation process.

3.1. Experimental setup and procedure

This study utilizes experimental data provided by Prof. Juan Manuel Belman Flores. The data obtained using a fully monitored, single-stage vapor compression refrigeration system, as shown in the schematic diagram in Figures 8. The system consist of two closed-loop secondary circuits connected to the evaporator and condenser, using water-glycol mixture (70/30 w/w) and water as secondary fluids, respectively. A comprehensive description of the system components is provided in Méndez-Méndez et al. (2023).

The refrigeration installation comprises three main circuits: the external evaporator loop, the refrigerant loop (compressor side), and the external condenser loop. Each circuit contains components designed for efficient heat transfer, flow monitoring, and pressure regulation:

- External Evaporator Loop
 - Pressure Transducers: Installed before and after the evaporator to monitor refrigerant pressure for performance evaluation.
 - Thermocouples: Measure refrigerant and water-glycol temperatures ($T_{in_{w_e}}$, $T_{out_{w_e}}$, T_{evap}) to track heat exchange.
 - Flowmeter: Monitors water-glycol mass flow rate (\dot{m}_{w_e}) entering the evaporator.

- Water-Glycol Tank and Pump: Maintain and circulate the secondary fluid through the evaporator.
 - Shut-Off Valves A & B: Allow isolation of the evaporator for maintenance or system adjustments.
 - Electronic Expansion Valve (EEV): Regulates refrigerant flow into the evaporator, ensuring stable superheating.
- Refrigerant loop (external Compressor loop)
 - Pressure Transducers: Measure refrigerant pressure at inlet and outlet ($p_{comp_{in}}$, $p_{comp_{out}}$) for system monitoring.
 - Thermocouples: Measure refrigerant temperatures (T_{evap} , $T_{comp_{out}}$) for energy analysis.
 - Liquid Receiver: Serves as a storage vessel to ensure a steady supply of liquid refrigerant to the expansion valve, accommodating fluctuations in refrigerant flow and system load.
 - Coriolis Flowmeter: Measures refrigerant mass flow rate (\dot{m}_{ref}) for precise control and system diagnostics.
 - Electrical Wiring (on compressor): Supplies power to the compressor and facilitates control signals.
 - Red flow line: Is for High-pressure, high-temperature refrigerant in superheated vapor and liquid states.
 - It Moves from compressor to condenser, liquid receiver, Coriolis flowmeter, and EEV.
 - Blue flow line: Is for Low-pressure, low-temperature refrigerant in saturated or superheated vapor state.
 - It Flows through evaporator, absorbs heat, evaporates, returns to compressor.
- External Condenser Loop with Chiller
 - Thermocouples: Monitor cooling water and refrigerant temperatures ($T_{in_{wc}}$, $T_{out_{wc}}$, T_{cond}) for performance tracking.

- Pressure Transducers: Measure refrigerant pressures at condenser inlet and outlet ($p_{cond_{in}}$, $p_{cond_{out}}$).
- Cooling Water Tank and Pump: Circulate the cooling water through the condenser and chiller.
- STAD Valve: Balances and regulates water flow in the condenser loop.
- Flowmeter: Measures cooling water mass flow rate (\dot{m}_{w_c}).
- Chiller: Cools the water leaving the condenser to ensure effective heat rejection, especially in high-load scenarios.
- Shut-Off Valves (C, D, E, F): Enable isolation of specific sections (e.g., pump, chiller, condenser) for maintenance.

The vapor compression circuit includes a reciprocating compressor with a displacement volume of 5.26m³/h at 2900 rpm, a single cylinder, and a net weight of 21kg. The system also includes a 3-liter capacity liquid receiver and a thermostatic expansion valve. The B3-030 Enfusion™ brazed plate heat exchanger (BPHE) from Danfoss were employed for the evaporator and condenser (Danfoss A/S, 2021). The BPHE consist of 10 plates for the evaporator and 20 plates for the condenser, arranged in a counter-current configuration.

Mass flowmeters are installed to measure the mass flow rates of refrigerant, water-glycol, and water in all cycles. Temperature sensors are used to perform an energy balance across both the evaporator and condenser by considering the refrigerant and water sides. Under the conditions specified above, the system operates with cooling capacities ranging from 0.5kW to 3kW.

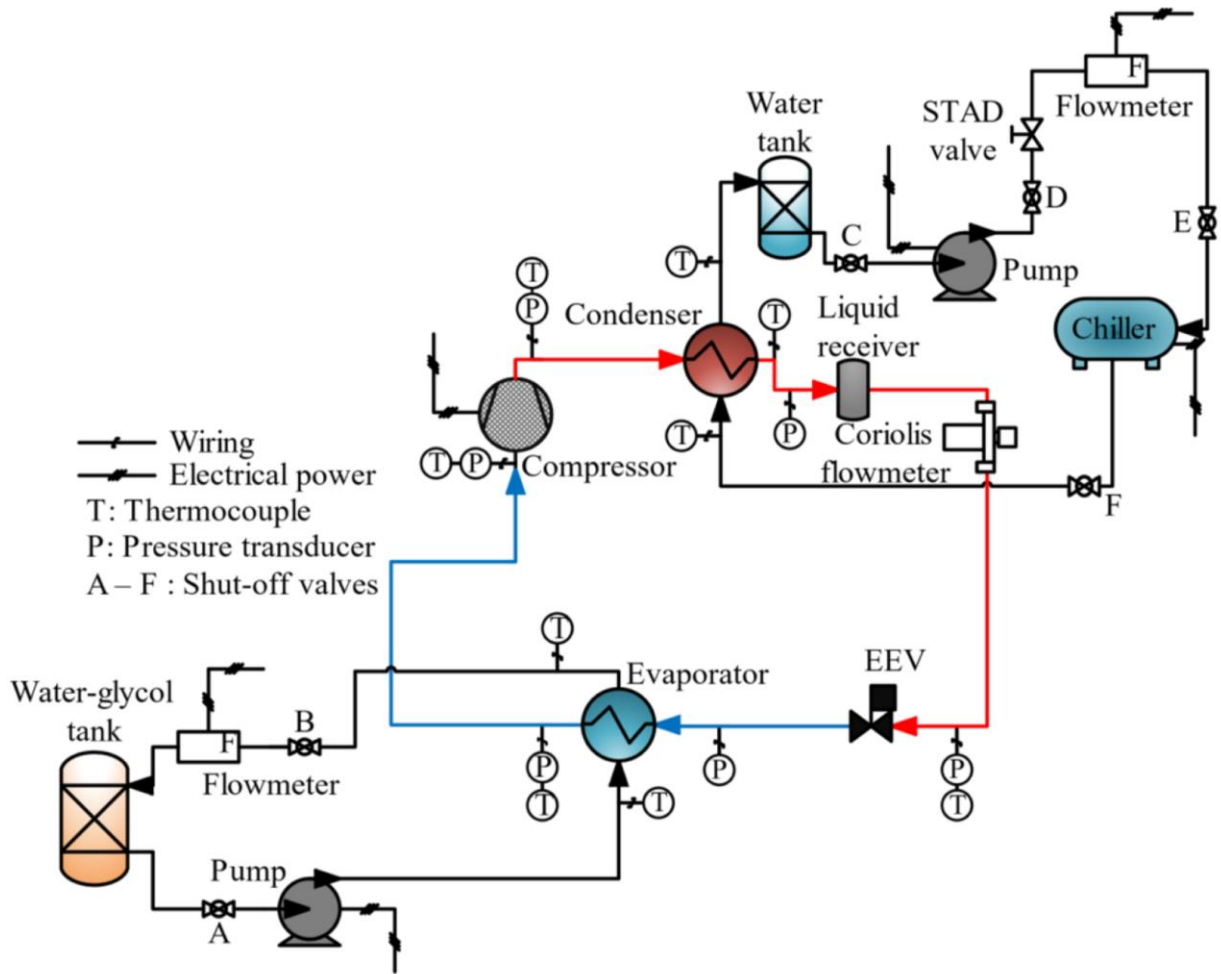


Figure 8: Instrumentation diagram of the refrigeration installation (Méndez-Méndez et al. 2023).

To evaluate the viability of low-GWP refrigerants R513A and R516A as a potential replacement for R134a in refrigeration applications, a series of experiments were conducted. These experiments were performed at seven distinct evaporating temperatures ($-12\text{ }^{\circ}\text{C}$, $-8\text{ }^{\circ}\text{C}$, $-4\text{ }^{\circ}\text{C}$, $0\text{ }^{\circ}\text{C}$, $4\text{ }^{\circ}\text{C}$, $8\text{ }^{\circ}\text{C}$, and $12\text{ }^{\circ}\text{C}$), to simulate typical operating ranges for cooling and heating applications. This setup resulted in a total of 21 unique operating points tested for each refrigerant.

During each experimental run, measurements were collected for temperature, pressure, and mass flow in the refrigerant circuit, as well as the flow rates of the secondary fluid through the evaporator and condenser. Heat transfer rates were calculated based on measured water temperatures and flow rates. COP values for heating and cooling modes were determined using

thermodynamic properties. These data were utilized as inputs to the model and for validating its outputs, as illustrated in Figure 9. A complete list of all measurements is provided in Appendix I.

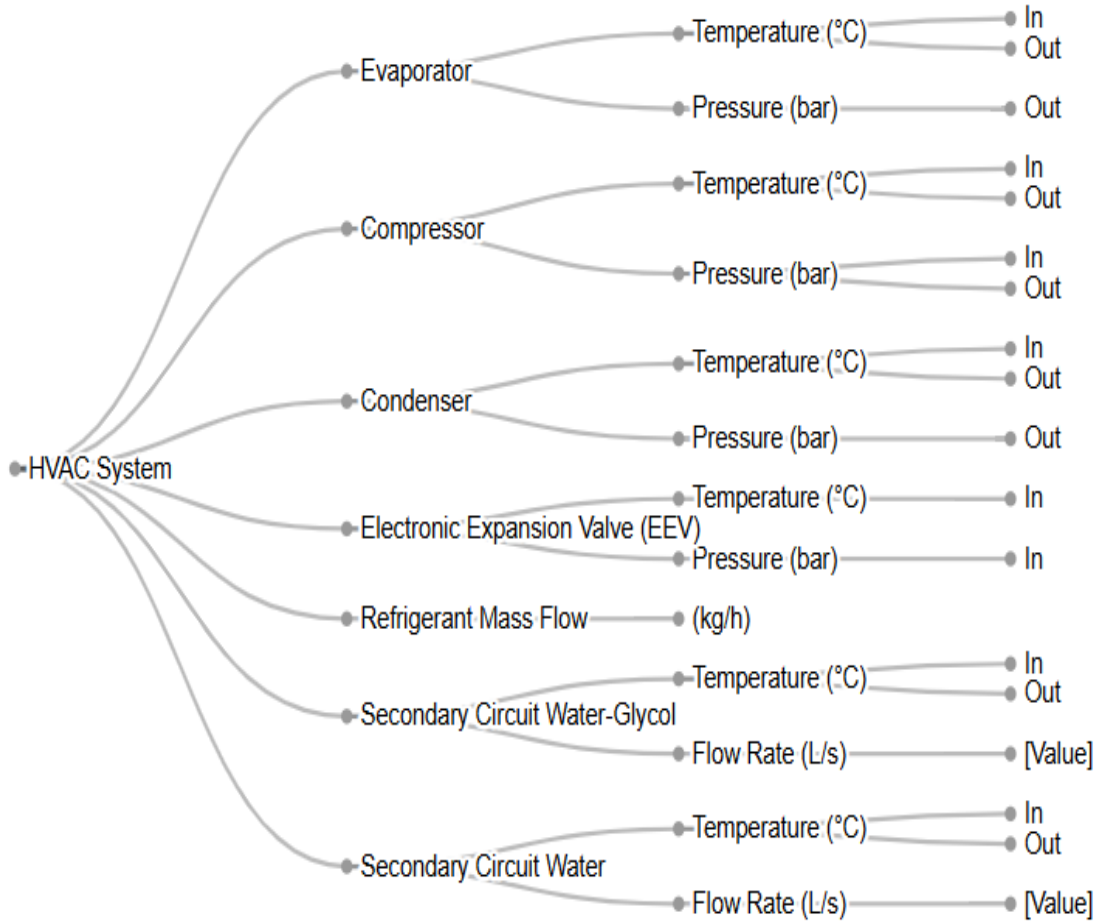


Figure 9: Flowchart of variable measures.

It is important to highlight that the experiments and the model were conducted under steady-state conditions. This ensures that all measurements are consistent over time and sufficient to determine the thermodynamic properties of the refrigerant and water at the inlet and outlet points of key components such as the compressor, condenser, evaporator, and expansion valve. These steady-state properties can be accurately calculated using CoolProp_v6.5.0.0, a robust and free software tool that provides precise thermodynamic data for a wide range of refrigerants and fluids. For the fluids R516A and R513A, which are not included in the library, these mixtures were created in CoolProp using the Mixture function and their respective molar mass percentages.

3.2. Preliminary calculations

This section plays a critical role in defining the intrinsic parameters and performance correlations of key components of the refrigeration system. These calculations are essential for accurately and reliably representing the system's behavior before detailing the mathematical model. For the compressor, both volumetric efficiency and isentropic efficiency are calculated using experimental data. Volumetric efficiency is determined based on the refrigerant mass flow rate and specific volume at the compressor inlet, with a correlation developed as a function of the compression ratio. Similarly, isentropic efficiency reflects the effectiveness of the compression process by comparing the actual enthalpy change to that of an ideal isentropic process. Empirical correlations, expressed as polynomial functions of the compression ratio, are derived to facilitate their application across varying operating conditions.

In the case of the heat exchangers, the primary parameter influencing the behavior of the refrigerant fluid is the heat transfer coefficient. Since this coefficient depends on complex processes like evaporation and condensation, it is challenging to model it analytically. Instead, experimental data related to heat and mass transfer within the heat exchangers are used to establish correlations involving dimensionless numbers, such as Reynolds (Re) and Prandtl (Pr) numbers, which effectively capture the heat transfer dynamics.

3.2.1. Volumetric efficiency of compressor

The volumetric efficiency, η_{vol} , of the compressor can be calculated using the mass flow rate of the refrigerant, \dot{m}_{ref} , as follows:

$$\eta_{vol} = \frac{\dot{m}_{ref} v_{compin}}{V_d} \quad (15)$$

where V_d is the compressor volumetric displacement, and v_{compin} is the specific volume at the compressor inlet.

The volumetric efficiency, η_{vol} , is computed for each tested operating point and refrigerant, with a correlation developed as a function of the compression ratio, $CR = p_{compout}/p_{compin}$, as shown in Eq. (16):

$$\eta_{vol} = a_1(CR)^2 + a_2(CR) + a_3 \quad (16)$$

Where $p_{comp_{out}}$, $p_{comp_{in}}$ are the compressor outlet and inlet pressures, respectively. Here, a_1, a_2, a_3 are polynomial coefficients obtained through regression.

3.2.2. Isentropic efficiency of compressor

The isentropic efficiency, η_{isen} , of the compressor reflects the effectiveness of the compression process by comparing the actual enthalpy change to that of an ideal isentropic process. The isentropic efficiency is given by:

$$\eta_{isen} = \frac{h_{comp_{out-isen}} - h_{comp_{in}}}{h_{comp_{out}} - h_{comp_{in}}} \quad (17)$$

where h is the enthalpy of the refrigerant. The subscripts $comp_{in}$ and $comp_{out}$ denotes enthalpies at the compressor inlet (suction) and outlet (discharge), respectively, while $h_{comp_{out-isen}}$ represents the enthalpy of the fluid at the compressor outlet, assuming an isentropic compression process.

The isentropic efficiency, η_{isen} , is calculated across all tested operating points for each refrigerant, and an empirical correlation based on the compression ratio CR is derived, as shown in Eq. (18):

$$\eta_{isen} = b_1(CR)^2 + b_2(CR) + b_3 \quad (18)$$

where b_1, b_2, b_3 are the polynomial coefficients of correlations determined through regression analysis.

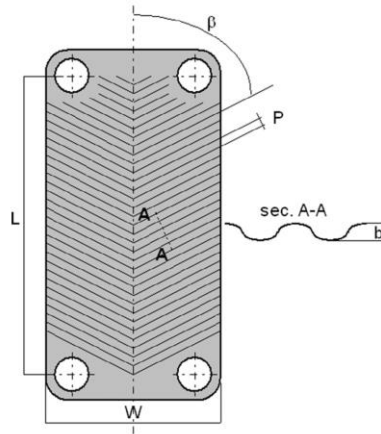
3.2.3. Heat transfer coefficient into a brazed plate heat exchanger

The heat exchangers in use are EnFusion™ brazed plate heat exchangers (BPHE), designed by Danfoss for compact and efficient heat transfer across a range of applications. The BPHE design provides a high heat transfer rate while maintaining a compact footprint, suitable for both

evaporation and condensation processes. The key parameters of the BPHE are outlined in Table 2, with a schematic of the BPHE configuration and operation illustrated in Figure 10.

Table 2: Geometrical characteristics of the BPHE (Longo et al. 2016).

Parameter	Measure/Type	
Plate length L_p (mm)	278	
Plate width W_p (mm)	72	
Area of the plate A (m ²)	0.023	
Corrugation type	Chevron	
Angle of the corrugation β (°)	65	
Corrugation depth b (mm)	2	
Corrugation pitch P (mm)	8	
Plate roughness R_a (μ m)	0.4	
	Evaporator	condenser
Total number of plates	10	20
Number of effective plates	8	18
Channels on refrigerant side	4	9
Channels on water side	5	10



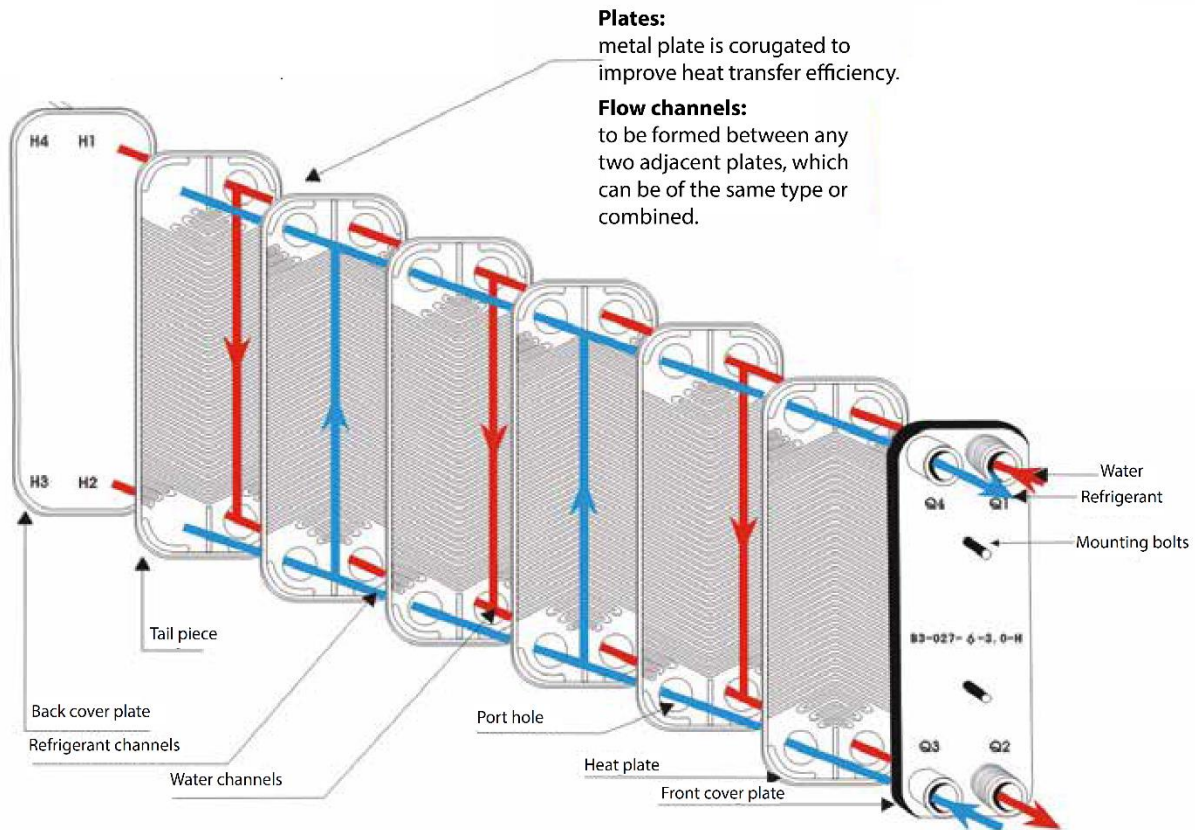


Figure 10: Operational diagram of the BPHE (Danfoss A/S, 2014).

The heat transfer coefficient (HTC) is a fundamental parameter for analyzing and optimizing heat exchangers and other thermal systems. HTC quantifies the rate of heat transfer between a solid surface and a fluid flowing over or around it, playing a vital role in determining the efficiency of thermal systems. Calculating the heat transfer coefficient can be challenging due to the complexity of the physical phenomena involved in the heat transfer, such as conduction, convection, and, in some cases, phase changes, particularly in multi-phase flow systems (Incropera, 1996).

In heat exchanger analysis, it is important to distinguish between local and average heat transfer coefficients. The **local HTC** represents the heat transfer coefficient at specific points within the heat exchanger, typically calculated at each differential volume along the fluid flow path. This provides detailed insights into variations in heat transfer due to changes in fluid temperature, flow conditions, or phase states along the heat exchanger.

On the other hand, the **average HTC** is a single, representative value calculated over an entire section of the heat exchanger, such as the single-phase or two-phase regions. It is derived as the mean of the local HTC values across that section. In this study, **average HTCs** for the single-phase and two-phase regions were calculated and used in the analysis, as they offer a practical and simplified approach for evaluating overall heat transfer performance. This methodology does not rely on a distributed model but instead assumes a representative value for each region to assess thermal performance.

Due to the complexities involved in calculating the heat transfer coefficient in different conditions, researchers often develop empirical correlations to predict the heat transfer coefficient based on dimensionless numbers. Commonly used dimensionless numbers include (Longo et al. 2022):

- Reynolds Number (Re): Indicates the flow regime (laminar or turbulent).
- Prandtl Number (Pr): Relates the momentum diffusivity to thermal diffusivity.

These correlations are typically derived from a large dataset of experimental results and are usually expressed as polynomial or power law equations.

3.2.3.1. Calculation of HTC for single-phase flow.

For single-phase water flow, the heat transfer coefficient, HTC_w , is calculated using a correlation developed by Longo and Gasparella, (2007) valid Prandtl numbers between $5 < Pr_w < 10$ and Reynolds numbers between $200 < Re_w < 1200$:

$$HTC_w = 0.277 \left(\frac{\lambda_w}{d_h} \right) Re_w^{0.766} Pr_w^{0.333} \quad (19)$$

where:

$$Re_w = \frac{G_w d_h}{\mu_w} \quad (20)$$

$$G_w = \frac{\dot{m}_w}{n_{plt_w} A_{ch}} \quad (21)$$

$$Pr_w = \frac{\mu_w c_{p_w}}{\lambda_w} \quad (22)$$

$$d_h = 2b \quad (23)$$

$$A_{ch} = bW_p \quad (24)$$

where \dot{m}_w , G_w , λ_w , μ_w are the mass flow rate, mass flux, thermal conductivity and viscosity of water, respectively. Also, b is the corrugation depth of plate BPHE. n_{plt_w} is the number of plates on the water side. Finally, d_h and A_{ch} are the hydraulic diameter and cross-sectional area of BPHE channel. W_p is the width of the plates.

On the water side, the average and local HTC within the BPHE vary minimally because the flow remains in the liquid phase, and the temperature change in water is relatively small. For the model of heat pump model, Eq. (19) can be applied directly to calculate HTC_w for both the evaporator and condenser.

The correlation of Eq. (19) is also applied in calculating the HTC of the refrigerant when it flows as a single-phase vapor in the evaporator and condenser.

3.2.3.2. Calculation of experimental HTC for refrigerant side.

To experimentally determine the refrigerant side heat transfer coefficient, the following procedure was applied to both the evaporator and condenser (Longo et al. 2016). First, the heat transfer rate, \dot{Q} , was calculated using the Eq. (25):

$$\dot{Q} = \dot{m}_w c_{p_w} |(T_{out_w} - T_{in_w})| \quad (25)$$

where \dot{m}_w is the water mass flow rate, c_{p_w} represents the specific heat capacity of water, $|(T_{out_w} - T_{in_w})|$ is the absolute temperature difference across the water side of the heat exchanger.

The overall heat transfer coefficient, U , is calculated as follows:

$$U = \frac{\dot{Q}}{A_{eff,BPHE} \Delta T_{ln}} \quad (26)$$

where $A_{eff,BPHE}$ denotes the effective heat transfer area of BPHE, and ΔT_{ln} is logarithmic mean temperature difference between the water and refrigerant, for the evaporator see Eq. 2, for the condenser see Eq. 8. The effective heat transfer area of the BPHE is defined as:

$$A_{eff,BPHE} = N_{eff-plates} W_p L_p \quad (27)$$

where $N_{eff-plates}$ is the effective number of plates, W_p the width of the plate, and L_p the length of each plate in the BPHE. Appendix II shows the experimental results for U for evaporator and condenser.

Finally, the average heat transfer coefficient for the refrigerant side, \overline{HTC}_{ref} , was calculated from the overall heat transfer coefficient, U , (Eq. 26) by determining the water side heat transfer coefficient (Eq. 19):

$$\overline{HTC}_{ref} = \left(\frac{1}{U} - \frac{1}{HTC_w} \right)^{-1} \quad (28)$$

In this study, wall thermal resistance was neglected in the calculation, which could lead to slight overestimations of the refrigerant-side HTC. This assumption was deemed acceptable for the brazed plate heat exchanger (BPHE) used, as its wall material and geometry contribute minimally to the overall thermal resistance. Local HTC values vary significantly within the BPHE due to evolving refrigerant flow patterns across single-phase, two-phase, and vapor regions, making this assumption acceptable within the scope of the experimental setup.

3.2.3.3. Develop of correlation for local HTC of refrigerant two-phase flow.

In the literature, several studies have developed experimental correlations to calculate the local heat transfer coefficient (HTC) during two-phase flow in BPHEs. In this work, local HTC values were used to estimate average HTC values for the two-phase region, as this approach aligns with the experimental and modeling methods employed. Specifically, two local HTC correlations were adapted—one for condensation and one for evaporation.

First, here are some definitions for two-phase flow:

The mass flux of the refrigerant is defined as:

$$G_{ref} = \frac{\dot{m}_{ref}}{n_{plt_{ref}} A_{ch}} \quad (29)$$

where \dot{m}_{ref} , and G_{ref} represents the mass flow rate, mass flux of the refrigerant, respectively. $n_{plt_{ref}}$ represents the number of plates on the refrigerant side, while A_{ch} is the cross-sectional area of BPHE channel.

The mean vapor quality, x_m represents the average of the vapor quality from the inlet to the outlet of a differential volume and is given by:

$$x_m = \frac{x_{in} + x_{out}}{2} \quad (30)$$

The Reynolds Number of refrigerant in the liquid phase, Re_{ref_l} is given by:

$$Re_{ref_l} = \frac{G_{ref} d_h}{\mu_{ref_l}} (1 - x_m) \quad (31)$$

where μ_{ref_l} , is the liquid phase viscosity of the refrigerant, and d_h is the hydraulic diameter.

The Prandtl number of the refrigerant in the liquid phase, Pr_{ref_l} , is given by:

$$Pr_{ref_l} = \frac{\mu_{ref_l} c_{p_{ref_l}}}{\lambda_{ref_l}} \quad (32)$$

where λ_{ref_l} is the thermal conductivity of liquid refrigerant, and $c_{p_{ref_l}}$ is its specific heat capacity.

Longo et al. (2015) presented a non-dimensional correlation for the convective boiling heat transfer coefficient in BPHEs, which was based on the Reynolds number of the liquid phase, Re_{ref_l} , and the Prandtl number, Pr_{ref_l} . In this study, the flow characteristics differs from those examined by Longo et al. (2015) due to lower mass flow rates. While Longo et al. (2015) results were predominantly influenced by nucleation effects, the flow in this case exhibits strong convective characteristics. As a result, the original correlation has been adjusted to match the experimental data used in this study.

For evaporation, the HTC correlation was derived using the modified Longo et al. (2015) equation, with an enlargement factor $\Phi=1.24$, expressed as:

$$HTC_{evap} = 0.408\Phi \left(\frac{\lambda_{refl}}{d_h} \right) Re_{refl}^{1.35} Pr_{refl}^{\left(\frac{1}{3}\right)} \quad (33)$$

On the other hand, Longo (2010) introduced local HTC correlations for condensation in BPHEs. However, the constants in these correlations were adjusted in this study to better fit the experimental data used in this study. The condensation heat transfer coefficient, HTC_{cond} , with the revised constants, is given by:

$$HTC_{cond} = 0.129\Phi \left(\frac{\lambda_{refl}}{d_h} \right) Re_{refeq}^{1.30} Pr_{refl}^{\left(\frac{1}{3}\right)} \quad (34)$$

All thermodynamics properties of R134a, R513A, and R516A were calculated using Cool-prop, assuming saturated liquid and vapor states at the saturation temperature, specific to the evaporation or condensation process in each case. The correlations of Eq.33 and Eq.34 were calculates only using the experimental data set of Méndez-Méndez et al. (2023), and valid for the mass flux $5 \frac{kg}{m^2s} < G_{ref} < 30 \frac{kg}{m^2s}$ and heat flux between 5-12kW/m².

3.2.3.4. Average HTC of refrigerant side.

For Evaporator:

Step 1: Calculate average HTC during two-phase flow:

- In an evaporator, the inlet quality ($x_{in_{evap}}$) can be calculated, while the final quality is always 1 (indicating complete evaporation).
- The local HTC is determined using Eq. (33) over the range from the initial quality to the final quality, discretized into steps.
- These local HTC values are then averaged by summing them across all intervals and dividing by the total number of steps. This approach ensures an accurate calculation of the average HTC over the two-phase region of the evaporator.

Step 2: HTC for superheated vapor flow:

- Once the refrigerant flow is entirely vapor, the $HTC_{sp,e}$ for this vapor flow is calculated using Equation (19), which accounts for the heat transfer characteristics in the vapor phase.

Step 3: Overall HTC for the refrigerant side:

- The overall HTC on the refrigerant side of the evaporator is then calculated by combining the contributions from both the two-phase and vapor flow regions.
- The proportion of the area occupied by the two-phase and superheated vapor flow sections is taken into account using the $F_{sp,e}$ factor. This factor governs how much area of each phase (two-phase vs. vapor) contributes to the overall HTC.

$$\overline{HTC}_{evap} = \left(\frac{1}{i} \sum_{x=x_{in\,evap}}^{x=1} HTC_{evap}(x_i) \right) (1 - F_{sp,e}) + HTC_{sp,e} F_{sp,e} \quad (35)$$

An example of how to use this method is presented in Appendix III.

For the condenser:

Step 1: Calculate HTC for vapor flow:

- Initially, the refrigerant enters the condenser in a superheated vapor state (typically at the condenser inlet). As the vapor cools, it eventually reaches a point where its quality becomes 1, indicating it has reached a saturated vapor state.
- The HTC for this vapor region is calculated using Eq. (19).

Step 2: Calculate average HTC for two-phase flow:

- once condensation begins, the refrigerant enters a two-phase region, where vapor and liquid coexist. This region extends from quality 1 down to quality 0.

- The local HTC in the condenser is calculated using Equation (34). These local HTC values are then averaged by summing them across all steps and dividing by the total number of steps. This process provides an accurate estimate of the average HTC for the two-phase region.

Step 3: Calculate HTC for liquid flow:

- After condensation process is complete, the refrigerant becomes a subcooled liquid.
- The HTC for this liquid phase is calculated using Eq. (19) as well.

Step 4: Overall HTC for the refrigerant side:

- The overall HTC on the refrigerant side of the condenser is determined by combining the contributions from all three regions: the vapor flow, two-phase flow, and liquid flow. The proportion of each region are considered using $F_{sp,c}$ and $F_{sc,c}$, which represent the fractions of the area occupied by the superheated vapor and subcooled liquid regions, respectively:

$$\overline{HTC}_{cond} = \left(\frac{1}{i} \sum_{x=1}^{x=0} HTC_{cond}(x_i) \right) (1 - F_{sp,c} - F_{sc,c}) + HTC_{sp,c} F_{sp,c} + HTC_{sc,c} F_{sc,c} \quad (36)$$

3.3. Mathematical model

The heat pump model comprises three interconnected sub-models: the evaporator, compressor, and condenser. The key assumptions in this model include:

- The pressure drop is negligible.
- The heat losses to the environment are negligible.
- The conduction effect of the metal plate in the BPHE is negligible.
- The electronic expansion valve maintains a constant superheating level in the evaporator.

- The expansion process is an isenthalpic process (no change in enthalpy).
- The evaporator operates with water containing 30% volume of ethylene-glycol.

3.3.1 Evaporator balance

The mean temperature of water in the evaporator, T_{mw_e} , is calculated using Eq. (37) based on the inlet and outlet water temperature in the evaporator ($T_{in_{w_e}}$ and $T_{out_{w_e}}$, respectively) to calculate the properties of the water.

$$T_{mw_e} = \frac{T_{in_{w_e}} + T_{out_{w_e}}}{2} \quad (37)$$

The heat transfer rate on the water side and refrigerant side of the evaporator are defined by Eqs. (38) and (39), respectively.

$$\dot{Q}_{evap} = \dot{m}_{w_e} c_{p_{w_e}} (T_{in_{w_e}} - T_{out_{w_e}}) \quad (38)$$

$$\dot{Q}_{evap} = \dot{m}_{ref} (h_{evap_{out}} - h_{evap_{in}}) \quad (39)$$

where \dot{m}_{w_e} and $c_{p_{w_e}}$ are the mass flow rate and specific heat capacity of water in the evaporator, respectively, and $h_{evap_{out}}$, $h_{evap_{in}}$ are the enthalpies of refrigerant at the outlet and inlet of the evaporator.

The equation of BPHE (brazed plate heat exchanger) as the evaporator is:

$$\dot{Q}_{evap} = U_{evap} A_{evap} \Delta T_{ln- evap} \quad (40)$$

where A_{evap} is the heat transfer area of the evaporator in the heat exchanger, which is equal to $A_{eff, BPHE}$ for the evaporator size (refer to Table 2).

The global heat transfer coefficient of the evaporator (U_{evap}), is given by:

$$U_{evap} = \left(\frac{1}{HTC_{w_e}} + \frac{1}{HTC_{evap}} \right)^{-1} \quad (41)$$

Where HTC_{w_e} is the heat transfer coefficient of water in the evaporator, calculated using Eq. (19) and T_{mw_e} to determine the properties, and \overline{HTC}_{evap} is the average heat transfer coefficient of refrigerant in the evaporator, calculated with the adjusted Eq. (35).

For the evaporator sub-model, there are four inputs: $T_{in_{w_e}}$, \dot{m}_{w_e} , $h_{evap_{in}}$, and \dot{m}_{ref} . Equations (38), (39), and (40) are solved using a numerical method to determine three outputs: T_{evap} , $h_{evap_{out}}$, and $T_{out_{w_e}}$.

3.3.2. Condenser balance

The mean temperature of water in the condenser T_{mw_c} is calculated using Eq. (42), based on the water temperature at the inlet and outlet of the condenser ($T_{in_{w_c}}$ and $T_{out_{w_c}}$, respectively) to calculate the properties of water.

$$T_{mw_c} = \frac{T_{in_{w_c}} + T_{out_{w_c}}}{2} \quad (42)$$

The heat transfer rate on the water side and refrigerant side of the condenser are defined by Eqs. (43) and (44), respectively.

$$\dot{Q}_{cond} = \dot{m}_{w_c} c_{p_{w_c}} (T_{out_{w_c}} - T_{in_{w_c}}) \quad (43)$$

$$\dot{Q}_{cond} = \dot{m}_{ref} (h_{cond_{in}} - h_{cond_{out}}) \quad (44)$$

where \dot{m}_{w_c} , and $c_{p_{w_c}}$ are the mass flow rate and specific heat capacity of water in the condenser, respectively, and $h_{cond_{out}}$, $h_{cond_{in}}$ are the enthalpies of the refrigerant at the outlet and inlet of the condenser.

The equation of the BPHE (Braze plate heat exchanger) as the condenser is:

$$\dot{Q}_{cond} = U_{cond} A_{cond} \Delta T_{ln-cond} \quad (45)$$

where A_{cond} is the heat transfer area of the condenser heat exchanger, which is equal to $A_{eff, BPHE}$ for the condenser size (refer to Table 2).

The global heat transfer coefficient of the condenser, (U_{cond}), is given by:

$$U_{cond} = \left(\frac{1}{HTC_{w_c}} + \frac{1}{\overline{HTC}_{cond}} \right)^{-1} \quad (46)$$

Where HTC_{w_c} is the heat transfer coefficient of water, calculated using Eq. (19) and the T_{mw_c} to determine the properties, and \overline{HTC}_{cond} is the average heat transfer coefficient of refrigerant in the condenser, calculated with Eq. (36).

For the condenser sub-model, there are four inputs: $T_{in_{w_c}}$, \dot{m}_{w_c} , $h_{cond_{in}}$, and \dot{m}_{ref} . Equations (43), (44), and (45) are solved using a numerical method to determine three outputs: T_{cond} , $h_{cond_{out}}$, and $T_{out_{w_c}}$.

3.3.3. Compressor

The mass flow rate of the working fluid through the compressor is defined by Eq. (47):

$$\dot{m}_{ref} = \frac{\eta_{vol} V_d}{v_{comp_{in}}} \quad (47)$$

where η_{vol} is the volumetric efficiency of the compressor, calculated using the experimental regression described in Section 3.2.1.

The enthalpy of refrigerant at the outlet of the compressor, ($h_{comp_{out}}$), is given by:

$$h_{comp_{out}} = h_{comp_{in}} + \frac{h_{comp_{in}} - h_{comp_{out-isen}}}{\eta_{isen}} \quad (48)$$

where η_{isen} is the isentropic efficiency of the compressor, calculated by the experimental regression explain in section 3.2.2.

The energy transferred from the compressor to refrigerant is defined by Eq. (49):

$$W_{comp} = \dot{m}_{ref} (h_{comp_{out}} - h_{comp_{in}}) \quad (49)$$

For the compressor sub-model, there are three inputs: T_{cond} and T_{evap} (necessary for calculating the volumetric and isentropic efficiencies of the compressor), and h_{compin} . The outputs of the model are \dot{m}_{ref} and $h_{compout}$, which do not require numerical methods for their calculation.

The coefficient of performance (COP) of the system is determined by Eqs. (50) and (51), where the power consumption of the compressor is directly measured.

$$\text{For Cooling: } COP_c = \frac{\dot{Q}_{evap}}{W_{comp}} \quad (50)$$

$$\text{For Heating: } COP_h = \frac{\dot{Q}_{cond}}{W_{comp}} \quad (51)$$

3.3.4. Heat pump model

To solve the heat pump model, the three sub-models were combined as shown in Figure 11. The model considered the conditions of the secondary fluids, specifically the water circulating through the condenser and evaporator. The evaporation and condensation temperatures of the refrigerant were determined iteratively using the trust-region dogleg algorithm, as illustrated in the flowchart in Figure 12.

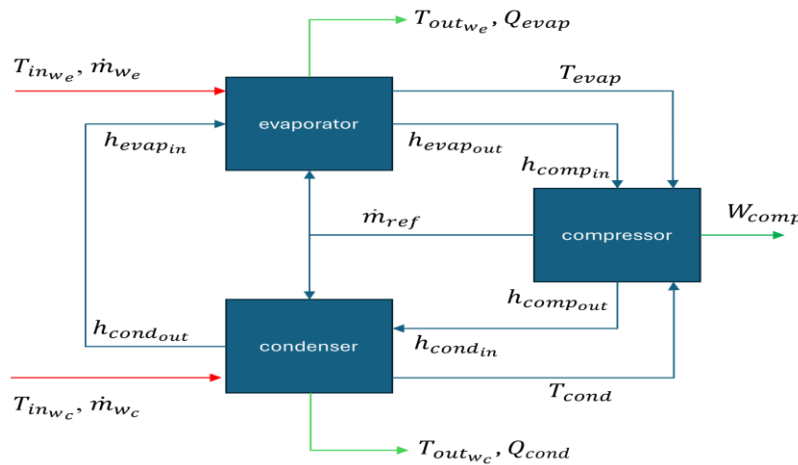


Figure 11: Modeling of system components.

The system in Figure 11 consists of an **evaporator**, **compressor**, and **condenser** that work together to transfer heat and maintain the refrigeration cycle.

- **Evaporator:**

- Water (or water-glycol) enters the evaporator at a temperature $T_{in_{we}}$ and a certain mass flow rate \dot{m}_{we} .
- Inside the evaporator, the water absorbs heat from the refrigerant, which causes the refrigerant to evaporate. This heat absorption is recorded as \dot{Q}_{evap} .
- The water exits the evaporator at a higher temperature $T_{out_{we}}$, having absorbed the heat.
- The refrigerant entering the evaporator has an enthalpy $h_{evap_{in}}$, and after evaporating, the refrigerant leaves the evaporator with a new temperature T_{evap} and enthalpy $h_{evap_{out}}$ (which is also the enthalpy entering the compressor as $h_{comp_{in}}$).

- **Compressor:**

- The refrigerant is compressed in the compressor, which increases its pressure and temperature.
- The work done by the compressor is represented as \dot{W}_{comp} .
- The refrigerant exits the compressor with a high temperature and pressure, now having an enthalpy $h_{comp_{out}}$, which moves towards the condenser.

- **Condenser:**

- The hot refrigerant enters the condenser, where it releases heat to the cooling medium (such as water).
- The cooling medium enters the condenser at a temperature $T_{in_{wc}}$ and leaves at a higher temperature $T_{out_{wc}}$, having absorbed the heat from the refrigerant.
- The refrigerant in the condenser loses heat and condenses back into a liquid. It enters with an enthalpy $h_{cond_{in}}$ and leaves the condenser as a liquid with enthalpy $h_{cond_{out}}$.
- The heat release by the refrigerant is \dot{Q}_{cond} .

- After leaving the condenser, the refrigerant, now a high- pressure liquid, flows back through the expansion valve, where its pressure is reduced. This process ensures the refrigerant is ready to re-enter the evaporator and repeat the cycle. Throughout the system, the refrigerant mass flow rate, \dot{m}_{ref} remains constant, ensuring a continuous and steady-state operation.

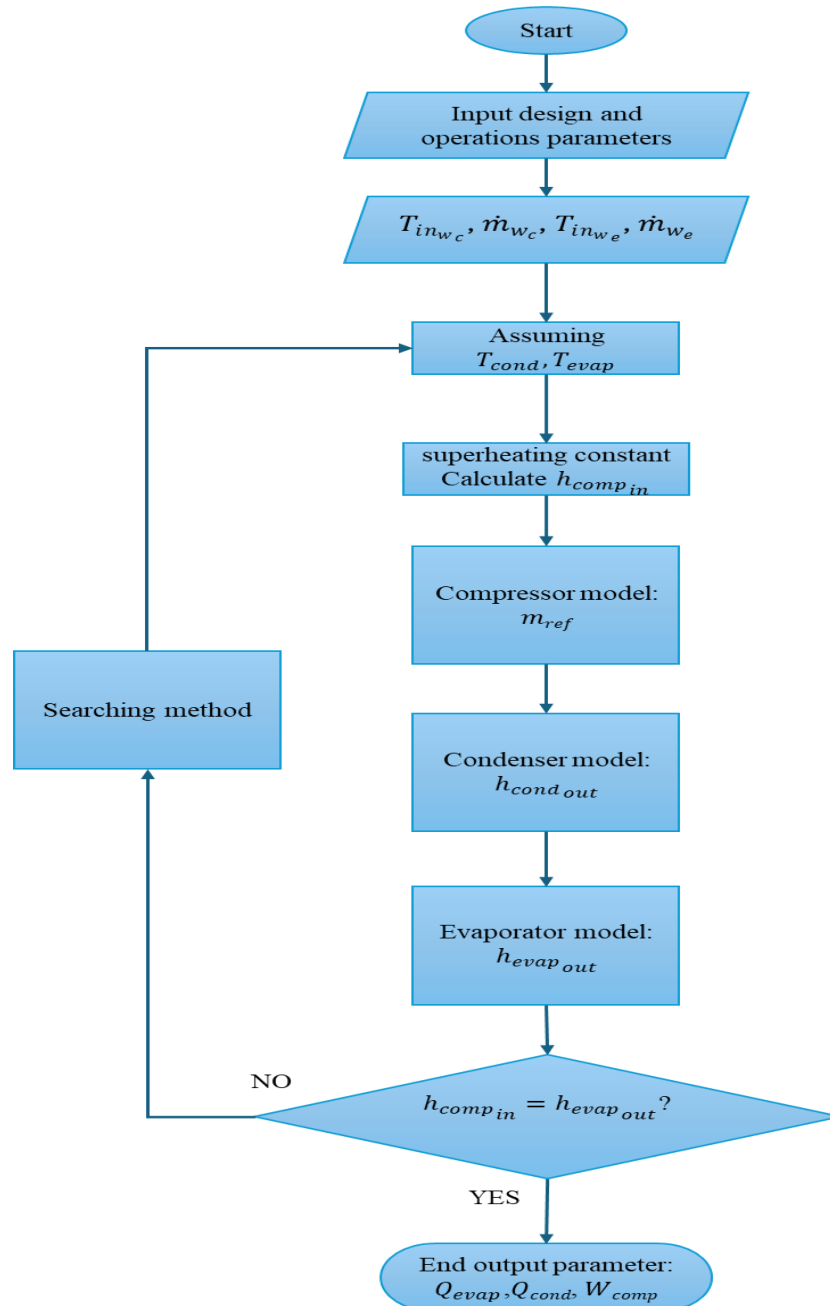


Figure 12: Fluxgram (flow diagram) of heat pump model solution using MATLAB.

The flow diagram in Figure 12 describes the step-by-step process for solving the heat pump model, and the process is as follows:

- **START:** The process begins.
- **Input Design & Operation Parameters:** Key parameters like inlet temperatures and mass flow rates for the condenser and evaporator are provided.
- **Assume T_{cond} and T_{evap} :** Initial guesses are made for the condenser and evaporator temperatures.
- **Calculate Compressor Inlet Enthalpy ($h_{comp_{in}}$):** Using the assumed temperatures and a superheating constant, the enthalpy at the compressor inlet is calculated.
- **Compressor Model (\dot{m}_{ref}):** The compressor model is used to compute the refrigerant flow rate.
- **Condenser Model ($h_{cond_{out}}$):** The condenser model calculates the outlet enthalpy of the refrigerant based on the refrigerant flow and heat exchange in the condenser.
- **Evaporator Model ($h_{evap_{out}}$):** Similarly, the evaporator model calculates the outlet enthalpy of the refrigerant after it absorbs heat.
- **Check if $h_{comp_{in}} = h_{evap_{out}}$:** The process checks if the enthalpy at the compressor inlet equals the enthalpy at the evaporator outlet.
 - If YES, the model ends and the output parameters (such as heat transfer rates: \dot{Q}_{evap} , \dot{Q}_{cond} , \dot{W}_{comp}) are finalized.
 - If NO, the process proceeds to a Searching Method.
- **Searching Method:** This step adjusts the assumed values for condenser and evaporator temperatures (T_{cond} and T_{evap}) and iterates the process.
- **Return to Assumption Step:** After adjustments, the process returns to the assumption of T_{cond} and T_{evap} , and the calculations are repeated until the enthalpies match.

The mathematical model for analyzing heat transfer coefficients and system performance was implemented using MATLAB, leveraging its numerical computation capabilities for solving complex thermodynamic equations. All correlations and experimental validation calculations were carried out within this framework.

3.4. Model validation parameters

A well-validated model ensures reliable predictions of a heat pump behavior under varying operating conditions, which is critical for both manufacturers and users. In this context, model validation refers to the process of comparing the predictions of a heat pump mathematical model with experimental data. The goal is to verify that the model accurately captures the physical behavior of the heat pump, including the heat transfer rates, energy consumption, and temperature changes, across a wide range of conditions.

The validation was conducted using experimental data obtained from a fully monitored vapor compression system described by Méndez-Méndez et al. (2023). These data sets included operational parameters for three refrigerants: R134a, R513A, and R516A. The experimental measurements covered varying inlet temperatures in the evaporator and condenser, as well as a range of mass flow rates, ensuring comprehensive validation across diverse operating scenarios.

The model predictions for key parameters were compared to the experimental values for heat transfer rates in the evaporator and condenser, compressor work, and COP. The accuracy of the model was assessed using statistical methods such as Mean Percentage Error (MPE) and Mean Percentage Absolute Error (MAPE). These metrics evaluate the average percentage difference between predicted values from a model and actual observed value, and are calculated as follows:

$$MPE = \frac{1}{n} \sum_{i=1}^n \frac{(y_i - \hat{y}_i)}{y_i} \quad (53)$$

$$MAPE = \frac{1}{n} \sum_{i=1}^n \frac{|y_i - \hat{y}_i|}{y_i} \quad (54)$$

where y_i represents the actual values (observed data), \hat{y}_i represents the predicted values from the model, and n is the total number of observations.

For validating a heat pump model, MPE and MAPE are useful in assessing the accuracy of the model in predicting key outputs, such as heat transfer rates (HTCs) of the evaporator and condenser, work of the compressor, and coefficient of performance (COP). Validation results

demonstrated strong agreement between the model and experimental data, with MPE and MAPE values for COP and HTC_s consistently below acceptable thresholds.

3.5. Simulations conditions

As mentioned in section 2.1.3, two specific cases were studied in the heat pump with simultaneous heating and cooling. The first case considered an application with a medium evaporation temperature, where the water-glycol inlet temperatures ranged from 0 to 5°C at the evaporator; and water inlet temperature from 35 to 40 °C at the condenser. The second case analyzed an application with a high evaporation temperature, with the water-glycol inlet temperatures ranging from 10 to 15 °C at the evaporator; and water inlet temperatures from 50 to 55 °C at the condenser. For both cases, the behavior of the three refrigerant fluids was analyzed, and the mass flow rate of the secondary fluids (water-glycol for the evaporator and water for the condenser) was varied between 0.05 kg/s and 0.15 kg/s to study performance variations.

4. RESULTS AND DISCUSSION

4.1. Experimental results

Appendix I presents the experimental data for the fluids R134a, R513A, and 516A conducted by Prof. Juan Manuel Belman Flores and his team, for more details see Méndez-Méndez et al. (2023). Figure 13 shows that the seven evaporation temperatures were set with high precision across all fluids. However, achieving a consistent condensation temperature between tests proved more challenging, reflecting the variability observed in the control of condensation parameters. This inconsistency in condensation temperature underscores the greater difficulty in stabilizing condenser conditions compared to the evaporator

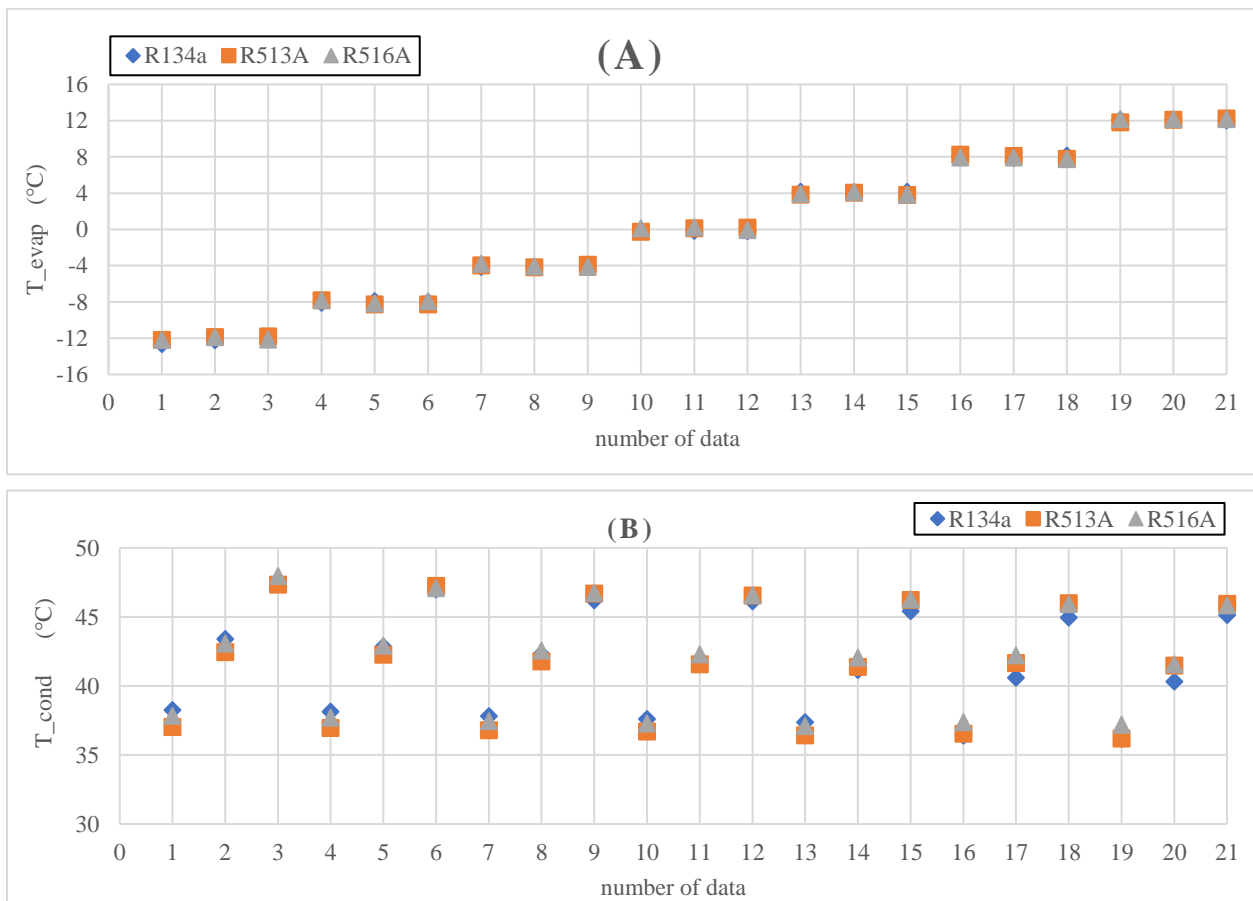


Figure 13: T_{evap} and T_{cond} vs number of data for R134a, R513A, and R516A.

In Figure 14A, the relationship between mass flow rate and evaporation temperature is clearly observed, with mass flow rate increasing as evaporation temperature rises. This trend is primarily attributed to the increase in the compressor volumetric efficiency, which is strongly

influenced by evaporation pressure (and thus evaporation temperature). For each evaporation temperature, the data include multiple condensation temperatures) for each refrigerant, yet there is minimal variation in mass flow rate values. This suggests that condensation temperature has a limited impact on mass flow rate. Figure 14B reinforces these observations. At a constant condensation temperature, substantial variation in mass flow rate is evident across the seven different evaporation temperatures (or pressures), confirming that evaporation temperature exerts a stronger influence on mass flow rate than condensation temperature.

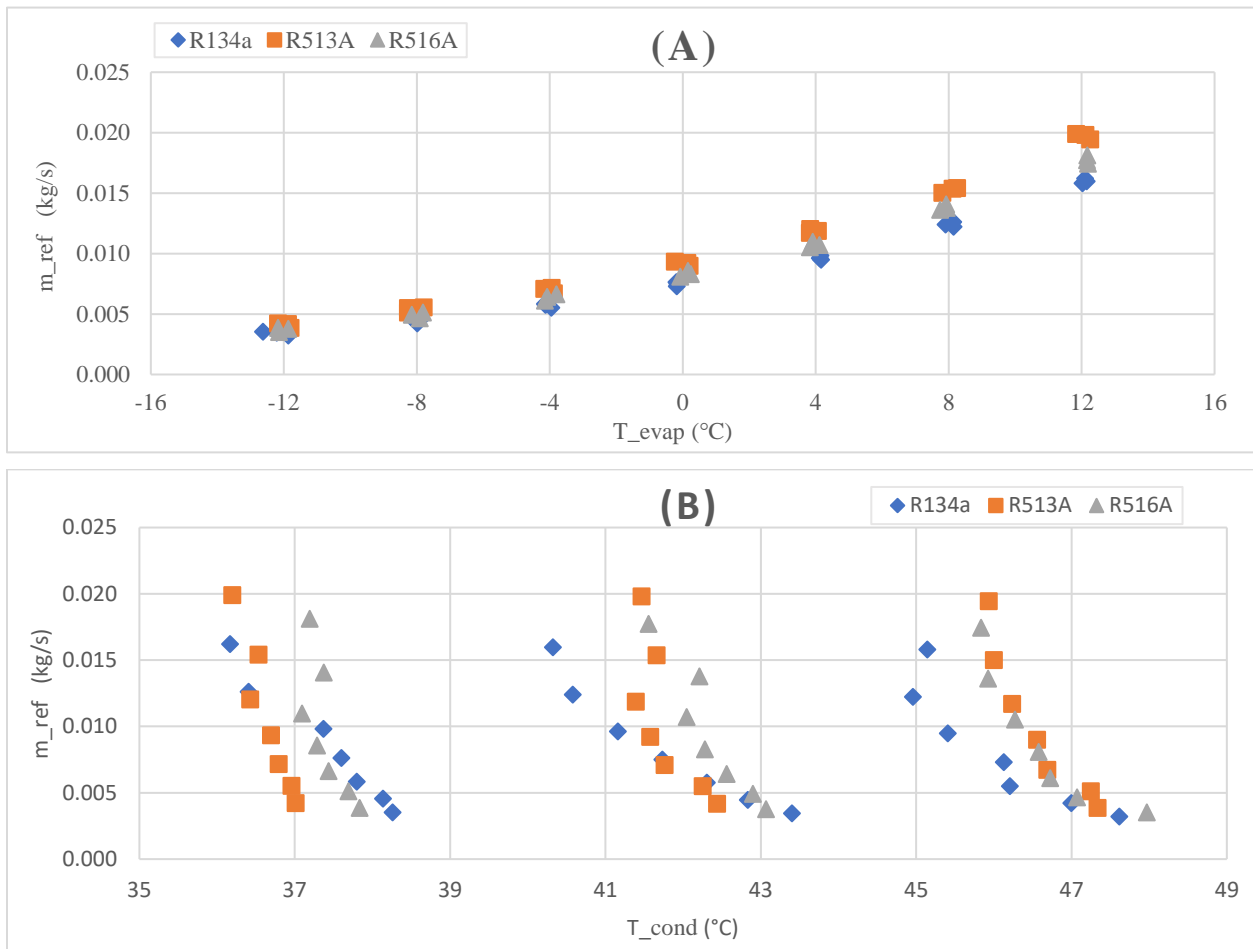


Figure 14: Effect of T_{evap} and T_{cond} on \dot{m}_{ref} .

Figure 15 shows, as expected, that heat transfer in both the evaporator and condenser, as well as the compressor work, are strongly influenced by the evaporation temperature. For all three

fluids, there are no significant differences in performance, suggesting that a R513A and 516A exhibits promising potential as replacements for R134a.

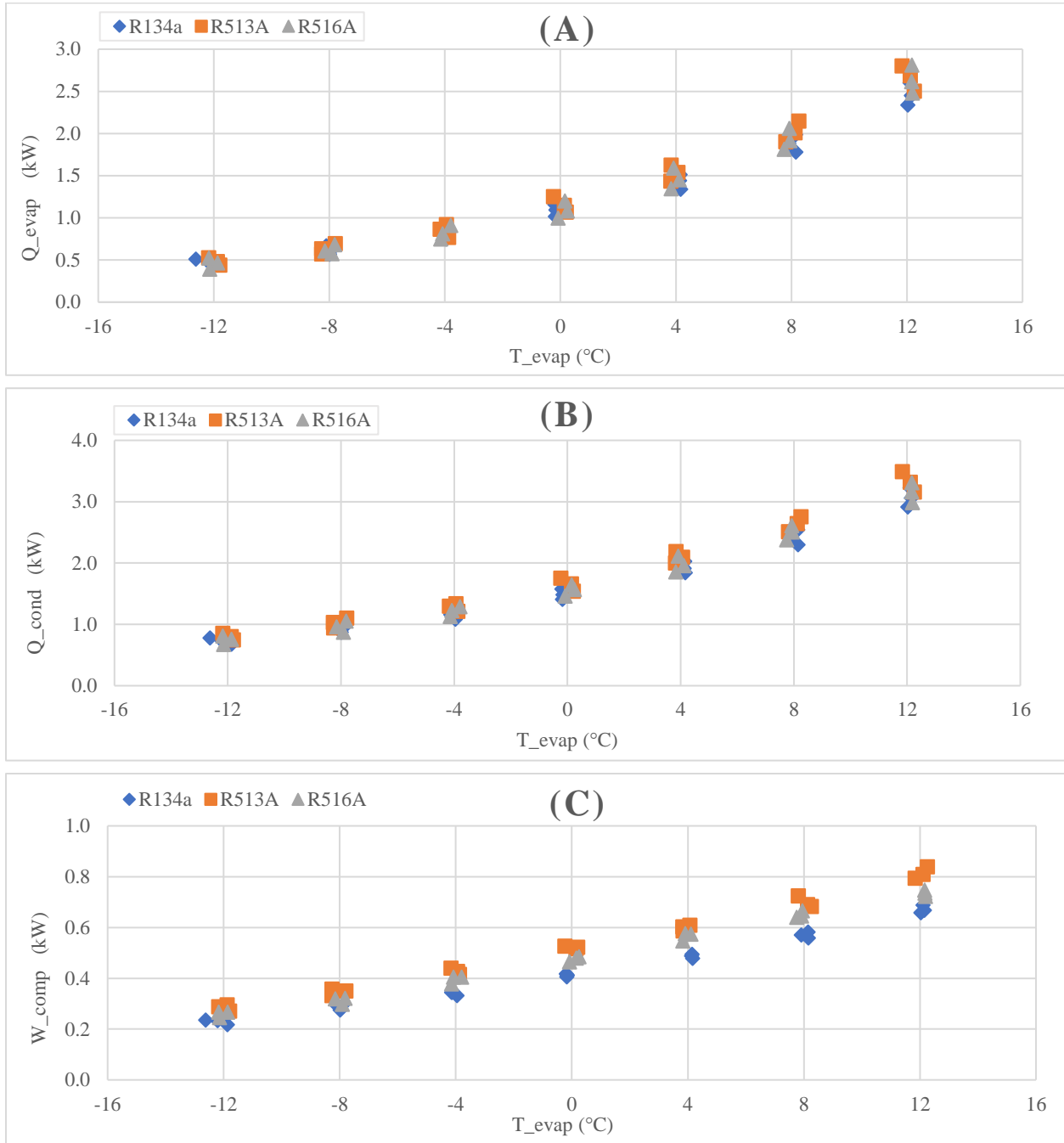


Figure 15: Q_{evap} , Q_{cond} , and W_{comp} vs T_{evap} for R134a, R513A, and R516A.

Figure 16 illustrates the COP for both cooling and heating modes across all three refrigerants. The results show that, compared to R134a, R513A exhibits a 15% lower COP in cooling mode, while

R516A shows a 10% reduction. In heating mode, the performance gap narrows, with R513A demonstrating an 11% decrease and R516A an 8% decrease.

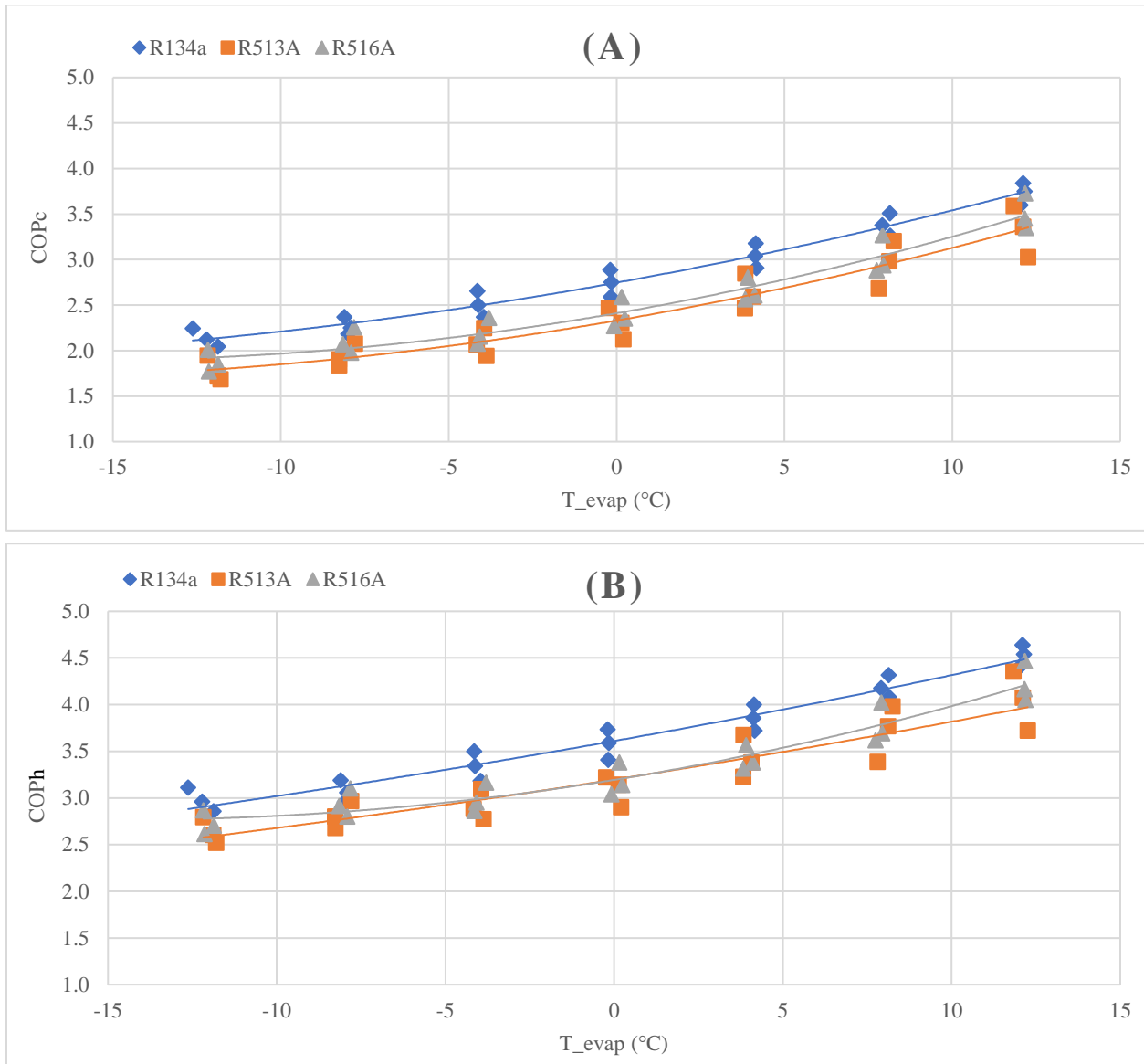


Figure 16: COP_h and COP_c vs T_{evap} for R134a, R513A, and R516A.

Figure 17 presents the overall heat transfer coefficient in both the evaporator and condenser for the three fluids, calculated as described in section 3.2.3. Similar trends are observed, consistent with findings from other authors (Longo, 2010; Longo et al. 2015). Notably, the heat transfer coefficient is generally higher in the evaporator than in the condenser, primarily due to the temperatures at which phase changes occur. Lower temperatures enhance heat transfer and exhibit

better thermodynamic properties, such as increased conductivity and reduced viscosity. When comparing the fluids, both R513A and R516A demonstrate slightly lower heat transfer capacities than R134a.

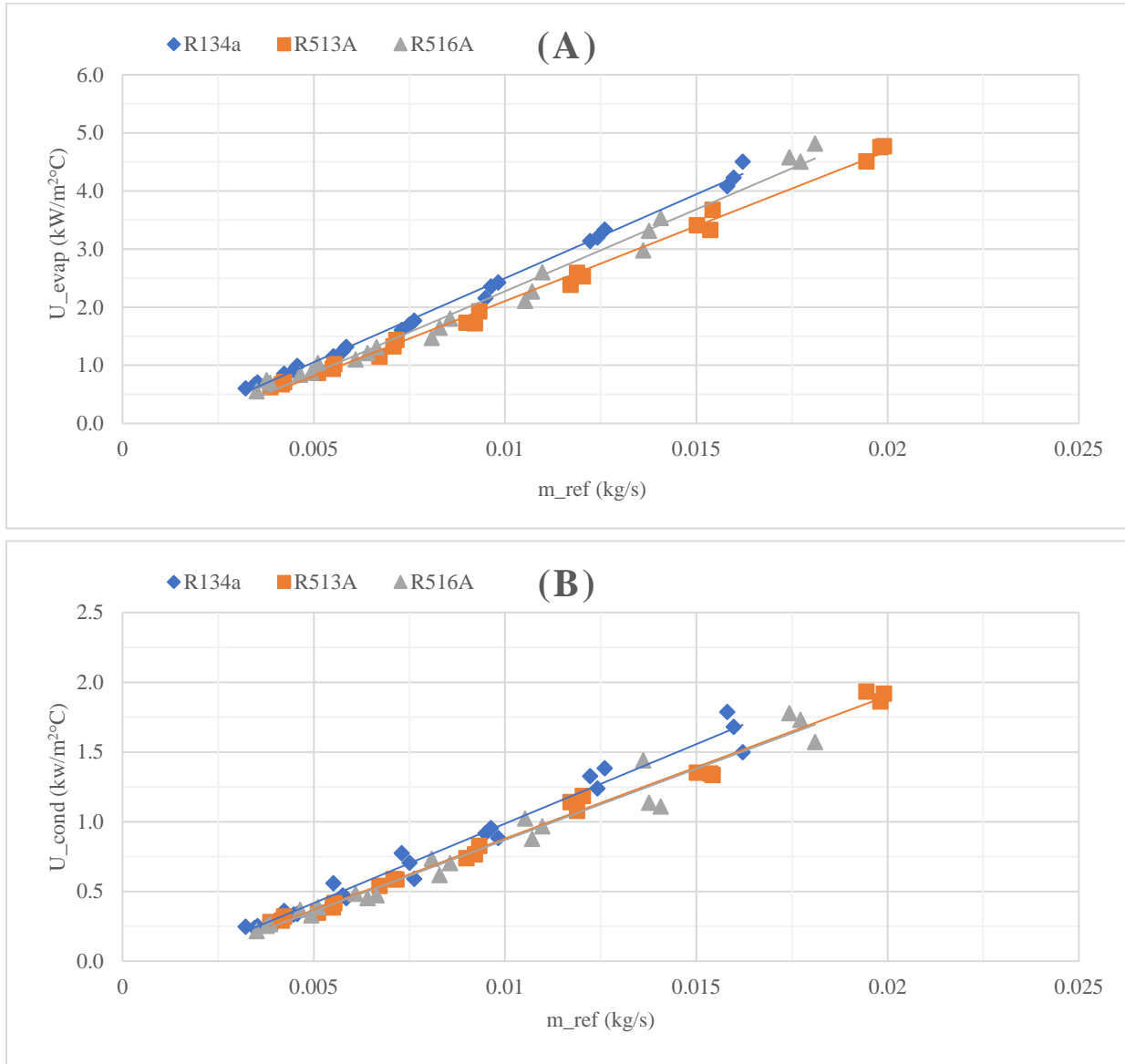


Figure 17: U_{evap} and U_{cond} vs \dot{m}_{ref} for R134a, R513A, and R516A.

The isentropic and volumetric efficiencies were calculated according to sections 3.21 and 3.2.2. As presented in Figure 18, a quadratic regression model is applicable to the volumetric efficiency data for all fluids, with a regression coefficient of 0.91. In contrast, the experimental data for isentropic efficiency exhibited greater dispersion. A regression analysis considering all

fluids together yielded a coefficient of 0.7. However, performing a separate regression for each fluid data points of each fluid improved the coefficient to 0.8.

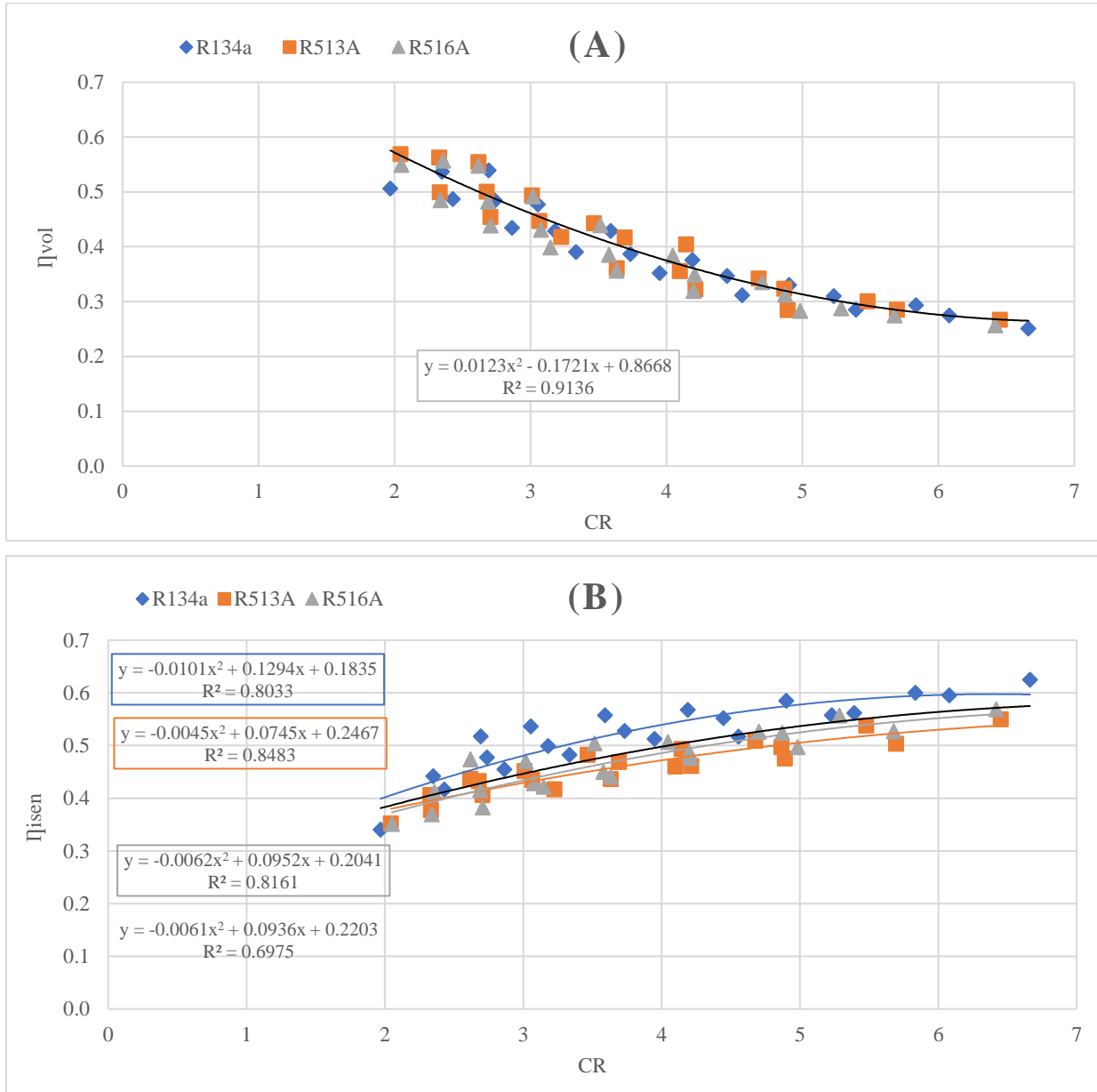


Figure 18: Volumetric and isentropic efficiency vs compression ratio.

4.2. Validation of mathematical model

This section presents the validation of the heat pump system model, focusing on key performance parameters such as temperature, heat transfer coefficients, heat loads in the evaporator and condenser, compressor work, and coefficient of performance (COP). These modeled parameters were systematically compared with experimental data to evaluate the model accuracy and reliability. Table 3 presents the mean percentage error (MPE) and mean absolute percentage error (MAPE) results for all refrigerants, highlighting the model key predictive outcomes.

Table 3: Mean percentage error (MPE) and mean absolute percentage error (MAPE) of R134a, R513A, and R516A.

Variable	R134a		R513A		R516A		Total	
	MPE	MAPE	MPE	MAPE	MPE	MAPE	MPE	MAPE
U_{evap}	0.32	1.95	-4.76	4.85	5.31	5.43	0.29	4.08
U_{cond}	12.03	12.03	-3.76	7.73	-10.36	10.84	-0.70	10.21
\dot{m}_{ref}	7.17	9.09	4.22	8.74	9.01	10.40	6.80	9.41
\dot{Q}_{evap}	-2.59	3.14	10.25	10.25	11.89	11.89	6.52	8.43
\dot{Q}_{cond}	1.73	4.72	9.98	10.66	14.59	14.69	8.77	10.02
\dot{W}_{comp}	4.57	6.37	-0.20	4.93	7.91	8.93	4.09	6.74
COP_c	-0.76	10.23	6.68	7.11	0.27	3.56	-0.93	6.97
COP_h	-0.04	2.56	13.79	13.79	9.38	9.38	7.72	8.58

It is important to note that MPE reveals the directional bias of the error, indicating whether values are consistently overestimated (positive MPE) or underestimated (negative MPE). In contrast, MAPE represents the magnitude of the error without regard to direction, with higher MAPE values indicating greater variability in error for a given refrigerant and variable, and lower MAPE values suggesting greater consistency. In the scientific literature on refrigeration models, an acceptable error range for model predictions often falls within 5–10% for most performance parameters, such as energy efficiency, heat transfer, and flow rates. This range is generally considered satisfactory for practical applications, though it may vary based on model design and parameter sensitivity (Li et al. 2024).

The heat transfer coefficient for the evaporator generally shows a MAPE below 6% for all fluids. However, the heat transfer coefficient for the condenser has a higher average MAPE, around 10% for all fluids. This difference is illustrated in Figure 17, which reveals a greater dispersion in the experimental data for the condenser's heat transfer coefficient compared to that of the evaporator. This variation in data dispersion makes it challenging for the model correlation to fully capture the experimental behavior.

The mass flow rate exhibited a similar pattern across all fluids, showing consistent overestimation with an average MPE of 6.8%. This relatively accurate prediction can be attributed to the volumetric efficiency, as shown in Figure 18, which had a regression coefficient above 0.9.

For the heat transfer prediction in the evaporator and condenser, the results were satisfactory for R134a, with errors below 5%. However, for R513A and R516A, the error exceeded 10%, likely due to the lower variability in the experimental data for R134a, as shown in Figure 15. Another contributing factor could be the differences in the boiling and condensation correlations used in the model. These correlations are calibrated with few data and might not perfectly account for the thermodynamic and transport property variations of R513A and R516A. For instance, the heat transfer performance is influenced by the refrigerant-specific coefficients in the correlations, which may lead to discrepancies when applied to blends like R513A and R516A. Addressing this limitation may require adapting or recalibrating the correlations to better match the experimental data for these fluids.

Finally, the model achieved an absolute error below 10%, which is attributed to the use of a specific regression for isentropic efficiency tailored to each fluid. Following the same trend, the parameters related to the evaporator exhibited better performance (lower error rate) compared to those associated with the condenser. Consequently, the cooling COP showed relatively low errors across all fluids, with an MPE of -0.93% and an MAPE of 6.97%. However, the heating COP had larger errors, with MPE and MAPE values of 7.72% and 8.58%, respectively.

These results suggest that the model effectively predicts the performance of the refrigeration system, demonstrating a strong correlation between the experimental and predicted data. Figures 19 to 21 further analyze the model accuracy by examining whether data points fall within acceptable error ranges for each parameter. For temperature prediction, a range of $\pm 1^\circ\text{C}$ was selected to assess the model's ability to capture experimental variations. For other parameters, a threshold of $\pm 10\%$ was used.

In Figure 19, the model accuracy in estimating evaporator parameters - particularly the evaporation temperature - is confirmed, with most data points within the $\pm 1^\circ\text{C}$ range. In contrast, the condensation temperature shows several points outside the range. Figure 20 indicates a slight tendency for the model to overestimate the condenser heat load, while it performs well in estimating the evaporator heat load and compressor work. The overestimation of the condenser heat load, as shown in Figure 20, could be due to inaccuracies in the condensation correlation, especially at low cooling capacities. This is because, at these lower capacities, the refrigerant may not experience a well-defined condensing process, leading to errors in the calculation of heat transfer. Finally, Figure 21 reveals that for the cooling COP, the majority of data points fall within the $\pm 10\%$ range. However, for the heating COP, a notable number of points lie outside this range, indicating greater variability in the heating performance predictions.

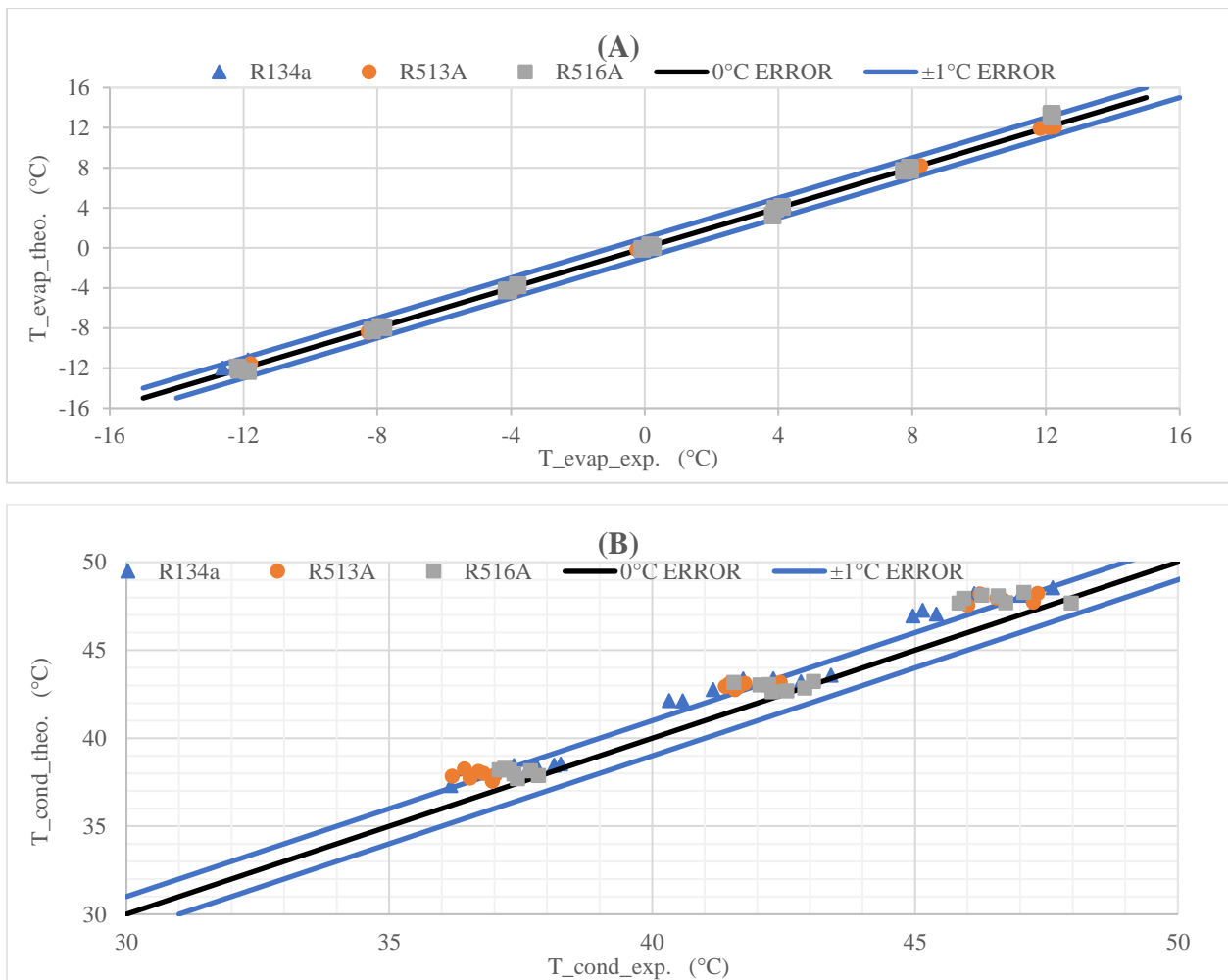


Figure 19: Theoretical vs experimental T_{evap} and T_{cond} .

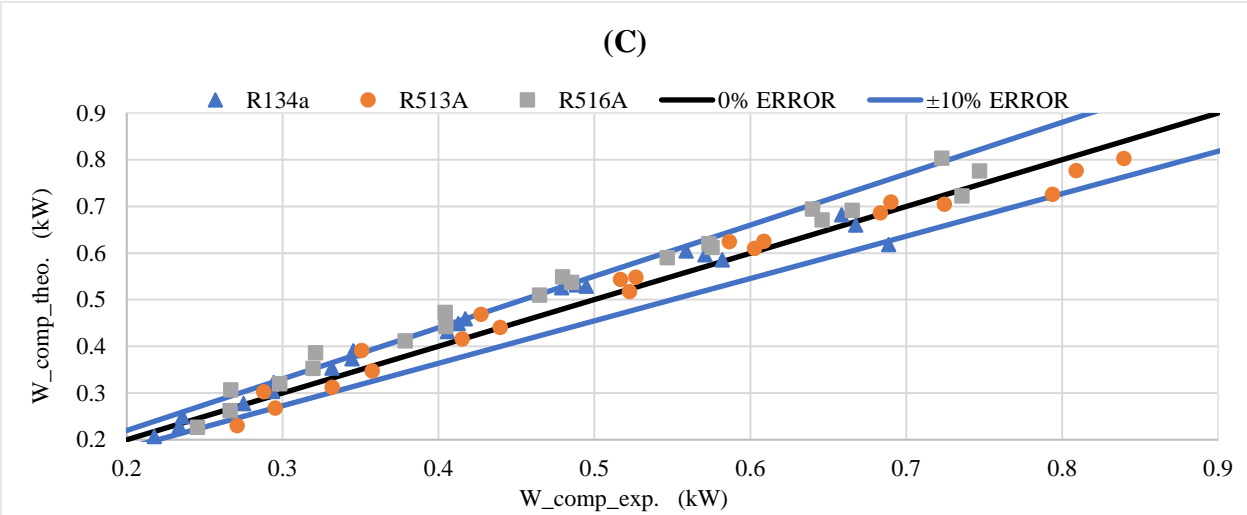
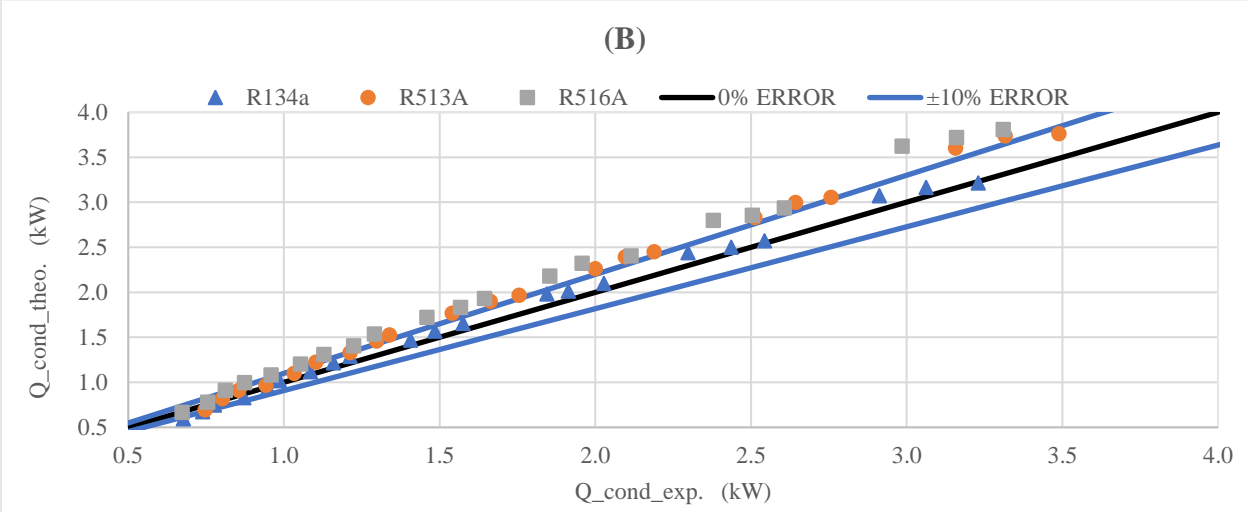
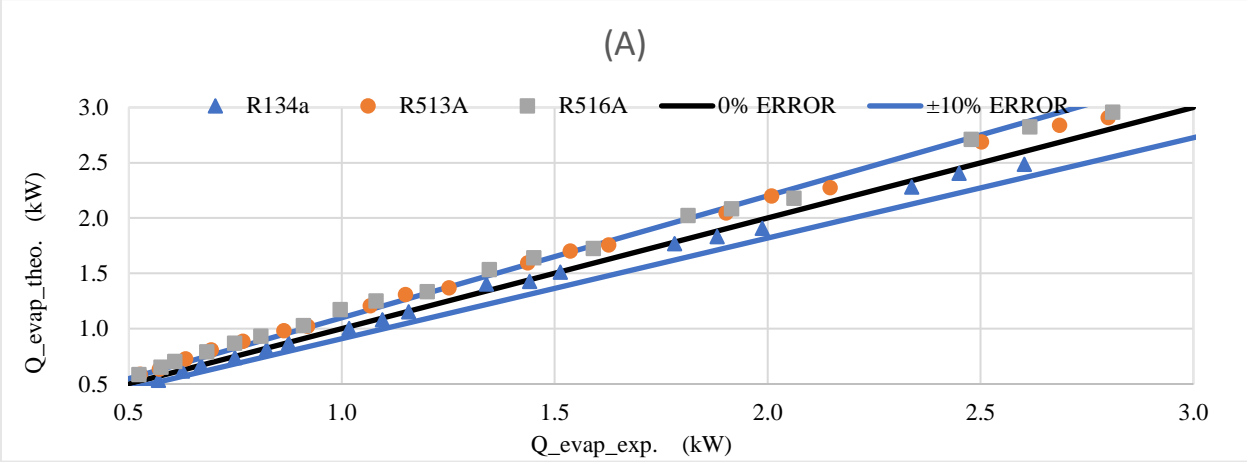


Figure 20: Theoretical vs experimental Q_{evap} , Q_{cond} , and W_{comp} .

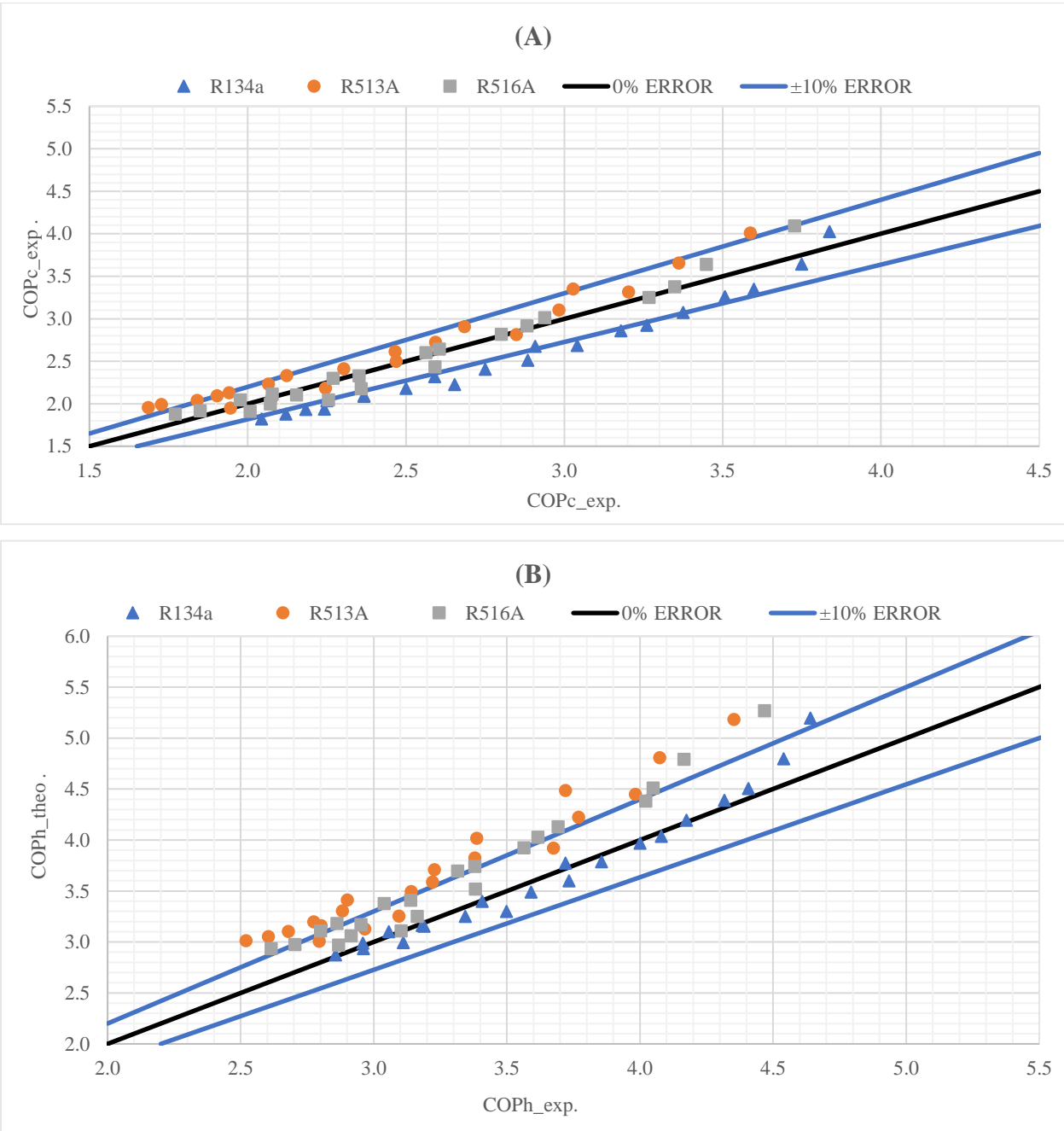


Figure 21: Theoretical vs experimental COP for cooling and heating.

Analysis of the experimental data presented in Appendix 1 revealed greater variability in controlling the condensation temperature. Specifically, the temperature difference between the water and the refrigerant in the condenser was smaller and more variable than that observed in the

evaporator for each test and fluid. This variability impacted the comparison with the condenser model, yet the results still fell within the acceptable error range, indicating the model robustness despite these fluctuations.

4.3. Simulation of systems

As explained in Section 3.5, the validated model is used to analyze and study the performance trends of the heat pump in two scenarios involving variations in the flow rate and inlet temperature of the water-glycol mixture in the evaporator and the water in the condenser. In all cases, the three refrigerants—R134a, R513A, and R156A—are simulated, with the main results focusing on the COP in cooling and heating modes. Tables 4 and 5 present the results obtained for the 36 simulated conditions per scenario. Regarding fluid performance differences, the trends are clear. In some cases, R134a achieves a higher COP than the other two fluids, R513A and R516A, while in other cases, the order reverses. The most important conclusion is that R513A and R516A exhibit similar behavior.

To better visualize the trends, Figure 22 illustrates the effects of the four variables on the R134a refrigerant. Figure 22A shows that, with fixed condenser conditions, increasing the inlet temperature or flow rate of the water-glycol mixture has no significant effect on COP. As expected, the cooling COP is lower than the heating COP due to the additional compressor work, which is converted into heat transferred in the condenser. Figure 22B presents conditions with a fixed evaporator, varying the inlet temperature and flow rate of the condenser water. While the condenser water temperature does not produce significant changes in the system COP, the flow rate does, as each increase results in a better COP. This improvement is likely because the condenser is slightly oversized, so a higher flow rate enhances the overall heat transfer coefficient. In contrast, the evaporator is ideally sized, so increases in temperature or flow rate do not further impact machine performance. Figure 23 shows the same behavior, even across different temperature ranges in both the evaporator and the condenser.

Table 4: Simulation results for the medium-temperature scenario.

Inputs				R134a		R513A		R516A	
\dot{m}_{w_e}	$T_{in_{w_e}}$	\dot{m}_{w_c}	$T_{in_{w_c}}$	COP_c	COP_h	COP_c	COP_h	COP_c	COP_h
0.05	0	0.05	35	1.91	2.97	1.82	2.87	1.81	2.86
0.05	0	0.05	40	1.93	2.99	1.83	2.88	1.87	2.92
0.05	0	0.10	35	2.28	3.35	2.28	3.36	2.27	3.35
0.05	0	0.10	40	2.31	3.39	2.36	3.44	2.39	3.48
0.05	0	0.15	35	2.47	3.56	2.46	3.54	2.45	3.54
0.05	0	0.15	40	2.48	3.57	2.55	3.64	2.52	3.61
0.05	5	0.05	35	1.82	2.87	1.66	2.70	1.66	2.70
0.05	5	0.05	40	1.84	2.89	1.67	2.72	1.70	2.74
0.05	5	0.10	35	2.25	3.32	2.05	3.12	2.07	3.14
0.05	5	0.10	40	2.26	3.34	2.12	3.19	2.15	3.22
0.05	5	0.15	35	2.37	3.45	2.19	3.26	2.21	3.28
0.05	5	0.15	40	2.45	3.53	2.29	3.37	2.26	3.34
0.10	0	0.05	35	2.12	3.19	2.14	3.21	2.09	3.16
0.10	0	0.05	40	2.14	3.21	1.70	2.74	1.72	2.76
0.10	0	0.10	35	2.33	3.37	2.57	3.66	2.51	3.60
0.10	0	0.10	40	2.29	3.36	2.48	3.57	2.51	3.60
0.10	0	0.15	35	2.63	3.72	2.91	4.02	2.87	3.98
0.10	0	0.15	40	2.57	3.66	2.82	3.92	3.06	4.18
0.10	5	0.05	35	2.04	3.11	1.94	3.00	1.92	2.98
0.10	5	0.05	40	2.08	3.15	1.96	3.01	1.98	3.04
0.10	5	0.10	35	2.52	3.61	2.62	3.71	2.58	3.67
0.10	5	0.10	40	2.50	3.58	2.58	3.67	2.61	3.71
0.10	5	0.15	35	2.92	4.04	3.01	4.12	3.00	4.10
0.10	5	0.15	40	2.90	4.01	3.01	4.13	3.05	4.17
0.15	0	0.05	35	2.17	3.24	2.18	3.25	2.12	3.19
0.15	0	0.05	40	2.27	3.35	1.59	2.63	1.61	2.65
0.15	0	0.10	35	2.22	3.29	2.39	3.47	2.33	3.41
0.15	0	0.10	40	2.15	3.22	2.25	3.33	2.27	3.34
0.15	0	0.15	35	2.42	3.51	2.80	3.91	2.73	3.83
0.15	0	0.15	40	2.36	3.44	2.65	3.75	3.23	4.36
0.15	5	0.05	35	2.09	3.16	1.98	3.04	1.98	3.04
0.15	5	0.05	40	2.14	3.21	2.02	3.08	2.08	3.14
0.15	5	0.10	35	2.40	3.48	2.55	3.65	2.50	3.59
0.15	5	0.10	40	2.29	3.37	2.45	3.54	2.51	3.60
0.15	5	0.15	35	2.86	3.96	3.09	4.21	3.03	4.15
0.15	5	0.15	40	2.81	3.91	3.27	4.40	3.31	4.44

Table 5: Simulation results for the high-temperature scenario.

Inputs				R134a		R513A		R516A	
\dot{m}_{w_e}	$T_{in_{w_e}}$	\dot{m}_{w_c}	$T_{in_{w_c}}$	COP_c	COP_h	COP_c	COP_h	COP_c	COP_h
0.05	10	0.05	50	1.78	2.83	1.64	2.68	1.66	2.70
0.05	10	0.05	55	1.83	2.88	1.78	2.83	1.79	2.84
0.05	10	0.10	50	2.24	3.31	2.07	3.14	2.10	3.16
0.05	10	0.10	55	2.38	3.46	2.20	3.27	2.22	3.29
0.05	10	0.15	50	2.43	3.52	2.16	3.23	2.18	3.25
0.05	10	0.15	55	2.49	3.58	2.35	3.43	2.37	3.45
0.05	15	0.05	50	1.59	2.63	1.41	2.44	1.44	2.46
0.05	15	0.05	55	1.64	2.68	1.48	2.51	1.50	2.53
0.05	15	0.10	50	1.98	3.04	1.74	2.79	1.76	2.80
0.05	15	0.10	55	2.08	3.15	1.84	2.89	1.87	2.92
0.05	15	0.15	50	2.11	3.18	1.78	2.83	1.82	2.87
0.05	15	0.15	55	2.16	3.23	1.90	2.95	1.92	2.98
0.10	10	0.05	50	2.05	3.11	1.59	2.63	1.62	2.66
0.10	10	0.05	55	1.75	2.80	1.72	2.76	1.73	2.78
0.10	10	0.10	50	2.68	3.78	2.70	3.80	2.74	3.84
0.10	10	0.10	55	2.70	3.80	2.92	4.03	2.94	4.05
0.10	10	0.15	50	3.06	4.20	3.10	4.22	3.12	4.25
0.10	10	0.15	55	3.20	4.33	3.25	4.38	3.27	4.40
0.10	15	0.05	50	1.86	2.92	1.69	2.74	1.72	2.76
0.10	15	0.05	55	1.93	2.98	1.48	2.51	1.51	2.54
0.10	15	0.10	50	2.63	3.72	2.53	3.62	2.57	3.66
0.10	15	0.10	55	2.70	3.80	2.65	3.75	2.68	3.78
0.10	15	0.15	50	3.08	4.20	2.87	3.99	2.92	4.03
0.10	15	0.15	55	3.13	4.25	2.99	4.11	3.02	4.14
0.15	10	0.05	50	2.15	3.22	1.45	2.48	1.47	2.51
0.15	10	0.05	55	1.64	2.68	1.56	2.59	1.57	2.61
0.15	10	0.10	50	2.56	3.65	2.62	3.72	2.67	3.76
0.15	10	0.10	55	2.52	3.61	3.11	4.23	3.13	4.26
0.15	10	0.15	50	3.07	4.19	3.42	4.56	3.45	4.60
0.15	10	0.15	55	3.44	4.58	3.57	4.71	3.59	4.74
0.15	15	0.05	50	1.92	2.97	1.72	2.77	1.75	2.80
0.15	15	0.05	55	1.98	3.04	1.34	2.36	1.36	2.38
0.15	15	0.10	50	2.63	3.72	2.62	3.71	2.63	3.73
0.15	15	0.10	55	2.63	3.73	2.69	3.79	2.73	3.83
0.15	15	0.15	50	3.23	4.36	3.30	4.44	3.34	4.48
0.15	15	0.15	55	3.46	4.60	3.42	4.56	3.45	4.59

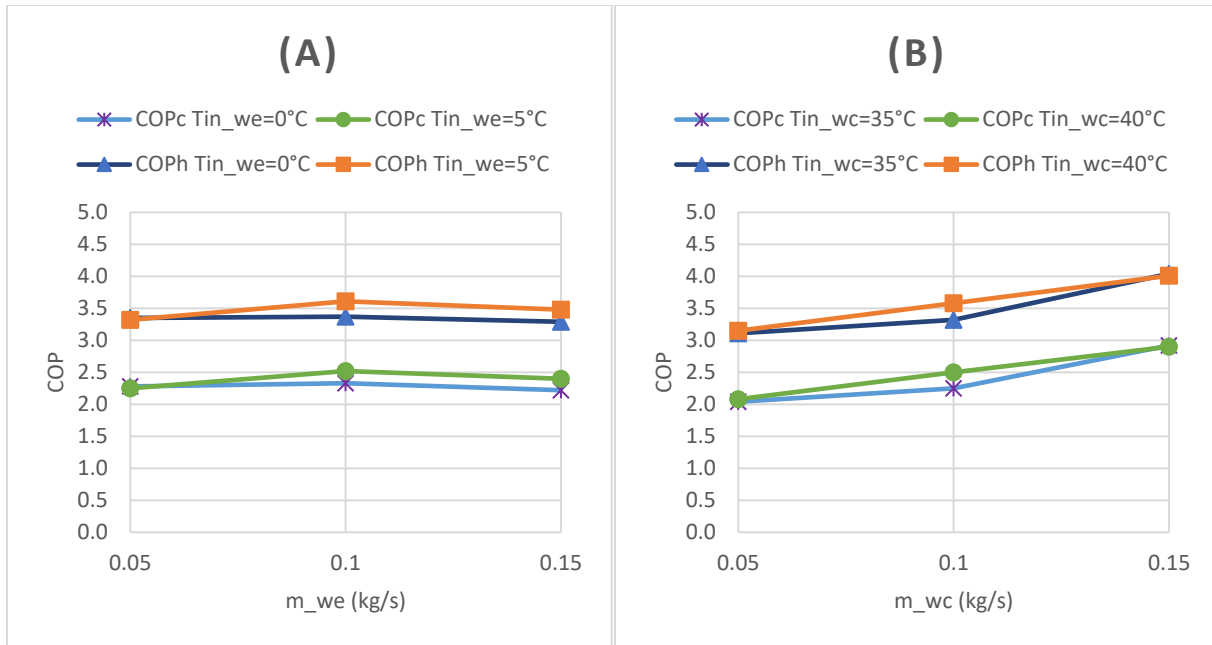


Figure 22: COP vs mass flow rate of water for R134a: (A) $\dot{m}_{w_c} = 0.1 \text{ kg/s}$ and $T_{in_{w_c}} = 35 \text{ }^\circ\text{C}$.
 (B) $\dot{m}_{w_e} = 0.1 \text{ kg/s}$ and $T_{in_{w_e}} = 5 \text{ }^\circ\text{C}$.

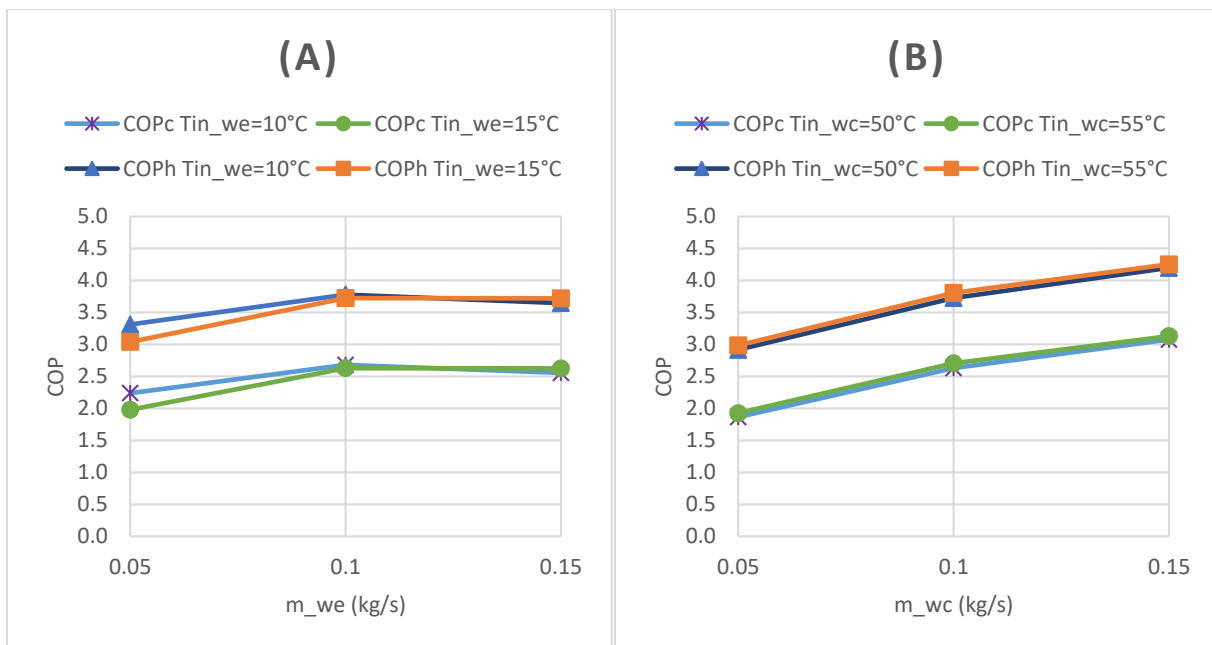


Figure 23: COP vs mass flow rate of water for R134a: (A) $\dot{m}_{w_c} = 0.1 \text{ kg/s}$ and $T_{in_{w_c}} = 50 \text{ }^\circ\text{C}$.
 (B) $\dot{m}_{w_e} = 0.1 \text{ kg/s}$ and $T_{in_{w_e}} = 15 \text{ }^\circ\text{C}$.

Figure 24 provides a detailed examination of the impact of water flow variation in both the evaporator and condenser with the heat pump operating on R134a. This analysis is presented through a heat map, with two distinct conditions inlet temperature conditions: one at 0°C and 40°C (Scenario 1) and another at 15°C and 55°C (Scenario 2) for the evaporator and condenser, respectively. In the first condition (Scenario 1), while variations in flow rates do not result in a significant spread between the lowest and highest COP values, there is still a noticeable trend where increasing the water flow rate in the condenser positively improves the COP. On the other hand, the optimal water-glycol flow rate of 0.1 kg/s in the evaporator for maximizing COP can be used as a reference for similar systems. Higher temperatures increase the sensitivity of COP to flow rate changes, emphasizing the importance of optimizing flow for maximum efficiency in high-temperature conditions. The COP can increase by approximately 70% from its minimum to its maximum. As expected, the higher-temperature scenario (Scenario 2) also favors an increase in COP, indicating that temperature conditions play a pivotal role in optimizing the heat pump efficiency.

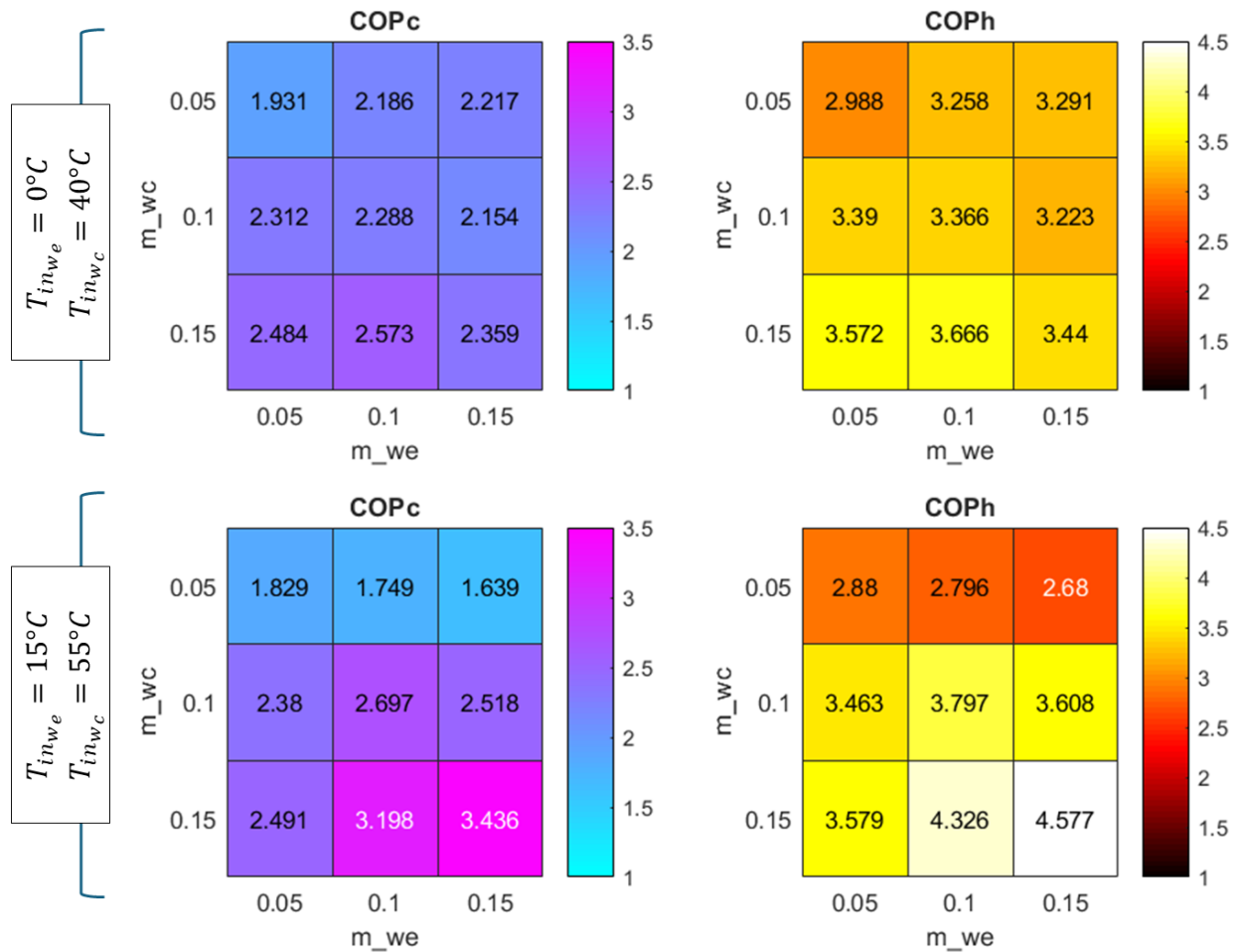


Figure 24: COP vs mass flow rate of water for R134a for two scenarios.

Finally, to provide a more detailed comparison between fluids, Figure 25 presents COP_c and COP_h for four conditions with water flow rates of 0.15 kg/s in both the evaporator and condenser. The results indicate a slight performance advantage for R516A, followed closely by R513A and R134a. This difference is more pronounced under the conditions of scenario 1. In Scenario 2, with higher temperatures—representative of potential applications in waste heat recovery systems operating in simultaneous cooling and heating mode—all three fluids perform effectively, with an average COP_c and COP_h values of 3.3 and 4.6, respectively. These findings align with reports from other studies that highlight the strong potential of low-GWP blends like R513A and R516A as viable replacements for the higher-GWP fluid, R134a.

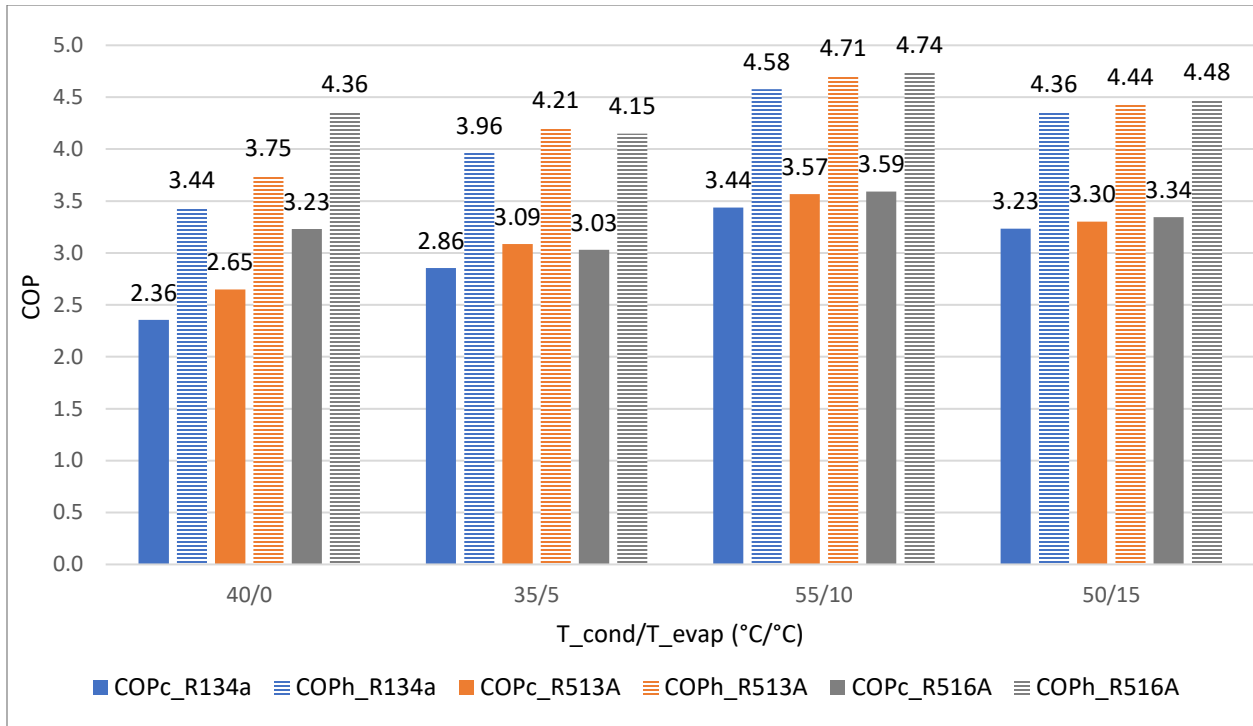


Figure 25: COP for all fluids, with $\dot{m}_{w_c} = 0.15 \text{ kg/s}$ and $\dot{m}_{w_e} = 0.15 \text{ kg/s}$.

5. CONCLUSION AND FUTURE WORKS

5.1. Conclusion

This research has successfully evaluated the performance of low-GWP refrigerants R513A and R516A as alternative solutions to R134a in simultaneous heating and cooling systems, focusing on their thermodynamic behavior and system efficiency under varying operational conditions. Through mathematical modeling and experimental validation, this study provided insights into the efficiency of R513A and R516A compared to R134a under different operational scenarios. The results demonstrated that, although R134a occasionally achieved a higher COP, R513A and R516A showed comparable and often favorable performance, particularly in scenarios involving heat recovery. This aligns with global sustainability goals, reinforcing the potential of these alternative refrigerants to reduce greenhouse gas emissions while maintaining energy efficiency.

Key outcomes were:

- **Comparable COP Performance:** Across both medium- and high-temperature scenarios, R513A and R516A achieved coefficients of performance (COPs) values similar to those of R134a. For instance, for the three fluids, the average COP in cooling mode (COP_c) was 3.3, while in heating mode (COP_h) it was 4.6 across the tested conditions, indicating that these refrigerants can effectively replace R134a in heat pump applications without significant efficiency losses.
- **High-Temperature Advantage for R516A:** Under high-temperature scenarios (e.g., condenser inlet temperatures of 50–55°C), R516A demonstrated a measurable advantage, achieving slightly higher COP values than R134a. This makes R516A particularly suitable for applications requiring greater thermal resilience, such as waste heat recovery systems.
- **Impact of Operational Conditions:** COP variability across different scenarios, highlighted the influence of operational parameters, including secondary fluid flow rates and inlet temperatures on system performance. For instance, lower mass flow rates (0.05 kg/s) generally reduced the system's overall COP, while higher mass

flow rates (0.15 kg/s) improved heat transfer and energy efficiency. These findings offer critical insights into optimizing heat pump performance for specific operational demands.

In conclusion, this study confirms that R513A and R516A are promising replacements for R134a refrigerants in heat pumps designed for simultaneous heating and cooling systems. These refrigerants exhibit lower global warming potential (GWP) while maintaining competitive coefficients of performance (COP) under diverse operating conditions. Their ability to achieve efficient performance in both heating and cooling modes highlights their operational flexibility and suitability for practical applications. These findings position R513A and R516A as effective alternatives that balance energy efficiency and system reliability, contributing to the advancement of next-generation refrigerant technologies.

5.2.Future works

Future research can build upon this work by:

- **Enhancing the Mathematical Model:** Improvements could focus on two key areas. First, expanding the dataset with extra experimental data, particularly with refined control over condenser conditions, to increase model accuracy. Second, applying AI-based methods to calculate the volumetric and isentropic efficiency of compressor, as well as the heat transfer coefficients of refrigerants in both the evaporator and condenser, could further enhance predictive capabilities.
- **Expanding Operating Conditions:** Investigating the performance of these refrigerants across a broader range of temperatures and flow rates will help determine their suitability for diverse climates and industrial processes. Such studies could identify optimal operational boundaries and guide usage recommendations for R513a and R516A in varied environments.
- **Optimization of Design and Control Strategies:** Future work can explore advanced design and control strategies for simultaneous heating and cooling applications. By incorporating dynamic control based on real-time demand changes, it may be

possible to improve COP and enhance energy efficiency under varying load conditions.

- **Lifecycle and Environmental Impact Assessment:** Conducting a comprehensive lifecycle assessment would allow for a more comprehensive evaluation of the environmental benefits of adopting R513A and R516A. This assessment could quantify both direct and indirect emissions, energy consumption, and end-of-life impacts, providing clearer insights into the long-time sustainability benefits of these low-GWP refrigerants.
- **Exploring Alternative low-GWP Refrigerants:** Future studies could also evaluate additional low-GWP refrigerants or blends that may offer similar or improved thermodynamic properties. Comparative analyses of various refrigerants in simultaneous heating and cooling systems could broaden the options for sustainable alternatives, enabling better alignment with global climate targets.

REFERENCE

AISSANI, H.; ZID, S.; BENCHARIF, M. Analysis of a simple vapor compression and ejector refrigeration systems working with eco-friendly refrigerants. **Journal of Renewable Energies**, v. 27, n. 2, 25 dez. 2024.

AL-SAYYAB, A. K. S. et al. Comprehensive experimental evaluation of R1234yf-based low GWP working fluids for refrigeration and heat pumps. **Energy Conversion and Management**, v. 258, 15 abr. 2022.

BELMAN-FLORES, J. M. et al. Experimental evaluation of R513A as a low GWP refrigerant to replace R134a in a domestic refrigerator. **International Journal of Refrigeration**, v. 142, p. 148–155, 1 out. 2022.

BELMAN-FLORES, J. M. et al. Drop-In Replacement of R134a in a Household Refrigerator with Low-GWP Refrigerants R513A, R516A, and R1234ze(E). **Energies**, v. 16, n. 8, p. 3422, 13 abr. 2023.

BLANCO OJEDA, F. W. A. et al. Experimental evaluation of low-GWP refrigerants R513A, R1234yf and R436A as alternatives for R134a in a cascade refrigeration cycle with R744. **International Journal of Refrigeration**, v. 144, p. 175–187, 1 dez. 2022.

BOBBO, S. et al. **A Technological Update on Heat Pumps for Industrial Applications**. **Energies** Multidisciplinary Digital Publishing Institute (MDPI), , 1 out. 2024.

BYRNE, P. Research Summary and Literature Review on Modelling and Simulation of Heat Pumps for Simultaneous Heating and Cooling for Buildings. **Energies 2022, Vol. 15, Page 3529**, v. 15, n. 10, p. 3529, 11 maio 2022a.

BYRNE, P. Modelling and Simulation of Heat Pumps for Simultaneous Heating and Cooling, a Special Issue. **Energies 2022, Vol. 15, Page 5933**, v. 15, n. 16, p. 5933, 16 ago. 2022b.

CHAVHAN, S. P.; POONAWALA, N. S.; GAWANDE, J. S. An Alternative Refrigerant to R134a in VCR System-A Review. **Engineering**, 2019.

CONTE, R. et al. Experimental investigation of large scroll compressors working with six low-GWP refrigerants. **Thermal Science and Engineering Progress**, v. 44, 1 set. 2023.

DAĞDIR, K.; BILEN, K. Usage of R513A as an alternative to R134a in a refrigeration system: An experimental investigation based on the Kigali amendment. **International Journal of Thermofluids**, v. 21, 1 fev. 2024.

DANFOSS A/S. © Danfoss A/S (RC-MCGP sw) 2014-11 Catalogue | **Heat Hexchanger**. [s.l: s.n.].

DANFOSS A/S. © Danfoss | **Climate Solutions | 2021.11 (Maneurop reciprocating compressors MT-MTZ)**. [s.l: s.n.].

DIREK, M.; SOYLU, E. The effect of internal heat exchanger using R1234ze(E) as an alternative refrigerant in a mobile air-conditioning system. **Journal of Mechanical Engineering**, v. 64, n. 2, p. 114–120, 2018.

DOMANSKI, P. A.; YANA MOTTA, S. **Low-GWP Refrigerants Status and Outlook**. Gaithersburg: [s.n.].

DUBEY, S. et al. Energy, environmental and economic analysis of low GWP refrigerant heat pumps for simultaneous heating and cooling applications. **Thermal Science and Engineering Progress**, v. 51, 1 jun. 2024.

EHPA. **What's a Heat Pump?**

FERNANDO, P. et al. Propane heat pump with low refrigerant charge: design and laboratory tests. **International Journal of Refrigeration**, v. 27, n. 7, p. 761–773, 1 nov. 2004.

GIRIP, A.; ILIE, A.; CALOTA, R. **Comparative study regarding retrofitting with a low GWP refrigerant in an ice rink with energy recovery implementation.** IOP Conference Series: Earth and Environmental Science. **Anais...Institute of Physics**, 2023. Disponível em: <<https://iopscience.iop.org/article/10.1088/1755-1315/1185/1/012012/pdf>>. Acesso em: 13 set. 2023

HU, Y. et al. Study on the impacts of refrigerant leakage on the performance and environmental benefits of heat pumps using R513A as replacement of R134a. **International Journal of Refrigeration**, v. 168, p. 399–410, 1 dez. 2024.

INCROPERA, F. **Fundamentals Of Heat And Mass Transfer.** [s.l.] Wiley, 1996. v. v7

ISLAM, M. A. et al. Thermodynamic and Environmental Assessment of Low-GWP Alternative Refrigerants for Domestic Cooling. **Journal of The Institution of Engineers (India): Series C**, v. 104, n. 2, 2023.

KERSEY, M. **Refrigerant Update: Hydrofluoroolefins (HFOs) and Future Architectures.** US: [s.n.]. Disponível em: <https://www.epa.gov/system/files/documents/2022-10/GC.Webinar-HFOs_2022.08.30_1.pdf>. Acesso em: 9 set. 2023.

KIM, S. et al. **Very Low GWP Refrigerant R-516A for R-134a replacement in Very Low GWP Refrigerant R-516A for R-134a replacement in Commercial Refrigeration Commercial Refrigeration Very Low GWP Refrigerant R-516A for R-134a replacement in Commercial Refrigeration.** [s.l: s.n.]. Disponível em: <<https://docs.lib.purdue.edu/iracc>>.

KUMAR, S. Y.; BHASKAR, H. B.; LOHITH, M. BASAVARAJU. N. Experimental Thermal Performance Comparison in the condenser of Heat Pump System using R22 and R134a Refrigerants. **International Journal of Research Publication and Reviews**, v. 5, n. 12, p. 941–946, dez. 2024.

LI, G. Performance evaluation of low global warming potential working fluids as R134a alternatives for two-stage centrifugal chiller applications. **Korean Journal of Chemical Engineering**, v. 38, n. 7, p. 1438–1451, 1 jul. 2021.

LI, K. et al. Refined one-dimensional modeling and experimental validation of scroll compressor with vapor injection for electric vehicles. **International Journal of Refrigeration**, v. 168, p. 469–483, 1 dez. 2024.

LI, W.; HRNJAK, P. Quantification of two-phase refrigerant distribution in brazed plate heat exchangers using infrared thermography. **International Journal of Refrigeration**, v. 131, p. 348–358, 1 nov. 2021.

LIU, Y. et al. Surface tension and parachor for a new low-GWP refrigerant R1123/R32/R1234yf and its constituent binary pairs. **International Journal of Refrigeration**, v. 132, p. 276–292, 1 dez. 2021.

LONGO, G. A. Heat transfer and pressure drop during HFC refrigerant saturated vapour condensation inside a brazed plate heat exchanger. **International Journal of Heat and Mass Transfer**, v. 53, n. 5–6, p. 1079–1087, 1 fev. 2010.

LONGO, G. A. et al. A new model for refrigerant boiling inside Brazed Plate Heat Exchangers (BPHEs). **International Journal of Heat and Mass Transfer**, v. 91, p. 144–149, 1 dez. 2015.

LONGO, G. A. et al. HFO1234ze(E) vaporisation inside a Brazed Plate Heat Exchanger (BPHE): Comparison with HFC134a and HFO1234yf. **International Journal of Refrigeration**, v. 67, p. 125–133, 1 jul. 2016.

LONGO, G. A. et al. Local heat transfer coefficients of R32 and R410A boiling inside a brazed plate heat exchanger (BPHE). **Applied Thermal Engineering**, v. 215, 1 out. 2022.

LONGO, G. A.; GASPARELLA, A. Refrigerant R134a vaporisation heat transfer and pressure drop inside a small brazed plate heat exchanger. **International Journal of Refrigeration**, v. 30, n. 5, p. 821–830, ago. 2007.

MÉNDEZ-MÉNDEZ, D.; PÉREZ-GARCÍA, V.; MORALES-FUENTES, A. Experimental Energy Evaluation Of R516a And R513a As Replacement Of R134a In Refrigeration And Air Conditioning Modes. **International Journal of Refrigeration**, jun. 2023.

MODI, S. D.; AHIR, S. N.; STUDENT, M. E. **Issue 1 | ISSN: 2456-3315 IJRTI1801004 International Journal for Research Trends and Innovation© 2018 IJRTI** |. [s.l: s.n.]. Disponível em: <www.ijrti.org>.

MOTA-BABILONI, A. et al. Experimental exergy analysis of R513A to replace R134a in a small capacity refrigeration system. **Energy**, v. 162, p. 99–110, 1 nov. 2018.

MOTA-BABILONI, A. et al. Experimental influence of an internal heat exchanger (IHx) using R513A and R134a in a vapor compression system. **Applied Thermal Engineering**, v. 147, p. 482–491, 25 jan. 2019.

PABON, J. J. G. et al. **Applications of refrigerant R1234yf in heating, air conditioning and refrigeration systems: A decade of researches. International Journal of Refrigeration** Elsevier Ltd, , 1 out. 2020.

PADMAVATHY, S. R. et al. Performance studies of low GWP refrigerants as environmental alternatives for R134a in low-temperature applications. **Environmental Science and Pollution Research**, 1 dez. 2021.

PRASAD, U. S. et al. Experimental and Simulation Study of the Latest HFC/HFO and Blend of Refrigerants in Vapour Compression Refrigeration System as an Alternative of R134a. **Processes**, v. 11, n. 3, 1 mar. 2023.

REGULATION (EU) NO 517/2014. Regulation (EU) No 517/2014. **Official Journal of the European Union**, n. fluorinated greenhouse gases and repealing Regulation (EC) No 842/2006, 16 abr. 2014.

SARRAF, K.; LAUNAY, S.; TADRIST, L. Analysis of enhanced vapor desuperheating during condensation inside a plate heat exchanger. **International Journal of Thermal Sciences**, v. 105, p. 96–108, 1 jul. 2016.

SCHULTZ, K.; KUJAK, S.; MAJURIN, J. **Assessment of next generation refrigerant R513A to replace R134a for chiller products**. Refrigeration Science and Technology. **Anais...International Institute of Refrigeration**, 2015. Disponível em: <<https://iifir.org/fr/fridoc/evaluation-du-frigorigene-r513a-de-la-prochaine-generation-pour-31199>>. Acesso em: 14 set. 2023

TOFFOLETTI, G. et al. Experimental comparison of cycle modifications and ejector control methods using variable geometry and CO₂ pump in a multi-evaporator transcritical CO₂ refrigeration system. **International Journal of Refrigeration**, v. 169, p. 226–240, 1 jan. 2025.

TRANE. Introduction to Decarbonization in HVAC. <https://www.trane.com/content/dam/Trane/Commercial/global/learning-center/engineers-newsletters/ADM-APN082-EN.pdf>, 2022.

UNEP. **OZONACTION FACT SHEET Refrigerant Blends: Calculating Global Warming Potentials**. 1 rue Miollis, Building VII Paris 75015, France: [s.n.]. Disponível em: <<http://ozone.unep.org/en/assessment-panels>>.

UNEP. **The Montreal Protocol on Substances that Deplete the Ozone Layer**. Disponível em: <<https://ozone.unep.org/treaties/montreal-protocol-substances-deplete-ozone-layer/text>>. Acesso em: 5 set. 2023.

UNITED NATIONS. **Kigali Montreal Protocol**. Disponível em: <<https://www.unep.org/ozonaction/who-we-are>>. Acesso em: 5 set. 2023.

VACCARO, G. et al. Experimental results on a chiller using a CO₂-DME mixture. **International Journal of Refrigeration**, v. 168, p. 662–672, 1 dez. 2024.

VUPPALADADIYAM, A. K. et al. **Progress in the development and use of refrigerants and unintended environmental consequences. Science of the Total Environment** Elsevier B.V., , 1 jun. 2022.

YANG, M. et al. Experimental study on R1234yf/R134a mixture (R513A) as R134a replacement in a domestic refrigerator. **Applied Thermal Engineering**, v. 146, p. 540–547, 5 jan. 2019.

YASSER, Z. K.; OUDAH, M. H. Experimental Comparison of Flow Boiling Heat Transfer in Smooth and Microfin Tubes Using R134a, R1234yf, and R513A. **International Journal of Refrigeration**, dez. 2024.

YILDIZ, A.; YILDIRIM, R. Investigation of using R134a, R1234yf and R513A as refrigerant in a heat pump. **International Journal of Environmental Science and Technology**, v. 18, n. 5, p. 1201–1210, 1 maio 2021.

YOU, Y. The Optimal Ratio of the Temperature Differences for Heat Transfer in Evaporator and Condenser. **International Journal for Research in Applied Science and Engineering Technology**, v. 12, n. 12, p. 757–760, 31 dez. 2024.

ZHANG, Z. et al. Theoretical and experimental research on the performance of twin screw compressor using R513A as R134a replacement. **Proceedings of the Institution of Mechanical Engineers, Part E: Journal of Process Mechanical Engineering**, v. 235, n. 2, p. 170–177, 16 ago. 2020.

APPENDIX I. EXPERIMENTAL DATA

Table 6: Experimental data for R134a.

Expected T_{evap} (°C)			-12			-8			-4			0			4			8			12		
Expected T_{cond} (°C)			35	40	45	35	40	45	35	40	45	35	40	45	35	40	45	35	40	45	35	40	45
Evaporator	Temperature (°C)	IN	-12.62	-12.21	-11.87	-8.10	-7.91	-7.99	-4.15	-4.12	-3.96	-0.19	-0.16	-0.17	4.15	4.13	4.16	8.14	7.91	8.15	12.10	12.15	12.03
		OUT	-7.14	-6.92	-6.66	-2.34	-2.32	-2.16	0.98	1.17	1.46	4.28	4.92	4.91	8.99	9.43	9.78	12.24	12.67	13.50	15.56	16.43	17.04
	Pressure (bar)	OUT	1.81	1.84	1.86	2.16	2.18	2.17	2.51	2.52	2.53	2.91	2.91	2.91	3.39	3.39	3.40	3.89	3.86	3.90	4.45	4.45	4.43
Compressor	Temperature (°C)	IN	0.81	0.97	1.06	2.03	2.46	2.87	6.09	6.69	6.67	9.23	10.11	9.85	12.23	12.89	13.77	15.49	16.15	17.48	18.82	19.00	20.03
		OUT	86.21	88.80	90.42	84.08	87.21	88.69	81.34	84.18	85.97	78.68	81.23	83.27	75.93	78.27	80.57	73.22	75.27	77.86	70.52	72.29	75.17
	Pressure (bar)	IN	1.79	1.82	1.86	2.11	2.09	2.09	2.42	2.42	2.43	2.85	2.84	2.84	3.29	3.28	3.25	3.78	3.76	3.78	4.63	4.35	4.31
		OUT	9.66	11.08	12.36	9.63	10.92	12.17	9.54	10.77	11.92	9.49	10.60	11.90	9.43	10.44	11.68	9.18	10.28	11.54	9.12	10.21	11.60
Condenser	Temperature (°C)	IN	75.71	77.61	78.53	73.50	75.94	77.60	72.92	75.51	76.17	70.55	72.82	74.15	67.95	70.09	71.83	65.28	67.11	69.13	63.10	64.60	66.92
		OUT	36.06	41.16	45.12	36.11	39.96	45.04	35.13	40.16	45.12	35.16	40.14	45.15	35.19	39.64	44.69	35.10	40.10	43.84	35.11	39.97	44.12
	Pressure (bar)	OUT	9.54	10.97	12.26	9.55	10.75	11.97	9.34	10.60	11.80	9.22	10.41	11.51	9.14	10.24	11.28	9.10	10.10	11.23	9.01	9.91	11.01
EEV	Temperature (°C)	IN	32.89	37.35	40.87	33.10	36.51	40.20	31.61	36.58	41.52	32.13	36.99	41.87	32.52	36.81	41.99	32.41	37.28	41.95	32.83	37.69	42.68
	Pressure (bar)	IN	9.03	10.43	11.81	9.04	10.30	11.36	8.72	9.83	11.09	8.51	9.62	10.94	8.59	9.69	10.76	8.65	9.67	10.49	8.49	9.49	10.45
Refrigerant mass flow (kg/h)			12.70	12.44	11.58	16.43	16.11	15.20	21.05	20.73	19.84	27.46	27.03	26.28	35.35	34.67	34.15	45.38	44.68	44.02	58.36	57.52	56.92
Secondary Circuit Water-glycol	Temperature (°C)	IN	-6.63	-6.21	-5.87	-2.10	-1.91	-1.99	1.85	1.88	2.04	5.81	5.85	5.82	10.14	10.13	10.16	14.13	13.91	14.13	18.11	18.14	18.02
		OUT	-9.99	-9.63	-9.27	-5.81	-5.60	-5.71	-2.07	-2.07	-1.95	1.76	1.75	1.67	5.90	5.83	6.01	9.67	9.41	9.57	13.50	13.58	13.45
	Flow rate (L/s)		0.04	0.04	0.04	0.05	0.05	0.04	0.06	0.06	0.05	0.08	0.07	0.07	0.10	0.09	0.09	0.12	0.11	0.11	0.15	0.15	0.14
Secondary Circuit Water	Temperature (°C)	IN	30.08	35.18	40.14	30.14	34.98	40.05	30.16	35.17	40.13	29.78	35.16	40.14	30.21	34.66	38.89	30.11	34.01	38.83	29.12	33.97	39.13
		OUT	33.26	38.28	43.15	33.64	38.45	43.45	34.01	38.97	43.88	33.87	39.21	44.14	34.43	38.83	42.97	34.47	38.32	43.17	33.51	38.32	43.52
	Flow rate (L/s)		0.058	0.057	0.054	0.067	0.065	0.061	0.075	0.073	0.069	0.092	0.088	0.084	0.115	0.110	0.108	0.140	0.135	0.127	0.176	0.168	0.159

Table 7: Experimental data for R513A.

Expected T_{evap} (°C)			-12			-8			-4			0			4			8			12		
Expected T_{cond} (°C)			35	40	45	35	40	45	35	40	45	35	40	45	35	40	45	35	40	45	35	40	45
Evaporator	Temperature (°C)	IN	-12.18	-11.88	-11.80	-7.79	-8.27	-8.26	-3.94	-4.16	-3.88	-0.24	0.14	0.21	3.83	4.07	3.82	8.25	8.12	7.81	11.83	12.11	12.26
		OUT	-7.63	-7.02	-6.78	-2.01	-2.58	-2.31	1.56	1.58	1.71	4.41	4.52	5.45	8.76	8.87	9.40	12.63	12.63	12.85	16.37	16.28	16.15
	Pressure (bar)	OUT	2.09	2.11	2.12	2.46	2.42	2.42	2.83	2.81	2.84	3.22	3.27	3.27	3.70	3.73	3.70	4.29	4.27	4.22	4.80	4.85	4.87
Compressor	Temperature (°C)	IN	0.93	1.84	3.34	3.58	4.32	5.80	6.23	7.12	8.28	8.20	8.37	9.51	11.19	11.57	12.41	14.40	14.46	14.88	17.49	17.78	17.76
		OUT	84.50	89.63	91.80	81.41	85.34	88.28	79.33	83.92	86.48	77.22	78.79	83.43	71.21	75.64	78.51	68.60	71.25	76.51	65.90	69.05	73.10
	Pressure (bar)	IN	2.01	1.99	1.98	2.33	2.31	2.33	2.69	2.71	2.69	3.02	3.00	3.03	3.58	3.59	3.59	4.16	4.14	4.11	4.71	4.74	4.72
		OUT	9.83	11.31	12.79	9.82	11.26	12.77	9.77	11.12	12.59	9.75	11.07	12.55	9.68	11.02	12.45	9.71	11.09	12.38	9.62	11.04	12.36
Condenser	Temperature (°C)	IN	75.37	79.20	80.63	72.70	76.24	77.92	70.18	73.48	75.38	67.56	70.75	73.05	64.95	68.09	70.54	61.94	64.67	67.65	59.29	62.03	65.31
		OUT	34.83	40.17	45.15	34.74	39.88	45.02	35.12	40.15	45.00	35.15	39.94	45.14	35.20	40.15	45.05	34.82	40.09	44.77	34.91	40.17	44.89
	Pressure (bar)	OUT	9.61	11.09	12.41	9.55	11.06	12.35	9.50	10.97	12.28	9.45	10.90	12.25	9.38	10.86	12.19	9.35	10.78	12.14	9.28	10.72	12.07
EEV	Temperature (°C)	IN	29.16	36.45	39.54	32.73	37.81	40.80	32.50	36.56	42.15	29.82	36.86	41.35	32.18	36.33	40.78	31.63	37.08	40.30	32.41	36.26	40.59
	Pressure (bar)	IN	8.99	10.67	11.93	8.97	13.43	11.70	9.02	10.38	11.67	8.90	10.82	12.18	8.94	10.83	12.15	8.86	10.73	12.08	8.85	10.72	12.01
Refrigerant mass flow (kg/h)			12.70	12.44	15.20	14.98	13.90	19.93	19.81	18.40	25.77	25.51	24.20	33.57	33.16	32.36	43.31	42.77	42.16	55.53	55.31	54.04	71.65
Secondary Circuit Water-glycol	Temperature (°C)	IN	-6.17	-5.91	-5.85	-1.72	-2.24	-2.19	1.99	1.90	2.28	5.78	6.26	6.15	9.95	9.98	9.82	14.22	14.20	13.70	17.94	18.11	18.18
		OUT	-9.55	-9.36	-9.33	-5.45	-5.97	-5.96	-1.93	-2.07	-1.77	1.68	2.12	1.99	5.68	5.65	5.54	9.73	9.69	9.19	13.28	13.44	13.56
	Flow rate (L/s)		0.04	0.04	0.03	0.05	0.05	0.04	0.06	0.06	0.05	0.08	0.08	0.07	0.10	0.10	0.09	0.13	0.12	0.11	0.16	0.16	0.15
Secondary Circuit Water	Temperature (°C)	IN	29.86	35.16	40.15	29.65	34.92	39.77	30.05	35.22	39.99	30.07	34.85	40.04	30.24	35.02	40.24	29.73	35.06	39.61	29.83	35.16	39.94
		OUT	33.13	38.40	43.37	33.20	38.45	43.28	33.99	39.07	43.81	34.24	39.03	44.10	34.56	39.28	44.47	34.14	39.41	43.98	34.26	39.55	44.32
	Flow rate (L/s)		0.063	0.059	0.056	0.074	0.070	0.064	0.081	0.081	0.076	0.101	0.095	0.091	0.121	0.118	0.113	0.149	0.145	0.137	0.188	0.181	0.173

Table 8: Experimental data for R516A.

Expected T_{evap} (°C)			-12			-8			-4			0			4			8			12		
Expected T_{cond} (°C)			35	40	45	35	40	45	35	40	45	35	40	45	35	40	45	35	40	45	35	40	45
Evaporator	Temperature (°C)	IN	-12.17	-11.86	-12.14	-7.82	-8.15	-7.91	-3.80	-4.08	-4.14	0.16	0.24	-0.08	3.92	4.11	3.83	7.92	7.95	7.75	12.17	12.16	12.19
		OUT	-7.38	-7.53	-7.83	-2.08	-2.32	-2.33	1.31	0.66	0.85	4.94	4.37	4.54	8.44	8.40	9.29	13.31	13.05	13.18	17.28	17.87	17.79
	Pressure (bar)	OUT	2.06	2.08	2.06	2.42	2.39	2.41	2.79	2.77	2.76	3.20	3.21	3.18	3.64	3.66	3.63	4.15	4.15	4.12	4.74	4.74	4.75
Compressor	Temperature (°C)	IN	1.83	1.89	1.88	6.23	5.79	5.99	5.40	5.13	5.65	8.12	7.78	8.30	9.72	10.95	12.03	14.57	14.58	15.34	17.99	18.69	19.27
		OUT	83.57	86.85	87.87	80.73	84.01	85.06	77.48	81.14	82.27	74.42	78.23	79.51	71.44	75.33	76.75	68.59	72.76	73.97	65.61	69.57	71.27
	Pressure (bar)	IN	1.96	1.97	1.97	2.32	2.28	2.34	2.66	2.62	2.60	3.06	3.06	3.01	3.54	3.54	3.44	4.13	4.07	3.98	4.69	4.56	4.57
		OUT	9.78	11.17	12.61	9.74	11.13	12.34	9.67	11.03	12.24	9.64	10.95	12.19	9.59	10.89	12.10	9.66	10.93	12.00	9.61	10.75	11.97
Condenser	Temperature (°C)	IN	74.28	77.41	78.12	71.80	75.03	75.80	69.22	72.42	73.45	66.73	70.16	71.17	64.45	67.92	69.08	62.15	65.82	66.81	59.66	63.14	64.43
		OUT	34.84	40.20	44.81	35.14	40.01	45.25	34.77	39.81	44.89	35.15	39.87	45.12	35.14	40.15	45.26	34.89	40.14	45.14	35.11	40.29	44.74
	Pressure (bar)	OUT	9.55	10.98	12.26	9.49	10.92	12.15	9.42	10.79	12.04	9.35	10.70	11.95	9.28	10.59	11.86	9.31	10.63	11.35	9.31	10.45	11.67
EEV	Temperature (°C)	IN	29.53	34.60	39.17	30.10	34.97	39.79	30.18	34.91	39.68	30.73	35.27	40.20	31.04	35.91	40.71	31.29	36.41	40.88	31.97	36.42	40.67
	Pressure (bar)	IN	8.97	10.41	11.64	8.97	10.37	11.55	8.90	10.27	11.45	8.89	10.21	11.43	8.85	10.14	11.37	8.93	10.22	11.32	8.90	10.07	11.23
Refrigerant mass flow (kg/h)			12.70	12.44	13.90	13.55	12.64	18.40	17.75	16.73	23.90	23.07	21.95	30.83	29.83	29.10	39.50	38.54	37.89	50.66	49.55	49.02	65.19
Secondary Circuit Water-glycol	Temperature (°C)	IN	-6.13	-6.39	-6.11	-1.88	-2.02	-1.89	2.30	1.97	1.96	6.27	6.28	6.07	9.84	10.14	9.93	14.00	13.95	13.87	18.21	18.31	18.13
		OUT	-9.48	-9.84	-9.80	-5.58	-5.70	-5.56	-1.54	-2.01	-1.99	2.16	2.17	2.00	5.60	5.94	5.72	9.41	9.40	9.41	13.65	13.64	13.51
	Flow rate (L/s)		0.04	0.04	0.03	0.05	0.05	0.04	0.06	0.06	0.05	0.08	0.07	0.07	0.10	0.09	0.09	0.12	0.11	0.11	0.17	0.15	0.14
Secondary Circuit Water	Temperature (°C)	IN	29.80	35.19	39.74	30.16	34.95	40.29	29.70	34.86	39.79	30.19	34.73	40.19	30.15	35.05	40.18	29.94	35.14	40.04	30.18	35.18	39.71
		OUT	33.06	38.37	42.85	33.69	38.45	43.72	33.57	38.68	43.58	34.29	38.81	44.23	34.41	39.26	44.26	34.31	39.41	44.22	34.60	39.55	44.07
	Flow rate (L/s)		0.060	0.057	0.052	0.071	0.066	0.061	0.080	0.077	0.071	0.096	0.092	0.086	0.119	0.112	0.109	0.143	0.140	0.136	0.179	0.173	0.164

APPENDIX II. AVERAGE HEAT TRANSFER COEFFICIENT EXPERIMENTAL ANALYSIS

Table 9: Average Heat transfer coefficient Experimental data for R134a.

Expected T_{evap} (°C)	-12			-8			-4			0			4			8			12			
	35	40	45	35	40	45	35	40	45	35	40	45	35	40	45	35	40	45	35	40	45	
Expected T_{cond} (°C)																						
Superheated (°C)	5.49	5.29	5.21	5.76	5.59	5.83	5.13	5.29	5.42	4.47	5.07	5.09	4.85	5.30	5.62	4.10	4.76	5.35	3.46	4.28	5.01	
Subcooling (°C)	2.05	2.09	2.35	1.87	2.72	1.81	2.52	2.00	0.94	2.29	1.44	0.83	2.03	1.37	0.57	1.16	0.33	0.97	0.91	0.21	0.88	
\dot{Q}_{evap}	0.51	0.49	0.44	0.67	0.63	0.57	0.88	0.82	0.75	1.16	1.10	1.02	1.51	1.44	1.34	1.99	1.88	1.78	2.60	2.45	2.34	
$\dot{Q}_{tp,e}$	0.50	0.47	0.42	0.65	0.60	0.55	0.85	0.80	0.72	1.13	1.06	0.98	1.47	1.39	1.29	1.94	1.83	1.72	2.55	2.38	2.26	
$\dot{Q}_{sp,e}$	0.02	0.02	0.01	0.02	0.02	0.02	0.03	0.03	0.03	0.03	0.03	0.03	0.04	0.05	0.05	0.05	0.06	0.06	0.05	0.07	0.08	
$\Delta T_{in-sp,e}$	2.20	2.44	2.53	1.76	2.05	1.61	2.62	2.45	2.28	3.24	2.69	2.65	2.89	2.43	1.98	3.51	2.97	2.33	3.99	3.37	2.72	
$\Delta T_{in-tp,e}$	4.05	4.01	4.02	3.81	3.82	3.79	3.66	3.64	3.60	3.56	3.52	3.47	3.41	3.36	3.47	3.23	3.20	3.12	3.13	3.14	3.13	
$\Delta T_{in-evap}$	3.94	3.93	3.95	3.67	3.71	3.61	3.61	3.58	3.52	3.55	3.49	3.44	3.39	3.32	3.38	3.24	3.20	3.08	3.14	3.15	3.11	
U_{evap}	0.71	0.67	0.60	0.99	0.92	0.86	1.32	1.25	1.16	1.77	1.71	1.61	2.43	2.36	2.16	3.34	3.20	3.14	4.51	4.23	4.09	
\dot{Q}_{cond}	0.78	0.74	0.68	0.99	0.95	0.87	1.21	1.16	1.09	1.58	1.49	1.41	2.03	1.91	1.84	2.54	2.44	2.30	3.23	3.06	2.91	
$\dot{Q}_{sp,c}$	0.14	0.13	0.11	0.17	0.16	0.14	0.22	0.21	0.18	0.27	0.25	0.23	0.32	0.30	0.28	0.39	0.36	0.33	0.46	0.42	0.39	
$\dot{Q}_{tp,c}$	0.63	0.60	0.55	0.80	0.77	0.71	0.97	0.93	0.89	1.28	1.21	1.17	1.68	1.59	1.56	2.14	2.07	1.95	2.75	2.64	2.50	
$\dot{Q}_{sc,c}$	0.01	0.01	0.01	0.01	0.02	0.01	0.02	0.02	0.01	0.03	0.02	0.01	0.03	0.02	0.01	0.02	0.01	0.02	0.02	0.00	0.02	
$\Delta T_{in-sp,c}$	17.99	17.21	15.33	16.74	15.94	14.01	15.75	14.55	12.08	15.08	12.75	11.06	13.23	11.85	11.31	11.20	11.09	9.71	11.78	10.04	8.78	
$\Delta T_{in-tp,c}$	6.62	6.69	5.96	6.27	6.12	5.23	5.74	5.25	4.17	5.78	4.52	3.92	5.00	4.35	4.41	4.00	4.33	3.81	4.76	4.04	3.62	
$\Delta T_{in-sc,c}$	6.93	6.95	6.06	6.85	6.22	5.82	6.12	5.90	5.44	6.43	5.65	5.40	5.91	5.62	6.07	5.53	6.25	5.46	6.42	6.10	5.40	
$\Delta T_{in-cond}$	7.47	7.50	6.64	7.05	6.85	5.85	6.49	5.95	4.70	6.47	5.09	4.39	5.56	4.84	4.87	4.44	4.75	4.19	5.21	4.40	3.94	
U_{cond}	0.25	0.24	0.25	0.34	0.33	0.36	0.45	0.47	0.56	0.59	0.70	0.77	0.88	0.95	0.92	1.38	1.24	1.33	1.50	1.68	1.79	

*Following the methodology described in Equations (1) through (8).

Table 10: Average Heat transfer coefficient Experimental data for R513A.

Expected T_{evap} (°C)	-12			-8			-4			0			4			8			12		
	35	40	45	35	40	45	35	40	45	35	40	45	35	40	45	35	40	45	35	40	45
Expected T_{cond} (°C)	35	40	45	35	40	45	35	40	45	35	40	45	35	40	45	35	40	45	35	40	45
Superheated (°C)	4.54	4.86	5.02	5.78	5.69	5.96	5.51	5.74	5.59	4.65	4.38	5.25	4.92	4.80	5.58	4.38	4.50	5.04	4.54	4.17	3.89
Subcooling (°C)	2.03	2.12	2.03	2.07	2.22	2.08	1.52	1.46	1.54	1.39	1.49	1.26	1.08	1.09	1.03	1.56	1.42	1.08	1.14	1.15	0.90
\dot{Q}_{evap}	0.53	0.48	0.44	0.69	0.63	0.57	0.92	0.86	0.77	1.25	1.15	1.07	1.63	1.54	1.44	2.15	2.01	1.90	2.80	2.69	2.50
$\dot{Q}_{tp,e}$	0.51	0.47	0.42	0.67	0.61	0.55	0.88	0.83	0.73	1.21	1.11	1.02	1.57	1.48	1.38	2.08	1.94	1.83	2.71	2.60	2.43
$\dot{Q}_{sp,e}$	0.02	0.02	0.02	0.03	0.03	0.03	0.04	0.04	0.03	0.04	0.04	0.04	0.06	0.05	0.06	0.07	0.07	0.07	0.09	0.08	0.07
$\Delta T_{ln-sp,e}$	3.18	2.85	2.6	1.86	1.94	1.48	2.05	1.93	2.29	3.10	3.44	2.41	2.97	2.82	2.05	3.26	3.29	2.55	3.29	3.46	3.58
$\Delta T_{ln-tp,e}$	4.04	3.95	3.90	3.86	3.81	3.82	3.57	3.68	3.71	3.54	3.63	3.40	3.51	3.24	3.36	3.17	3.28	3.05	3.19	3.06	3.00
$\Delta T_{ln-evap}$	4.01	3.89	3.84	3.69	3.66	3.56	3.47	3.54	3.61	3.53	3.62	3.34	3.49	3.22	3.27	3.17	3.28	3.03	3.19	3.07	3.02
U_{evap}	0.72	0.67	0.62	1.02	0.94	0.87	1.44	1.33	1.16	1.93	1.73	1.73	2.53	2.59	2.39	3.68	3.33	3.41	4.77	4.76	4.51
\dot{Q}_{cond}	0.86	0.80	0.75	1.10	1.03	0.94	1.34	1.30	1.21	1.76	1.66	1.54	2.19	2.10	2.00	2.76	2.64	2.51	3.49	3.32	3.16
$\dot{Q}_{sp,c}$	0.18	0.17	0.15	0.22	0.21	0.18	0.26	0.25	0.22	0.31	0.30	0.28	0.37	0.36	0.33	0.43	0.40	0.38	0.50	0.46	0.44
$\dot{Q}_{tp,c}$	0.67	0.62	0.59	0.87	0.80	0.74	1.06	1.03	0.97	1.42	1.34	1.25	1.79	1.72	1.65	2.29	2.21	2.11	2.95	2.82	2.69
$\dot{Q}_{sc,c}$	0.01	0.01	0.01	0.02	0.02	0.02	0.02	0.02	0.02	0.02	0.02	0.02	0.02	0.02	0.02	0.04	0.04	0.03	0.04	0.04	0.03
$\Delta T_{ln-sp,c}$	16.74	16.56	15.45	15.87	15.49	14.76	13.88	13.26	12.68	12.66	12.38	11.48	11.10	11.01	9.81	11.05	10.15	9.45	9.68	8.95	8.18
$\Delta T_{ln-tp,c}$	5.58	5.73	5.62	5.59	5.63	5.77	4.81	4.65	4.81	4.53	4.63	4.48	3.97	4.19	3.79	4.52	4.32	4.09	4.01	3.96	3.63
$\Delta T_{ln-sc,c}$	5.91	5.98	5.93	6.04	5.97	6.21	5.77	5.60	5.73	5.73	5.77	5.69	5.46	5.64	5.30	5.81	5.68	5.66	5.61	5.54	5.37
$\Delta T_{ln-cond}$	6.48	6.67	6.44	6.40	6.47	6.55	5.52	5.33	5.44	5.13	5.24	5.04	4.47	4.70	4.24	4.99	4.75	4.49	4.39	4.31	3.95
U_{cond}	0.32	0.29	0.28	0.42	0.39	0.35	0.59	0.59	0.54	0.83	0.77	0.74	1.18	1.08	1.14	1.33	1.35	1.35	1.92	1.86	1.93

*Following the methodology described in Equations (1) through (8).

Table 11: Average Heat transfer coefficient Experimental data for R516A.

Expected T_{evap} (°C)	-12			-8			-4			0			4			8			12		
	35	40	45	35	40	45	35	40	45	35	40	45	35	40	45	35	40	45	35	40	45
Expected T_{cond} (°C)	35	40	45	35	40	45	35	40	45	35	40	45	35	40	45	35	40	45	35	40	45
Superheated (°C)	4.79	4.33	4.31	5.74	5.83	5.58	5.10	4.74	4.99	4.79	4.12	4.61	4.52	4.28	5.46	5.38	5.10	5.43	5.11	5.71	5.60
Subcooling (°C)	2.84	2.72	3.02	2.40	2.74	1.67	2.52	2.60	1.69	1.99	2.27	1.31	1.80	1.75	0.86	2.34	1.92	0.64	1.93	1.12	0.95
\dot{Q}_{evap}	0.52	0.47	0.39	0.68	0.61	0.58	0.91	0.81	0.75	1.20	1.08	1.00	1.59	1.45	1.35	2.06	1.92	1.81	2.81	2.62	2.48
$\dot{Q}_{tp,e}$	0.51	0.45	0.38	0.66	0.58	0.55	0.88	0.78	0.72	1.16	1.05	0.96	1.54	1.41	1.29	1.99	1.85	1.74	2.72	2.51	2.38
$\dot{Q}_{sp,e}$	0.02	0.02	0.01	0.03	0.03	0.02	0.03	0.03	0.03	0.04	0.03	0.04	0.05	0.05	0.06	0.08	0.07	0.07	0.09	0.10	0.10
$\Delta T_{ln-sp,e}$	3.01	2.73	3.40	1.65	1.89	2.10	2.77	3.05	2.89	3.09	3.54	3.27	3.10	3.41	2.39	2.43	2.64	2.44	2.68	2.13	1.92
$\Delta T_{ln-tp,e}$	4.10	3.42	3.85	3.74	3.95	3.85	3.81	3.65	3.73	3.64	3.56	3.70	3.33	3.47	3.53	3.20	3.160	3.36	3.19	3.22	3.01
$\Delta T_{ln-evap}$	4.05	3.40	3.83	3.56	3.77	3.72	3.76	3.63	3.69	3.62	3.56	3.68	3.32	3.47	3.47	3.17	3.14	3.31	3.17	3.16	2.94
U_{evap}	0.70	0.75	0.55	1.04	0.88	0.84	1.32	1.21	1.10	1.80	1.65	1.47	2.60	2.27	2.11	3.54	3.32	2.98	4.82	4.50	4.58
\dot{Q}_{cond}	0.81	0.76	0.67	1.05	0.96	0.87	1.29	1.22	1.13	1.64	1.57	1.46	2.11	1.96	1.85	2.61	2.51	2.38	3.31	3.16	2.99
$\dot{Q}_{sp,c}$	0.16	0.15	0.13	0.20	0.19	0.16	0.24	0.22	0.20	0.29	0.27	0.24	0.34	0.32	0.29	0.40	0.38	0.34	0.47	0.45	0.39
$\dot{Q}_{tp,c}$	0.63	0.59	0.53	0.83	0.75	0.70	1.02	0.97	0.91	1.33	1.27	1.20	1.74	1.60	1.55	2.16	2.08	2.02	2.79	2.68	2.56
$\dot{Q}_{sc,c}$	0.02	0.02	0.02	0.02	0.02	0.01	0.03	0.03	0.02	0.03	0.03	0.02	0.03	0.03	0.02	0.05	0.04	0.02	0.06	0.03	0.03
$\Delta T_{ln-sp,c}$	17.48	16.77	16.09	15.75	15.85	13.29	14.98	14.44	12.48	13.07	13.31	10.74	12.01	11.78	9.72	11.83	11.11	8.71	10.46	9.36	8.15
$\Delta T_{ln-tp,c}$	6.46	6.34	6.71	5.80	6.25	5.08	5.83	5.82	5.04	5.04	5.51	4.32	4.76	4.86	3.96	5.18	4.86	3.65	4.68	4.05	3.76
$\Delta T_{ln-sc,c}$	6.33	6.24	6.42	6.07	6.29	5.73	6.20	6.12	5.87	5.87	6.16	5.54	5.82	5.90	5.49	6.00	5.87	5.40	5.81	5.62	5.47
$\Delta T_{ln-cond}$	7.37	7.24	7.54	6.59	7.08	5.74	6.59	6.54	5.63	5.66	6.14	4.80	5.29	5.40	4.38	5.68	5.33	4.00	5.09	4.42	4.06
U_{cond}	0.27	0.25	0.22	0.39	0.33	0.37	0.4729	0.45	0.48	0.70	0.62	0.73	0.97	0.88	1.02	1.11	1.14	1.44	1.57	1.73	1.78

*Following the methodology described in Equations (1) through (8).

**APPENDIX III. EXAMPLE OF HEAT TRANSFER COEFFICIENT
CALCULATION FOR REFRIGERANT SIDE**

This example illustrates how the average heat transfer coefficient on the refrigerant side is calculated for the evaporator:

$$n_{plt_{ref}} = 4$$

$$n_{plt_w} = 5$$

$$N_{eff-plates} = 8$$

$$L_p = 0.269 \text{ m}$$

$$W_p = 0.085 \text{ m}$$

$$b = 0.002 \text{ m}$$

$$T_{evap} = -12^\circ\text{C}$$

$$\dot{m}_{ref} = 0.016 \text{ kg/s}$$

$$x_{in_{evap}} = 0.3$$

- Using Eq. (33) to calculate the heat transfer coefficient (HTC_{evap}) for each quality of vapor:

$$HTC_{evap} = 0.408\Phi \left(\frac{\lambda_{refl}}{d_h} \right) Re_{refl}^{1.35} Pr_{refl}^{\left(\frac{1}{3}\right)}$$

x	$HTC_{evap} \left(\frac{W}{m^2K} \right)$
0.3	23167
0.4	18865
0.5	14796
0.6	10990
0.8	7491
0.9	4364
1.0	1732

- To calculate the average heat transfer coefficient (HTC_{evap}) for the two-phase flow region in the evaporator, the following equation is used:

$$\left(\frac{1}{i} \sum_{x=x_{in_{evap}}}^{x=1} HTC_{evap}(x_i) \right) = 11630 \frac{W}{m^2K}$$

3. The superheating is assumed to be constant at 5K. The heat transfer coefficient in the superheating zone is calculated using the T_{evap} and the properties of the refrigerant for saturated vapor. Using Eq. (19):

$$HTC_{sp} = 0.277 \left(\frac{\lambda_{sp}}{d_h} \right) Re_{sp}^{0.766} Pr_{sp}^{0.333} = 739 \frac{W}{m^2K}$$

4. Finally, for the average heat transfer coefficient in the evaporator on the refrigerant side, and considering that 20% of the total area of the evaporator corresponds to the superheating zone ($F_{sp,e} = 0.2$), the calculation follows Eq. (35):

$$\overline{HTC}_{evap} = \left(\frac{1}{i} \sum_{x=x_{in\,evap}}^{x=1} HTC_{evap}(x_i) \right) (1 - F_{sp,e}) + HTC_{sp,e} F_{sp,e}$$

$$\overline{HTC}_{evap} = 11630(1 - 0.2) + 739(0.2) = 9451 \frac{W}{m^2K}$$